LITHOS

New insights from plumbing system below composite mafic volcanoes: post-glacial volatile contents and magmatic fluids from Villarrica magmas

--Manuscript Draft--

Manuscript Number:	LITHOS12050R1
Article Type:	Regular Article
Keywords:	Composite volcano, Mafic magma, Melt inclusions, Noble gas, Eruptive Paroxysm
Corresponding Author:	Philippe Robidoux, Ph.D. University of Chile Santiago, CHILE
First Author:	Philippe Robidoux, Ph.D.
Order of Authors:	Philippe Robidoux, Ph.D.
	Yves Moussallam
	Estelle F. Rose-Koga
	Andrea Luca Rizzo
	Guillaume Georgeais
	Joao Lages
	Gilles Lévresse
	Simona Ferrando
	Alessandro Aiuppa
Abstract:	Villarrica volcano, in the southern Andes, is a composite mafic volcano whose persistent open-vent activity is punctuated by frequent Strombolian/Hawaiian eruptions and, more rarely, by more energetic (sub-Plinian) events. Here, we investigate the volatile composition of the parental melts that sustain this activity, and the conditions of pre-eruptive magma storage, by characterizing the composition of olivine-hosted melt and fluid inclusions. We concentrate on inclusions entrapped in minerals from pyroclastic materials erupted from both Villarrica summit and from its flank Minor Eruptive Centers (MECs) post the 14.5-13.5 kyr caldera collapse event that formed the Licán ignimbrite. Our micro-FTIR and SIMS measurements indicate that the Pucón eruption records the highest volatile contents, with 6.0 wt.% H2O, >1500 ppm CO2, 1330 ppm S, 1556 ppm Cl, and 2055 ppm F. These volatile contents imply a volatile-saturated magma originating from a depth of 14.4 to 17 km below Villarrica. Results for other flank eruptions highlight a similarly deep (17–21 km depth) source for basaltic CO2-rich mafic magmas erupted at regional MECs (Los Nevados, Caburgua). Melt inclusion results also reveal that deep rising mafic magma batches, when temporarily stored at 1–5 km depth, produce the more differentiated and degassed magma batches that sustain the decadal-old persistent effusive-explosive eruptive activity at Villarrica. Helium isotope ratios (3He/4He; Rc/Ra when corrected for atmosphere) measured in bulk noble gases from olivines (Fo75–88) indicate that the parental magmatic fluid signature (Rc/Ra = 6.7–7.6; CO2/3He = 4.7–7.5E+08) is only recorded during central paroxysmal subplinian eruption, and that this primitive gas signal is diluted in lateral MECs (Rc/Ra<6.5; CO2/3He = 1.4x10+9–3.1x10+10).
Suggested Reviewers:	George Zellmer G.F.Zellmer@massey.ac.nz Expert of volatile studies in subduction settings and dedicated to volcanic hazard mitigation.
	John Stix john.stix@mcgill.ca Internationally recognized volcanologist who treated several studies of degassing mafic magmatic systems.
	Jeffrey Witter

	jeff@innovategeothermal.co Geologist who completed his PhD thesis and work on the venting system of the Villarrica volcano, covering various aspects of geochemical studies of the system during the 2000s.
	Takeshi Kuritani Hokkaido University Faculty of Science kuritani@sci.hokudai.ac.jp Expert on studies of magmatic processes in similar active volcanoes, where experimental and geochemical tools have helped to assess magma genesis as a characterisation of magmatic differentiation for basalt-to-andesitic melt compositions.
Opposed Reviewers:	

« New insights from plumbing system below composite mafic volcanoes: post-glacial volatile contents and magmatic fluids from Villarrica magmas »

Author names and affiliations: Philippe Robidoux[a], Yves Moussallam[b,c], Estelle F. Rose-Koga[d], Andrea Luca Rizzo[e,f], Guillaume Georgeais[b], Joao Lages[g,h], Gilles Lévresse[i], Simona Ferrando[j], Alessandro Aiuppa[g,h]

[a] Department of Geology, Facultad de Ciencias Físicas y Matemáticas, Universidad de Chile, 8370450 Santiago, Chile

[b]Lamont-Doherty Earth Observatory, Columbia University, New York, USA

[c]American Museum of Natural History, Department of Earth and Planetary Sciences, NY 10024, New York, USA

[d]Institut des Sciences de la Terre d'Orléans (ISTO), CNRS UMR 7327, Université d'Orléans, BRGM, 1A rue de la Férollerie, 45071 Orléans, Cedex 2, France

[e]University of Milano Bicocca, Dipartimento di Scienze Dell Ambiente e della Terra (DISAT), Milano, Italy

[f]Istituto Nazionale di Geofisica e Vulcanologia (INGV), Sezione di Milano, Milano, Italy, Via Alfonso Corti, 12, 20133 Milano MI

[g]Dipartimento DiSTeM, Universitá degli Studi di Palermo, Palermo, Italy

[h]Istituto Nazionale di Geofsica e Vulcanologia (INGV), Sezione di Palermo, Via Ugo La Malfa 153, 90146, Palermo, Italy

[i]Centro de Geociencias, UNAM Campus Juriquilla Blvd. Juriquilla 3001, Querétaro 76230, Mexico

[j]Simona Ferrando, Department of Earth Sciences, University of Torino, Via Valperga Caluso 35,10125, Torino, Italy

Corresponding author.

Dr. Philippe Robidoux

Department of Geology, Facultad de Ciencias Físicas y Matemáticas, Universidad de Chile, Plaza Ercilla 803, 8370450, Santiago, Chile

E-mail address: robidouxphilippe@gmail.com

Cover letter

CENTRO DE EXCELENCIA EN GEOTERMIA DE LOS ANDES

FACULTAD DE CIENCIAS FÍSICAS Y MATEMÁTICAS UNIVERSIDAD DE CHILE

Santiago, August 26, 2024

Dr. G. Shellnutt,
Editorial Board Member of Lithos

Paper LITHO12050 "New insights from plumbing system below composite mafic volcanoes: post-glacial volatile contents and magmatic fluids from Villarrica magmas" by Robidoux et al.

Dear Editor,

Following your e-mail of July 7, 2024, we have strongly revised the manuscript based on detailed and constructive comments made by the two reviewers and yours.

To summarize, the research objective and focus have been limited to the main finding, which is to portrait the compositional and depth characteristics of the deep and shallow zone transporting magmatic fluids in the Villarrica composite volcanic system. For this matter, the reformulation of the abstract, the introduction, as well as the conclusion have been oriented around this theme. The figures and supporting tables have been reduced and organized to condense the dense information. The Appendix (B) contains all the supported datasets as recommended by reviewers and bulk rock trace/REE not used in the analyses and discussion.

As recommended by the reviewers, the Methods section has been implemented with the required supporting information, and specific methods have been reinstated in Appendix A. The Methods section is now clearer and directly accessible for specific data productive as a treatment. In the Discussion section, the geobarometric modeling has been rewritten (discussion in Sections 5.1, 5.2), clarifying the main scientific findings on the importance of recognizing the two depth zones for mafic magmas, while the role of magmatic fluids structured to cover a volcanic-arc scale (5.3) as a locally specific polygenetic volcanic complex (5.4) perspective.

I am including, in the next pages the ''*Revision Notes*'', a detailed response to all the comments and a brief explanation on how the manuscript has been modified. The new version of the manuscript is joined to the submission files as "*Revision, changes marked*", hoping the revision files will meet Lithos requirements for publication.

However, please let me know if any additional change needs to be done.

Waiting for your communication,

Best Regards,

Philippe Robidoux

Plaza Ercilla 803, Santiago – Chile. Tel: 5 (6) 951232150 Email Institucional: robidouxphilippe@gmail.com

CENTRO DE EXCELENCIA EN GEOTERMIA DE LOS ANDES

FACULTAD DE CIENCIAS FÍSICAS Y MATEMÁTICAS UNIVERSIDAD DE CHILE

Revision Notes

COMMENTS FROM EDITORS AND REVIEWERS
Dear Dr. Robidoux,

Thank you for submitting the manuscript entitled "New insight from plumbing system below composite mafic volcanoes: post-glacial volatile contents and magmatic fluids from Villarrica magmas" to Lithos. Below and attached are the comments of two reviewers that evaluated your manuscript. The reviewers are supportive of publication after major revisions.

The scientific concerns highlighted by the reviewers are straight forward. However, the primary concern is that the manuscript is unfocused and difficult to appreciate. It is a necessity to streamline the text (and appendices) and focus on the main conclusions of the study. This will require tough decisions on which data to include and which data to exclude.

In the revised version of the manuscript please provide point-to-point responses to the reviewers' comments and make sure the text, tables, figures (no more than 15), highlights (no more than 85 characters + spaces), and references (no more than 80) are properly formatted. The guidelines will be strictly enforced.

All the best.

Greg Shellnutt

Co-Editor-in-Chief

Reviewer #1: Review of "New insight from plumbing system below composite mafic volcanoes: post-glacial volatile contents and magmatic fluids from Villarrica magmas" by Robidoux et al submitted to Lithos (LITHOS12050)

Dear Editor,

I have now read the submitted manuscript. The authors present a very large data set of detailed textural features of olivines, olivine chemistry, melt and fluid inclusions, noble gas chemistry and whole rock major and trace elements. These data are presented for a time series of explosive eruptions from Villarrica volcano and some nearby centres which may be connected to the same plumbing system. The data are of good quality and methods and QC are mostly well-discussed, and a huge amount of information related to corrections and methods is presented in 14 separate appendices. It was unclear, however, what the main focus was, and I struggled to understand what the main conclusions were. The discussion also goes down many paths of trying to understand the whole system (depths of melting, mantle sources, inputs, components, depths of crystallisation, types of eruption, plumbing systems) but doesn't go into a lot of detail about any of them, and this combined with very busy figures and the majority of the work being in all the appendices makes this very difficult to read. The dataset is good and there are some great ideas here but the manuscript, figures and supplementary information need to be organised in a more streamlined way that will assist the reader in following the main scientific points. I support publication in Lithos after major revisions.

PR: The authors are very grateful for the straightforward critique and suggestions that help focus and structure the manuscript's research findings. We agree that the dense aspect of the data collection required a firm polishing and re-structuring from the main text for improving the quality and clarity of the manuscript. To assist in this matter, we provide a point-by-point response to the comments and assure that all observations have been positively addressed. Please be aware that line numbers from original version are modified. We agree on the reformulation of the aim/focus, condense the supporting data into a single structured appendix file as suggested, then all figures have been reviewed to simplify the illustration information.

To alleviate the writing problem, the method section is divided into a "Global Strategy=state of the art" and “Petrologic Approach” sections. The readers should now have a better understanding of the scientific objective being “to resolve the scenario of magma supply evolution at the Villarrica composite volcanic system by characterizing the variation of pre-eruptive volatiles as supplied by magmatic fluids beneath Villarrica, including its surrounding volcanic centers. "

As now stated in the new manuscript form, is to present (1) detailed measurements are provided to characterize Villarrica mafic magmas thought pre-eruptive conditions for melting (melt major volatile contents), then use (2) volatile tracers of the magmatic fluid source composition (isotopic noble gases). In order to improve the readability of the method, we have implemented the necessary details as recommended by Reviewer 1, then expanded into five subsections. The reason behind keeping an appendix to support this section (now simplified as Appendix A) is to give access to PEC details and strategy behind data filters, which are too much detail for the method part itself. If some of this is judged not necessary for the journal, we would be happy to eliminate this information.

Finally, we have restructured the discussion section into 5 sections that reflect the main discoveries revealed after respecting the state of the art for the scientific approach. The five scientific headlines of those discoveries are closely related dataset information that fortalice (1) better constrain on volatile geobarometric model (section 5.1 to 5.2) and (2) put into perspective the magmatic fluid characteristics of Villarrica and MECs (5.3 and 5.4). The conclusion is rewritten as a synthetic affirmation of these findings, which are presented with certainty and summarized in 3 paragraphs.

Main comments of the Reviewer #1 (R1):

1. The abstract seems to present the work in the context of the lateral evolution of this volcanic area (with comparisons between the main stratovolcano, the peripheral/parasitic groups of small cones and some 'monogenetic' cones further north but still in the same area). However, the discussion looks at the data more in a chronological order. Both are good approaches, but this needs to be more focussed in my opinion.

PR: Corrected by re-writing abstract, as recommended including comments of reviewers 1 and 2. The chronological order is now kept consistent in the results and discussion sections.

2. The abstract is very undigestible. It quickly moves from mafic explosive eruptions to very specific data details, with no setting up of the context or establishing a question to be answered. Maybe instead of putting in a conclusion from every dataset and every set of samples you can focus on the big picture conclusions?

PR: Corrected by re-writing abstract, listing instead the solid discovery lines and less secondary plan details.

3. It's not really clear whether the focus of this is the chronological evolution of the magmatic fluids at Villarrica and the surrounding centres (which this unique and detailed dataset can clearly address) or mantle sources, depths of melting, sediment/slab input etc. It's enough if you just focus on one of these things. In my opinion the manuscript is just trying to answer too many questions.

PR: Corrected in Abstract, Introduction and Discussion is reviewed accordingly to keep consistent on the focus. The main objective line is “to characterize the magmatic plumbing system that sustains the variety of eruption styles at Villarrica by studying the pre-eruptive volatile contents in the source parental magmas of both central and peripheral volcanic centers “.

4. Reading the manuscript didn't take me too long, but I spent over a day in total going through all 14 appendices. This is just too many and it was very frustrating that the text kept referring to all of the separate sheets all the time. I had to have them all open at the same time and keep flicking between them! Please go back through and consider

which pieces of data/methods explanation/corrections/summaries are constantly referred to during the results and discussions and would actually be better in the manuscript itself. You could also consider putting all of the separate sheets into one excel of multiple tabs with a 'contents page' at the front. The first appendix is 18 pages long and contains information on the ou could also consider putting all of the separate sheets into one excel of multiple tabs with a 'contents page' at the front. The first appendix is 18 pages long and contains information on the models which I think should really be in the text itself. Note that the table captions didn't always match the header, e.g. tab would say table A.10 but the caption would say A.9.

PR: One single file is created as Appendix B to resume the entire set of table files. The Appendix A is used as a supportive document (essentially 7 pages + references apart). Then Appendix B (Table A.1 to A.10) is supportive of the magma chemistry characterization for this research project.

5. The figures are very full of symbols, lines, vectors and labels which means they need careful study to pull out the relevant aspects that are referred to in the text. I find figure 7 in particular very 'busy'. Are all of the background datasets in these figures necessary? Is there a more clear way of presenting the data? For example, could some of the arrows showing processes by taken off and placed to the side or underneath the data?

PR: All figures are now reviewed to erase/simplify some symbols, particularly, figures 2, 5, 6, 7, 8. The figure 7 (trace element/REE ratios) is not used anymore since representing information that are not used to reach the goal of the present investigation.

6. There are quite a few places in the text where a reference is given that doesn't really relate to the preceding statement or idea, or is rather ambiguous. An example is lines 36-38 where the references given are more general review style papers but the sentence is about 'complex transport history at Villarrica'. This might seem like a minor detail, but I think it's a little misleading for a reader as it makes it seem like a lot of work has already been done on e.g. Villarrica when actually these articles are cited more for their concepts/theory. Some sentence restructuring would help this.

PR: Corrected for Line 36-38 and other sentences with supported citations are reviewed elsewhere in all parts of the manuscripts.

Detailed comments of the Reviewer #1 (R1):

Title: New insight from plumbing system below composite mafic volcanoes - I think this is missing an article, or a plural. New insights from the plumbing system?

PR: New insights

Start of introduction: This is the context that is missing from the abstract

PR: Agreed. The problematic is re-written for improving understanding of the main objective.

Lines 10-12: It's not clear why there is suddenly mention of recharge bodies, also what mechanism are you referring to here? The reader may not be familiar with Moitra et al and the references therein

PR: The shift from Strombolian to major explosive paroxysm is the main concern from the pre-eruptive volatile perspective, but not only at central crater. We reformulate in introduction as "*However, geological evidence also exists for more energetic Vulcanian to sub-Plinian eruptions (Silva et al., 2010; Costantini et al., 2011; Lohmar et al., 2012) and for mafic ignimbrite-forming eruptions (Moreno and Clavero, 2006), as observed elsewhere as a consequence of fast ascent, decompressional degassing, and fragmentation of basaltic magma (Moitra et al., 2018; Stix, 2007; Heinrich et al., 2020).* "

Lines 24-32: This is set out quite clearly. I suggest you stay with this as a primary focus and make sure all the data and interpretations are leading to this goal

PR: Agreed.

Line 33: What is the difference between a magmatic fluid and a volatile?

PR: This question is very important for expert as non-expert readers; thus we give the formal definition and add the section "Global Strategy" for explaining the importance of it. From the melt inclusion perspective, "magmatic fluids" are the volatile exsolved from the melt (and therefore present as a bubble in the melt inclusion). The volatile element concentration of a melt inclusion is the concentration of a volatile element in the glassy silicate melt, except for CO_2, for which it has been shown (e.g Moore et al., 2015) that a significant proportion of CO_2 can be exsolved in the bubble (when present) of the melt inclusion. In that specific case the total CO_2 concentration of the melt inclusion is the sum of the CO_2 concentrations in the glassy silicate, plus that in the bubble.

Line 43 and 58: In general, what is meant by degassing? Or variably degassed magma?

PR: Degassing is the process of governing volatile loss from the liquid silicate melt. Upon ascent a magma degasses. A melt inclusion will trap a magma at a given P, T condition, at a certain depth. Variably degassed magma would imply variability, in term of volatile element content measured in that MI, relating the volatile element concentration to the saturation process, therefore to a depth range.

Lines 47-57: This paragraph is much more clear and focussed, base the abstract and discussion around these questions

PR: Agreed.

Line 78: Note that the fumaroles in figure 1 are not really discussed in the text

PR: We agree. The figure 1 is thus modified to present geographical information only.

Line 79: Subduction 45 Myrs old, note that earlier you say 12-20 Myrs

PR: Corrected to "Volcanism in the Andes is the result of the subduction of the Nazca (10–60 My old) and Antarctic oceanic plates (<12–24 My old)". These are the ages consulted in Stern, 2004.

Methods: Where are the solubility models to calculate the saturation depths? These are a critical part of the discussion so need to be in the manuscript, not in the appendix (in my opinion). I couldn't find them in the appendix A (I see they are marked as dashed lines on figure 4 but it's not clear how they are derived.

PR: Details are now added in Method section 3.2.4 Correction for CO_2 contents and solubility models.

Line 148: I see from the appendix A that the whole rock analyses were conducted at Actlabs. Please report data quality here, accuracy on standards, duplicates and blanks.

PR: Data accuracy on standards, duplicates and blanks are now reported in new Appendix C.

Lines 171-173: This has already been said, but before it was R/Ra not Rc/Ra - what is the difference?

PR: R/Ra is the form without atmosphere correction. Rc/Ra is the form including correction for atmosphere. The form Rc/Ra is the form discussed in this manuscript, but some authors may not have done such corrections.

Lines 197-198: Please take lines 20-24 from Appendix A and put them here so that there is some explanation of these stats.

PR: Agreed and implemented in "3.1 Pyroclastic deposit classification and fragment size distribution".

Line 217: I'm interested why you plotted the whole rock data on the K2O vs. SiO2 instead of the more conventional TAS diagram - have high K2O rocks been found in this area?

PR: It is preferred here to focus on K2O (according to Peccerillo and Taylor, 1976) diagram classification as for distinguishing sodium from potassium enrichment between bulk rock and MI datasets. We suggest the use of the reference in bibliography is not necessary in this case, because classical petrological works as this require an in-text citation only.

Appendix C: What are the ratios with * at the bottom? Also, note that La/Ta is listed in the 'REE curve' but Ta isn't a REE

PR: *is the ratio used for building binary ratio diagram. Now this information is specified below the table (now Table A.2 in Appendix B). The binary diagrams are not used anymore in this paperwork.

Line 227: This sentence regarding the grouping of the olivine textures is very hard to follow

PR: The olivine crystals from each eruptive event were grouped and characterized for its dominant MI textures (Table A.3). In this study, olivine hosted MI are referred to as "MI populations" when they are derived from the same layer of a volcanic deposit.

Appendix D: What is meant by 'without fluids'?

PR: *Those inclusions without bubbles are assumed without fluids like category of olivines susceptible for not preserving magmatic fluids in their hosted MIs (now specified in Table A.3).

Line 290: 'F content susceptible to represent' - something not quite right with this sentence. 'F content may represent…?'

PR: Sentence eliminated

Line 305: n = 31. Note that the table in appendix J only has 25 samples.

PR: It is 25 measured density data, but 31 MI used for Mimic model.

Line 307: Please explain what the Mimic model is rather than just referring to a paper and the appendix.

PR: Since no heating experiment was performed on the naturally quenched MIs of this study, the instrumental evaluation of the CO_2 content here is compared with an experimental and computational method of CO_2 content reconstruction of the MIs containing shrinkage bubbles (MIMIC model from Rasmussen et al 2020).

Line 331: I like that the heading here is a statement of the results. Could you do this for the rest of the discussion headers? Or make them all consistent.

PR: Agreed, the discussion section titles are adjusted to be statements.

Appendix L: This seems like a great summary, maybe this should go in the manuscript itself?

PR: Yes, will be used as Table 3. Very useful for future consultations and investigators dedicated to this type of research. It represents an abstract dataset for MI quality and can be used for re-sampling volcanic layers for future inclusionists.

Line 339: Watch spelling and grammar here

PR: New sentence as "The highest volatile content in the MI collection is found in the Pucón ignimbrite at Villarrica.".

Line 350: Figure 5 - I like this figure, but why is the monogenetic cone Caburgua put first chronologically? I might have missed this, but is there any evidence that it precedes the other stages of Villarrica that you have presented here?

PR: Now clarified in the chapter 2. With new sentence "*Since Caburgua have been classified between 8,6 and 6, Kyr AP according to stratigraphic relationship with Villarrica Unit 2 (Moreno and Clavero, 2006), Caburgua cone could exceed the age of Pucón ignimbrite, but younger than Licán Ignimbrite (Hickey-Vargas et al., 2002).*"

Line 367: On figure 5d it looks like all of the samples have a very similar trapping MI temperature

PR: The figure 5d is now modified with two vertical axis; one for trapping °T and the other for quenching °T. The scale is now adjusted for showing the drastic variations.

Lines 348-371: This is interesting, but it's just not clear to me how this fits in with the focus of the study. The main thing here seems to be the link between explosivity, cooling rates and water contents (and H+ diffusion). I'm not sure whether this section is about volcanic style, or is a discussion of the interpretation of the water data because of possible effects of diffusion.

PR: The section is about the causes of volatile loss; therefore, the text was modified to clarify our intentions. We added the following sentence "*This section discusses melt inclusion volatile loss between two large sets of pre-eruptive conditions that chronologically describe Villarrica mafic magmas from the Pucón Ignimbrite (~3.7 kyrs) to decadal old central crater conditions*"

Line 389: '<17.0km, this study' (you don't need to refer to it as this study, if this is new data from a figure or table?

PR: Ok, this text is erased.

Line 391: I went through the 18 pages of Appendix A and couldn't find where you have worked out these pressure ranges. Maybe I missed it. But this information, seeing as it is key for one of the figures and the conclusions, should probably be in the main text.

PR: The pressures ranges are now written for Pucón event directly inside the manuscript (sections 5.1-5.2). Table A.8 is the reference for these detailed results and finally we found that an Appendix supportive section was not necessary.

Section 4.2 This section seems to mostly be in chronological order, which I think works. But it's really hard to follow what the ideas are as there is just so much data sprinkled throughout. Could you have a beginning paragraph where you do a broad overview of the main findings, then maybe some subheadings? E.g. changes in volatile contents, saturation depths, etc. Having all the information dispersed throughout makes it pretty hard to read.

PR: Agreed, while keeping chronological order, we rather now focus on the most important discovery line "
5.2 Deep reservoir inferred from CO_2-rich mafic magmas and volatile saturation at Villarrica and MECs"

Line 423: TCMS I assume is Trans Crystalline Mush System - please define

PR: Yes, now defined.

Line 428: Reference here to Blundy and Cashman - again this makes it seem like that reference is specifically about the Chaimilla event, not a theoretical concept you are applying. Just restructure the sentence

PR: Agreed, this reference is erased and not specific the case.

Line 442: 9km doesn't seem very deep?

PR: The use of "relatively" is added, considering that for Los Nevados it is the minimum depth value for no-CO2 corrected MIs.

Lines 451-453: 'The basement characteristics involve compositional heterogeneities of the transported magmas in the region of Villarrica according to our new bulk rock composition results' - I'm not clear what is meant by this.

PR: The word basement should be replaced by "mantle".

Section 4.3 I found it very hard to relate this section to the rest of the paper - it felt like a lot of generalised ideas were put together based on a few whole rock samples and put into the conclusions from the other datasets. I don't really get thelink between volatile saturation depth and subduction components.

PR: Agreed. The section is eliminated and volatile saturation story line focused in a sections 5.1+5.2. The subduction component is only discussed in relation to slab and cortical contamination tracers with Rc/Ra. The petrogenetic section about trace/REE is not relevant for this study but an extension to justify selection of geochemical markers.

Figure 7a and 7b: Note that in figure 7a you have used Th/La to show sediment addition, but in figure 7b the same ratio is used to show hydrous silicate melt… are these related? This doesn't seem very convincing.

PR: Agreed. Due to the complexity of the geomarker selection strategy, a matter rather to be studied in other investigation with minor eruptive centers and monogenetic systems, we prefer not using figure 7.

Line 465: This is the first mention of a granitic lithic contaminated scoria… again, this doesn't seem to really fit the focus of the study, it's just an interesting side note.

PR: Agreed. The granitic lithic were necessary to analyze and to compare with contaminated scoria from Pucón P2-P3 Ignimbrite, but, the trace element ratio is now eliminated from this study.

Section 4.4: This seems more on track with what the paper is focussing on. Just a thought with the atmospheric component, does the presence of the lava lake at Villarrica affect any of this?

PR: Thanks for the mention. The only certain data-supported idea that would insist is that the atmospheric component is stronger for magmas with evidence of shallow transport; therefore, if the lava lake from the main conduit crystallizes olivines and their FIs at shallow levels (Moussalam et al., 2023), perhaps ^{4}He will increase.

Line 547-548: why would the complex plumbing system of the volcano lower the He ratio? Explain more what you mean by this - something to do with greater evolution and fractional crystallisation?

PR: Agreed. This sentence is not using the specific geologic term and therefore sentence modified to "*we argue that the $^{3}He/^{4}He$ signature below Villarica is confirmed to be within the MORB range and that the cortical contamination plays an important role in lowering the original mantle $^{3}He/^{4}He$.*".

Figure 9: It's not clear to me why K2O is on there - you have used it as an index of evolution but these are all pretty similar… also, why is there such a big difference between your data and the literature data? Is it because of the types of samples that you have focussed on?

PR: Specific to bulk rock (not MI), the K_2O is useful to evaluate differentiation as continental contamination. We propose the following sentence to clarify: "bulk rock compositions indicating crustal interaction, such as Sr/Y ratios (> 20), and K_2O (wt%) content (Fig. 8cd)." Concerning the difference between datasets, we suggest that the type of samples may affect such differences, since this study mainly use bulk pyroclastic materials. If any additional information is required on this issue, please let us know.

Line 576: This is the first mention of fO2…

PR: Mistake, it was calculated in all MI; but fO_2 is not part of the discussion.

Conclusions: This is more of a summary of thoughts rather than a summary of the results and interpretation - the middle section seems to contain further discussion of new ideas rather than conclusions. Please refocus these conclusions – maybe you could frame them in the chronology that you have set up in figure 5 and parts of the discussion.

PR: The conclusion is now re-written and confirming statement titles of discussion and focuses on the main discoveries.

Figures: These are well produced with meaningful figure captions, but as I mentioned in the main comments, very very full of data and labels

PR: Agreed, we now suggest a reviewed version of the figures.

Tables: table 2 seems relevant but I'm not sure why table 1 is here while there is so much more relevant data (the MIs, FIs, noble gases…) hidden in the appendices.

PR: Table 1 is to present physical volcanology results from selected deposits where olivines-MI were separated.

Reviewer #2

This study adds several new pieces to the complex puzzle of the intricate scenario characterising volcanic systems extending across the lithosphere. I think (feel) that the amount of data is large, complementary, and helpful in constraining the general petrological picture. However, it is tough to follow the paper; consequently, it could be nice to re- organise it to attain a more straightforward and readable shape. I suggest to briefly and easily re-organise and make clear the following aspects by authors:

1) re-organise in a more proper and consequential order the abstract,

2) evidence of your new data and those deriving from previous studies in the text, tables, figures and supplementary materials (a unique Excel file with several sheets is appropriate for me),

3) in the introduction, please focus on the state of the art plus open questions and why this study is essential to clarify them,

4) avoid repetition of several topics and data in the methods, results and discussion parts,

5) the authors (if I understand right) measured several geochemical data sets (bulk rock compositions, volatiles inside MI and FI, isotopes, etc.); they should make more straightforward what they are using to improve the petrological scenario,

6) the title can probably also be revised to be more informative about the paper's scientific content.

I marked up several minor revisions, considerations, and notes directly on the submitted PDF; they could improve the clarity of this article. I also checked the list of references, and they are all appropriate and quoted, but many of them are reported only in the list and are not in the text.

Chieti, 06/07/2024

Sincerely, Gianluca Iezzi

PR: The authors are glad to follow the comments and suggestions to improve structure organization of the publication work. The dense information can be classified in two groups of datasets to resolve the main problematic: the microanalytical compositional photoshoot on the MIs and then the bulk Fis and whole rock geochemistry that frame the composite volcano into the context of magmatic fluid supply. In this sense, the introduction was re-written, containing a state-of-the-art scientific method explanation. We provide a point-by-point response to the comments and confirm minor comments are responded here. Please be aware that line numbers from original version are modified and that comments from reviewer were copied and pasted in this revision note section in order to deliver less quantity of documents for the review.

To contest main comments, we confirm (1) re-organizing the whole abstract, (2) Appendix B building to include necessary Table datasets, (3) state of the art section clarified into the introduction section, (4) elimination of repetition information through the text, (5) clarification in introduction and method of what the methods are being used for concerning petrological scenario, (6) proposing an adapted title for the paper and sub-discussion sections.

Finally, we have restructured the discussion section into 5 sections that review the two main strategies (A, B) as part of the state of the art for the scientific approach:

A) Characterize Villarrica mafic magmas thought pre-eruptive conditions for melting:

Discussion sections=

5.1 Mafic magmas degas and transit from deep to shallow volatile saturation levels

5.2 Deep reservoir inferred from CO2-rich mafic magmas and volatile saturation at Villarrica and MECs

B) **Volatile tracers of the magmatic fluid source composition**

Discussion sections=

5.4 Magmatic fluid evidence for atmospheric and crustal-derived components

5.5 Olivine FIs record primitive magmatic fluid during Villarrica subplinian climax

Detailed comments of the Reviewer #2 (R2):

Abstract

Mention of Masaya, Tongariro volcanoes

PR: Eliminated

Following glacial retreat

PR: "Following the glacial retreat..."

2.6wt.%

PR: "2.6 wt.%"

Channeled word correction

PR: Channelled

resulting in the formation of

PR: "forming"

Introduction

L12: report Moitra et al., 2018 in reference list

PR: Done

L15: report Stix et al., 1998 in reference list

PR: Done

L65: Correct year publication of Lages et al., 2021b

PR: Order a and b inverted

L81: Correct DeMets et al., 2001 citation

PR: DeMets, 2001

L114: do you sampled six new rocks, is it? Please make it clear here and in Table 1.

In Tab. 1: The columna D Fisher, 1966 is not clear to me...Table 1: the samples TVP03, 04, 05 are not reported.

PR: No, we sampled more, but we modified the introduction text for methodology and Table 1 references as symbol explanation. "Primary volcanic clast size: Fisher (1966)" refer to Fisher 1966. The Table 1 have the sample series name now adapted and clarified.

L245: are relativelly heterogeneous

PR: Ok

L242: The sentence here is already reported: "A description of the MIs is given in Appendix D (following the classification of Robidoux et al., 2018). "

PR: Agreed on eliminating the sentence

L307: Rasmussen et al. (2021)

PR: Rasmussen et al. (2020)=specifically the shrinkage bubble topic publication.

L337: Several simples are offset from the 1:1 line; have you some explanations for them?

PR: Yes, thank you for the observation. We add the following: " The SIMS divergence from 1:1 water line in figure A.2 is mainly due to the precision for smaller MI. The carbon dioxide 1:1-line offsets are larger when MIs hold shrinkage bubbles."

L354-359: the relations between cooling/quenching rates, size of clast, versus composition of the magma must be considered. SiO2-poor magmas can nucleate very rapidly, while SiO2-moderate and -rich are progressively more reluctant to nucleate. This is analysed in Vetere et al. (2915) and Giuliani et al. (2020).

PR: We agree on suggestion, but decided to eliminate the focused text on PEC. We observed that the dominant mafic character of Pucón MIs over Chaimilla and Chaillupén (Fig. 2), is consistent with the lowest crystallinity and differentiation processes that agrees with high cooling/quenching rates. Despite not developing the main text in this direction, we agree this argument applies since "*less differentiated MIs that represent low SiO_2 magmas are expected to nucleate crystals very quickly, while SiO_2-moderate and -rich magmas are increasingly reluctant to nucleate (Vetere et al., 2015; Giuliani et al., 2020)*". In this order of thought, the high-SiO_2 samples from this study (differentiated endmember MECs and the 2015 samples) coincide with the PEC-identified features in Figure 2 (orange arrow).

L361-363: This can be explained also by a more rapid cooling than for large clasts

PR: We agree, *smaller clast size favors a high cooling rate (e.g. Loyd et al., 2013).* Despite of this observation that concern a smal group of MIs, we prefer not focusing on PEC diffusion process, which is not the main objective of this study.

Section Discussion References: Giordano et al. (2008); Putirka et al. (2008); Boschetty et al. (2020); Marziano and Whitam (2012), Lohmar et al., 2008, Inamans (1952)

PR: Now these citation-references are added in reference list. Marziano et al. (2012) as Witham et al. (2012) citations are corrected. Lohmar, 2008 (thesis work) and Inman (1952) also corrected and considered in reference list. The references from figure 7 are not considered in manuscript and Appendix.

Notes on Figures:

Figure 2: Add symbology for PEC-MI (circles)

PR: Rephrased to "Figure 2 – Major element compositions. The post entrapment-corrected MIs (colored circles) with their major element contents as a function of SiO_2 wt.% (see corrected dataset in Appendix I). The bulk rock analyses are shown by colored squares for each series. "

Figure 3: there is no "a)"

PR: Ok, now "a)" added

Figure 6: kb/km should be the inverse

PR: Agreed

Abstract

Villarrica volcano, in the southern Andes, is a composite mafic volcano whose persistent open-vent activity is punctuated by frequent Strombolian/Hawaiian eruptions and, more rarely, by more energetic (sub-Plinian) events. Here, we investigate the volatile composition of the parental melts that sustain this activity, and the conditions of pre-eruptive magma storage, by characterizing the composition of olivine-hosted melt and fluid inclusions. We concentrate on inclusions entrapped in minerals from pyroclastic materials erupted from both Villarrica summit and from its flank Minor Eruptive Centers (MECs) post the 14.5-13.5 kyr caldera collapse event that formed the Licán ignimbrite. Our micro-FTIR and SIMS measurements indicate that the Pucón eruption records the highest volatile contents, with 6.0 wt.% H_2O, >1500 ppm CO_2, 1330 ppm S, 1556 ppm Cl, and 2055 ppm F. These volatile contents imply a volatile-saturated magma originating from a depth of 14.4 to 17 km below Villarrica. Results for other flank eruptions highlight a similarly deep (17–21 km depth) source for basaltic CO_2-rich mafic magmas erupted at regional MECs (Los Nevados, Caburgua). Melt inclusion results also reveal that deep rising mafic magma batches, when temporarily stored at 1–5 km depth, produce the more differentiated and degassed magma batches that sustain the decadal-old persistent effusive-explosive eruptive activity at Villarrica. Helium isotope ratios ($^3He/^4He$; Rc/Ra when corrected for atmosphere) measured in bulk noble gases from olivines ($Fo_{75–88}$) indicate that the parental magmatic fluid signature (Rc/Ra = 6.7–7.6; $CO_2/^3He$ = 4.7–7.5E^{+08}) is only recorded during central paroxysmal subplinian eruption, and that this primitive gas signal is diluted in lateral MECs (Rc/Ra<6.5; $CO_2/^3He$ = 1.4x10^{+9}–3.1x10^{+10}).

Keywords

Composite volcano, Mafic magma, Melt inclusions, Noble gas, Eruptive Paroxysm

Highlights

- Pucón Ignimbrite represent Villarrica postglacial primitive mafic magma.
- Polygenetic eruptive vents source >17 km depth CO_2-rich volatile melts.
- Villarrica and lateral vent degas mafic magma at < 5km storage depths.
- Shallow atmospheric and mixed crustal ^{4}He in volcanic arc fluids.
- Sublplinian paroxysm preserve MORB-like ^{3}He/^{4}He fluid ratios.

1. Introduction

Villarrica, located at 39°24'S and 71°55'W (Fig. 1a), is one of the few composite volcanoes worldwide hosting an active lava lake (e.g., Witter et al., 2004; Moussallam et al, 2016, 2023). The volcano, one of the most active of the Southern Andes Volcanic Zone (SVZ) that formed as a consequence of the subduction of the 12–20 My-old Nazca plate beneath the South American plate (Jarrard, 1986; Stern, 2004), typically produces Strombolian/Hawaiian volcanic activity at its central (summit) vent. However, geological evidence also exists for more energetic Vulcanian to sub-Plinian eruptions (Silva et al., 2010; Costantini et al., 2011; Lohmar et al., 2012) and for mafic ignimbrite-forming eruptions (Moreno and Clavero, 2006), as observed elsewhere as a consequence of fast ascent, decompressional degassing, and fragmentation of basaltic magma (Moitra et al., 2018; Stix, 2007; Heinrich et al., 2020). Postglacial volcano stratigraphy also indicates frequent outbursts of voluminous lava flows accompanied by small explosive eruptions, resulting in the formation of spreading clusters of minor eruptive centers (MECs) (Moreno and Clavero, 2006). Examples of these volcanic centers are Caburgua-Huelemolle Small Eruptive Centers (CHSEC), located in the southern sector of lake Caburgua, a few kilometers northeast of the Villarrica stratovolcano, and the small eruptive centers on Villarrica flank itself (McGee et al., 2017). As seen at other mafic volcanoes worldwide (Smith and Németh, 2017; Robidoux et al., 2020), MECs can allow characterizing magma transport from the volcanic edifice towards its peripheries.

Stratigraphic mapping at Villarrica over the last few decades has led to an improved model of the eruptive sequence (Moreno and Clavero 2006) as monitoring and risk management programs (Muñoz et al., 2024). However, understanding how magma origin, evolve and eruptive properties control the switch between such different activity styles at Villarrica (Moreno and Clavero, 2006) requires a thorough examination of pre-eruptive magma conditions since volatiles are especially key factors in controlling eruptive style and explosivity at basaltic volcanoes (Cashman et al. 2017), and the study of melt inclusions (MIs; e.g., Wallace et al., 2021) hosted in mafic phenocrysts from volcanic rocks is especially suitable for investigating pre-eruptive conditions. Hence, our attempt here is to characterize the magmatic plumbing system that sustains the variety of eruption styles at Villarrica by studying the pre-eruptive volatile contents in the source parental magmas of both central and peripheral volcanic centers. Our aim, in particular, is to determine whether magmas erupted at the post-glacial regional edifices (MECs), and at the flank volcanic centers that formed within the current 2 km-wide caldera (Villarrica Unit 3, <~ 3.7 Kyr AP; Moreno and Clavero, 2006), share the same characteristics (same volatile content) as those erupted at the volcano summit. We complement this analysis of Villarrica pre-eruptive magma conditions (from melt inclusion major volatile contents) with the determination of volatile chemistry and isotope compositions (noble gases) in fluid inclusions (Fis), in the attempt to characterize the magmatic fluid source.

2. Tectonic context and post glacial magmatic volatile background

Villarrica is part of the oblique Villarrica-Quetrupillán-Lanín chain in front of the Southern Volcanic Zone (SVZ). It is bounded by the Juan Fernandez Ridge at its northern edge (~33°S) and the Chile Rise to the south (~46°S) (Fig. 1 a). Volcanism in the Andes is the result of the subduction of the Nazca (10–60 My old) and Antarctic oceanic plates (<12–24 My old) beneath the South American continental plate (Stern, 2004), which is moving obliquely (20–30°) to the NE a rate of 7–9 cm/yr (DeMets, 2001). The basement beneath the Pleistocene-to-Holocene SVZ stratovolcanoes consists of continental crust which is ~ 35–60 km in thickness, above a shallowly dipping (< 25°) Benioff zone (Tassara and Echaurren, 2012). Where the mantle wedge is less well developed (~ 50 km thick), the overlying crust is much younger, with Paleozoic pre-Andean basement and Mesozoic-Cenozoic igneous rocks (Stern, 2004). Within the tectonic context, Villarrica has undergone eruptions of magma evolving at shallow crustal depths, sourced from > 45 km depth in the MOHO-lithospheric mantle (Tassara and Echaurren, 2012; Hickey-Vargas et al., 2016).

Villarrica volcano is close to densely populated urban and tourist areas, and has persistent degassing (e.g., Moussallam et al., 2016; Liu et al., 2019) and frequent effusive and explosive activity (Costantini et al., 2011). Petrological studies and the interpretation of seismic and geodetic data indicate a wide range of pre-eruptive magma storage conditions, in the range of 1.5–8 km in depth (Lohmar et al. 2012; Delgado et al., 2017; Lehr et al., 2022), considering volatile saturation conditions farther below ~12 km depth (Cortés et al., 2024). Pressures conditions determined with crystallization geothermobarometric methods delivered 0.9–3.5 kb values using augite-melt pair (Cortés et al., 2024) and may reach > 7 kb with olivine-augite pair models to represent post-1971 actual crater conditions (Boschetty et al., 2022) (8.1±1.7 kb; Morgado et al., 2015). According to mineral-liquid geothermobarometry, the last Strombolian paroxysm, characterized by lava fountaining, may have been sourced from magma stored at conditions of 0.2–3.5 kb pressure range and a temperature around ~1140 °C (Romero et al., 2022, Moussallam et al., 2023). Farther beyond Villarrica flank and regional MEC such as CHSEC, between 10.8 and 11.4 1.7 kb were measured in Caburgua according to olivine-augite phenocrysts (Morgado et al., 2015). Since Caburgua have been classified between 8,6 and 6, Kyr AP according to stratigraphic relationship with Villarrica Unit 2 (Moreno and Clavero, 2006), Caburgua cone could exceed the age of Pucón ignimbrite, but younger than Licán Ignimbrite.

Three major evolutionary steps define the construction and collapse of Villarrica stratovolcano, with respect to past deglaciation ages (Moreno and Clavero, 2006; Watt et al., 2013). The occurrence of major VEI events has been identified from volcano stratigraphy and ^{14}C geochronology, from the oldest identified intra-glacial Pyroclastic Deposit of 40–14 ky to several post-glacial to Holocene events (Moreno and Clavero, 2006). The history associated with the development of the stratovolcano is divided into Villarrica units 1, 2, and 3. We focus here on Unit 3 of Villarrica because it represents the series of volcanic layers that cover the current structure of Caldera 2 (Fig. 1b; Moreno and Clavero, 2006), which formed after the 14.5–13.5 ky BP (^{14}C date) Licán ignimbrite and reached a minimum depth of 1.5 km (6.8 kb) and marked the end of a major volcanic cycle at Villarrica (Lohmar et al., 2012).

At central crater, so far 5 eruptive events, Pucón Ignimbrite, Chaimilla (Pioli et al., 2015), 1971, 1984 and 2015 have been studied to quantify S and Cl contents in MIs by electron microprobe. These studies report maximum contents of 1230 ppm S and 963 ppm Cl (Pioli et al., 2015; Cortés et al., 2024; Mason et al., 2024). In sequences from Chaimilla fallout, the 1971 to 2000s tephra series, H_2O and CO_2 were determined by Fourier Transform Infrared Microspectrometry (FTIR) technique used and the following maximums values were determined; 2.7 wt.% and 500 ppm, respectively (Pioli et al., 2015; Cortés et al., 2024). Elsewhere on NE Villarrica flanks, in the Los Nevados sector (Gr. 2), the H_2O and CO_2 contents have reached values up to 3.0 wt.% and 1586 ppm, respectively (Robidoux et al., 2021).

3. **Methodology**

3.1 Global Strategy

The method proposed here to investigate pre-eruptive conditions is based on the study of MIs hosted in mafic phenocrysts from volcanic rocks. The idea behind this approach is to characterize the chemistry of the magmatic fluids associated with eruptive products coming from a deeper source in the volcano-magmatic plumbing system of the whole Villarrica complex. Specifically, to study the "magmatic volatile" content at saturated conditions, this study relies on the MIs which represent, at a given pressure and temperature, trapped silicate melt, with in some cases, magmatic fluids produced and exsolved during igneous processes. Those fluids are assumed to be the source of volatile elements (H_2O, CO_2, S, Cl, F; e.g. Wallace et al., 2021) and for this reason, the term "magmatic fluids" here refers to the exsolved gases that moves through magmatic conduits to the surface.

It is possible to trace the origin of the magmatic fluids by measuring the specific noble gas isotopic $^3He/^4He$ ratio of fluid inclusions (FIs) in olivine phenocrysts, at the time of eruption (e.g. Hilton et al., 2002). For example, previous authors showed that $^3He/^4He$ measurements in olivine-hosted FIs from the 2015 Villarica eruption have an isotopic signature as high as 6.7 Ra (Lages et al., 2021b). This is still lower than the typical homogeneous Andean signature in the mantle along the South American Arc of 8–9 Ra

(Lages et al., 2021a,b). Even though, uncertainties exist on local cause behind variation on isotopic helium variations at this volcano (Lages et al., 2021a). To explore further on this issue, we investigate $^3He/^4He$ variations in olivine-hosted FIs from magma batches generated within the post-glacial eruptive period at Villarrica. This latter implies sampling additional regional MECs and several pyroclastic deposits pertaining to central crater explosive paroxysm that were supplied by mafic magmas.

3.2 Petrologic Approach

The major eruptive events have been studied through a series of n = 15 volcanic rock units sampled from Villarrica and the MECs (Table 1). The most well-documented explosive mafic eruptions at Villarrica were selected because they were produced chronologically after the Licán ignimbrite, so that we can focus on the syn- to postglacial context of the actual Villarrica edifice. The list of samples and analytical methods is given in Tables 1 and 2, with full details of the methodology given in Appendix A “Supplementary Material Methodology Review” as result tables in Appendix B (Tables A.1 to A.10).

To obtain preserved volcanic rock products, volcanic deposits known from literature were systematically sampled between 2017 and 2022 on Villarrica flanks (Fig. 1), targeting juvenile pyroclasts representing rapid cooling rates to best preserve original fluids and volatile compositions from melt as fluid inclusions (MIs and FIs) (Lloyd et al., 2013; Wallace et al., 2021). Total grain size distributions (TGSDs) of entire fall deposits are examined to confirm the fragmentation processes associated with sampled outcrop pyroclast deposits known from the literature in order for name assignation of pyroclastic flow deposits, surge and fallout deposits (details in Appendix A). Olivine-hosted MIs are carefully exposed by polishing single crystals (see details of analytical methods in Appendix A; e.g. Rose-Koga et al., 2021). Special attention was given to the diversity of naturally quenched and preserved MI textural groups (Roedder, 1984) and textural statistics on MI typologies (Robidoux et al., 2018). Quantitative parameters related to post-entrapment crystallization (PEC) are reported in Table 3 and Appendix B and the PEC correction procedure is detailed in Appendix A.

3.2.1 Bulk rock chemistry of sampled volcanic pyroclasts

Bulk rock chemistry was carried out to compare with literature compositional ranges of magmas. n = 26 bulk rock samples are analysed by inductively coupled (IC) plasma mass spectrometry (PMS) as plasma-optical emission spectroscopy (POES). The methods determine the major, trace and rare earth element compositions of the collected samples (Table 2, A.1, A.2). Powders are prepared at the U. Mayor, Escuela de Geologia using a sample pulveriser and sent to a private laboratory for analysis (ActLabs, Canada). The standards, duplicates and blanks accuracy are detailed in Appendix C for the following analysis: major/trace elements fusion ICPOES/ICPMS, fluorine titration for FeO content and H_2O content by gravimetry.

3.2.2 Electron microprobe analysis (EMPA)

To provide the chemistry of the major elements from pre-eruptive magmatic processes, the selected MIs were measured with n = 163 electron microprobe analysis (EMPA) in mineral samples as for the glass inclusions they host (Table 2, A.1). The surfaces were probed with an electron microprobe analyser (EMPA), model JXA-8200 (JEOL), equipped with five wavelength dispersive X-ray spectrometers and one energy dispersive X-ray spectrometer analyser, at the HPHT (high pressure/high temperature) laboratory of the Istituto Nazionale di Geofisica e Vulcanologia (INGV) in Rome (see technical conditions in Robidoux et al., 2021).

3.2.3 Volatile element contents of glass inclusions

Volatile element contents (H_2O, CO_2, Cl, F, S) in glassy MIs, embayments and matrix glasses were determined using a Cameca IMS 1280 ion microprobe at the CRPG-CNRS-Nancy. The smallest range of MIs sizes (2-100 µm) was selected for SIMS (Table A.3), and a total of n = 57 MIs were measured to allow double calibration of CO_2 and H_2O, on the smallest MIs measured by microFTIR (here using abbreviation FTIR for consistency) (Table 1, Table A.1, A.5-A.7); a total of n = 37 inclusion duplicates were obtained by both SIMS and FTIR to fit for correlation tests (Table A.7), while n = 167 MIs FTIR analyses were performed on the total set of inclusions.

SIMS concentrations were determined using calibration curves (Fig. A.1). Maximum errors, based on reproducibility over 10 cycles of analyses, were less than 15% for CO_2, 3% for Cl, 4% for S, and 5% for H_2O and F. The FTIR technique, in comparison, determines the content of water and carbon species according to the Beer-Lambert law, following the same procedure for data treatment as Robidoux et al. (2021). The parameters of the volatile element content calculations are described in detail in Appendix A.

3.2.4 Correction for CO_2 contents and solubility models

Due to the need to account for the shrinkage bubble for the CO_2 content estimation (e.g. Rasmussen et al., 2020), the Raman microspectrometer was used for the measurement of CO2 in 25 bubbles (diameter 2 to 20 µm) of 25 unexposed MIs. The instrument is the Horiba Jobin Yvon high-resolution HR800 LABRAM of the Interdepartmental Center 'G. Scansetti' (Dipartimento di Scienze della Terra, University of Torino). The excitation source was a 532 nm green laser, with power at the emission source of 100 mW (e.g. Robidoux et al., 2017, 2018). The analyses were performed with a confocal setup, with the resulting spot size, calibration and spectral treatment (e.g. Frezzotti et al., 2012), being the same procedure as in Robidoux et al. (2018). The CO_2 bubble contents have been calculated starting from the Fermi diad split. The CO_2 Raman spectrum is characterized by two intensity peaks at ~1285 and ~1380 cm^{-1}, defined as Fermi diad peaks; in melt and fluid inclusions, the Fermi diad split is proportional to the fluid density inside the bubble (Esposito et al., 2011; Frezzotti et al., 2012; Remigi et al., 2021). The chosen densimeter is able to accommodate a large range of Fermi diad space (102,65 – 105,47 cm^{-1}) that fit the polynomial equation from the previous authors and the used instrumental setting (Robidoux et al., 2018). The MIs not corrected for CO_2 content (no shrinkage bubbles) are used in solubility model from Iacono-Marziano et al. (2012) to calculate isobars, degassing curves and calculate saturation depths. The selected MIs corrected for CO_2 contents (µRaman or alternative model Mimic from Rasmussen et al., 2020) are treated with the same criteria. The degassing curve models are proposed as second alternative to minimum saturation pressure conditions.

3.2.5 Bulk analysis of isotopic noble gases

To explore the source and spatial distribution of magmatic fluids and volatiles, eleven isotopic analyses of He-Ne-Ar were carried out in fluid inclusions (FIs) trapped in olivine crystals from the Villarica volcanic system at the laboratory of INGV, Sezione di Palermo (Italy). These measurements were combined with three other samples previously studied by Lages et al. (2021b), which are part of the same suite of samples. Those FIs occur within pyroclasts of mafic composition for each investigated eruptive event, and the whole-rock composition was also analyzed (Table 2, Table A.2). Approximately 0.1–1.2 g of unaltered crystals were hand-picked for noble gas analysis. After cleaning in an ultrasonic bath under nitric acid, acetone and deionised water, the crystals were loaded into a single-stage crusher and then baked under pumping to achieve ultra-high vacuum conditions. After crushing, the gas mixture released from the opening of the fluid inclusions was purified in a preparation system capable of separating noble gases from the main components, and then further separating helium from neon from argon (see Rizzo et al., 2018, 2022, Lages et al., 2021a, 2021b for further details).

Two distinct split-flight-tube mass spectrometers (Helix SFT-Thermo) were used to measure the isotopes of helium (^3He and ^4He) and ^{20}Ne, independently. The $^3He/^4He$ ratios are stated in Rc/Ra units, where Ra represents the $^3He/^4He$ of atmospheric air, which is 1.39 × 10^{-6}. The analytical error for the ^{20}Ne (1σ) was <0.8%. The He-isotope ratio measurements had an uncertainty (1σ) of less than 6%. According to Rizzo et al. (2018), the ^{20}Ne has been corrected for isobaric interferences at m/z values of 20 ($^{40}Ar^{2+}$). A multicollector mass spectrometer (GVI Argus) was used to measure the stable argon isotopes (^{36}Ar, ^{38}Ar, and ^{40}Ar) with an analytical uncertainty of $^{40}Ar/^{36}Ar$ < 0.2%. For the elemental and isotopic recalculations of He, Ne, and Ar, a pre-purified air standard separated into tanks was utilized. The standards for ^{4}He, $^{3}He/^{4}He$, ^{20}Ne and ^{40}Ar had analytical reproducibilities of less than 2.4%, 2.6%, 2.5% and 2.4%, respectively, over a period of >1 year for He and Ne and ~ 4 years for Ar. For He, Ne, and Ar, the typical blanks were at least two orders of magnitude lower than samples and standard signals. Additional information regarding sample preparation and analytical techniques can be found in Rizzo et al. (2018, 2022) and Lages et al. (2021a, 2021b).

Helium isotopic ratios are expressed as Rc/Ra, where Rc is the air-corrected $^{3}He/^{4}He$ ratio of the sample, determined using the $^{4}He/^{20}Ne$ ratios. The Rc/Ra value is equal to:

$[(R_m/R_a)(He/Ne)_m - (He/Ne)_{air}]/[(He/Ne)_m - (He/Ne)_{air}]$, where "m" and "air" denote air and measured values, respectively.

Because the argon concentration in the atmosphere is much higher than in magmatic fluid inclusions, it was necessary to make a correction, which assumes that all of the ^{36}Ar in the gas phase is atmospheric in origin. Thus, in the samples with $^{40}Ar/^{36}Ar$>300, the ^{40}Ar concentration can be corrected as follows:

$^{40}Ar^* = {}^{40}Arm-[(^{40}Ar/^{36}Ar)air \times {}^{36}Arm]$, where m is the measured value and $^{40}Ar^*$ is the corrected isotope value.

4. Results

4.1 Pyroclastic deposit classification and fragment size distribution

Sample collection and preparation for the study of volatiles in glassy inclusions (e.g. Lloyd et al., 2013) and olivine separation for bulk isotopic noble gas analyses (Robidoux et al., 2021) were carried out to select material below lapilli size granulometry. Both the pyroclasts of this size and the olivine mineral inclusions will have cooled rapidly, providing ideal trapping conditions for the inclusion in the host mineral and avoiding significant loss of H_2O due to H+ diffusion (Gaetani et al., 2012). The study covers all the pyroclastic deposits in both the monogenetic center, MECs and the adjacent Villarrica stratovolcano. At each site, ~5,000 grams of sample were sieved in the laboratory to retrieve the granulometric parameter and compare it with datasets in the literature from Silva et al. (2010).

The full description of the samples is resumed by 3 undergraduate theses at Universidad Mayor (Santiago, Chile) and summarized in Table 1, where key statistical parameters for the distribution are the median Mdφ (50), then the graphical standard deviation σ (φ). The comparison with datasets from Silva et al. (2010) classification fields confirm volcanostratigraphy assignations (details in Appendix A). To compare the different volcanic deposits, the median weight was calculated for grain size distribution in pyroclastic flow deposits, surge, and fallout deposits (Table 1, and Appendix A). The Pucón ignimbrite data represents the initial fall deposit (TVP10E; Md = -1.547; σ = 1.449) and matches the onset of the “Pb” eruptive phase of the Pucón ignimbrite (Moreno & Clavero, 2006), preceding the ignimbrite pyroclastic flow sequence (P1, P2; Silva, 2010, and references therein). The extreme end member for well-sorted and small fragments is associated with the Chaimilla and Caburgua fallout deposits (TVP06 series; Md = -0.97 to 1.1; σ = -2.1 to -1.41). Los Nevados, Chaillupén and the March 2015 Villarrica volcanic episode all fall below -2 and -6 Mdφ (50), due to the sampling collection of single lapilli- to bomb-sized fragments.

4.2 Bulk rock geochemistry

The major element compositions of the bulk rock samples are presented in Table A.2. The rocks are classified within the CA and HK-CA series fields (Fig. 2a), according to Peccerillo and Taylor (1976) diagram classification as for distinguishing sodium from potassium enrichment between bulk rock and MI datasets. The Villarrica samples are heterogeneous at Pucón, ranging from basaltic to andesitic (SiO_2=52.1–61.9 wt.%, K_2O=0.52–1.47 wt.%, MgO=2.52–4.84 wt.%), homogeneous at Chaimilla (SiO_2=~53.1 wt.%, K_2O=0.57–0.61 wt.%, MgO=3.9–4.0 wt.%), and overlapping in SiO_2 concentration with the lava fountain scoria composition from 2015 (SiO_2=~53.1 wt.%, K_2O=0.77–0.86 wt.%, MgO=5.31–5.56 wt.%). The range of bulk rock compositions for MEC is restricted to basaltic andesites at Los Nevados (SiO_2=52.3–55.1 wt.%, K_2O=0.67–1.02 wt.%, MgO=4.10–4.47 wt.%) and Chaillupén (SiO_2=53.5–54.5 wt.%, K_2O=0.77–0.84 wt.%, MgO=4.84–5.07 wt.%), but strictly basaltic at Caburgua (SiO_2=50.8–51.9 wt.%, K_2O=0.67–0.75 wt.%, MgO=6.87–6.97 wt.%).

The trace element compositions of the Villarrica rocks show a slight enrichment in light rare earth elements (LREEs), compared to the moderate and heavy rare earth elements, typical of MORB (Appendix C; Hickey-Vargas et al., 2016). The rocks are slightly enriched in large-ion lithophile elements (e.g., Cs, Rb, Sr, and Ba) relative to N-MORB, but overlap with E-MORB. Most samples have low contents of the high field strength elements (HFSE) Ta, Nb, Zr, and Hf. A detailed systematic use of slab-fluid ratios is resumed in Table A.2 as calculated geochemical ratios (Robidoux et al., 2020).

4.3 Olivine texture, chemistry, and MI description

The olivine crystals from each eruptive event were grouped and characterized for its dominant MI textures (Table A.3). In this study, olivine hosted MI are referred to as "MI populations" when they are derived from the same layer of a volcanic deposit. The percentage variations of the MI typologies (Robidoux et al., 2018) are classified according to the "cooling rate-dependent" textural description of MI typologies of Roedder (1984). Olivine crystals with no MIs are assigned to “G1”, then the MI typologies are coded, e.g. starting with homogeneous glassy MI assigned to "G2", MI with bubbles to “G3”, and MI with bubbles and oxides to “G4”.

The “G2” group is particularly variable in the Pucón products and reaches the highest percentages in the P2 sequence (>35%). The percentage of olivine crystals with preserved “primary MIs” (G2+G3+G4) also follows a certain order in term of the amount of olivine crystals in each volcanic deposit (considering that all the MI typologies are subject to PEC); from Pucón Ignimbrite, Chaimilla to the March 2015 eruption, the amount of olivine crystals with primary MIs (G2+G3+G4) decreases, so does the percentage of olivine crystals with vapor bubbles (G3+G4).

Olivine Mg# are listed in Table A.4. At the central eruptive vent of Villarrica, the Pucón olivine crystals are Mg-rich ($Fo_{76–88}$), and those from the 2015 eruption have the lowest Fo content (Fo_{76}), although fewer samples were analyzed, which could introduce a sampling bias. The Chaimilla olivine crystals are relatively heterogeneous in composition ($Fo_{76–85}$, Fo_{80}±3%). The MECs show slightly less Mg-rich olivine crystals compared to Villarrica ($Fo_{73–86}$). Los Nevados olivine crystals are heterogeneous in composition ($Fo_{75–85}$, Fo_{80}±3%), Chaillupén has olivine crystals with high Mg# ($Fo_{84–86}$, Fo_{84}±1%), and lastly the Caburgua olivine crystals have heterogeneous Mg# ($Fo_{73–84}$, Fo_{80}±4%).

4.4 Major element content from glass inclusions

The inclusions shown in Figure 2 have been corrected for post-inclusion crystallisation of the corresponding phenocryst-host according to the method of Robidoux et al. (2021), following the method of Danyushevsky and Plechov, using the Petrolog 3 program (Danyushevsky, L. V., & Plechov, 2011). This data treatment considers the diffusive exchange of FeO and MgO along the walls of the inclusion and the olivine host, and then the loss of Fe from the inclusion into the olivine host. Recalculated compositions from MIs in samples are given in Table A.8 for the corresponding olivine host crystals.

The corrected MI compositions (Fig. 2; Appendix A) required in 94 samples a range of 0.6–43.5 and average 15.7% olivine to be added. The Fe-loss implied adding a range of 0.3–3.4 and average of 2.1 wt% FeOT. The total iron content assumes that Fe2+ = ΣFe, the best-fit FeOT/MgO regression line was used at each group of volcanic centres, ranging with modelled bulk rock iron species ratios with Fe2+/Fe3+ = 1.1–4.1.

The MIs from the Pucón ignimbrite were classified as basaltic to basaltic andesites and a few andesites were observed (SiO_2 = 47.3–62.8 wt.% and K_2O=0.19–1.60 wt.%); data plot in the field from calc-alkaline (CA) to high potassium calc-alkaline (HKCA) rocks (Fig. 2). The Chaimilla series is slightly richer in K_2O (0.20–1.67 wt.%), and olivine-hosted MIs were mostly classified as basaltic andesites, whereas MIs from the 2015 eruption were basaltic-andesites, with lower K_2O contents (0.78–0.91 wt.%).

The total MIs reported by Robidoux et al. (2021), regardless of the specific eruptive center (Gr. 1, 2), were more differentiated in the Los Nevados MEC (47.6–58.0 wt.% SiO_2; 0.27–1.21 wt.% K_2O), with Chaillupén ballistics representing the most felsic MIs (57.1–59.0 wt.%; 0.93–1.35 wt.% K_2O). Caburgua represents intermediate differentiated MIs (51.1–59.3 wt.% SiO_2), but the alkaline content is highest in these samples (0.62–1.78 wt.% K_2O).

4.5 MI description and MI volatile concentrations

The water and carbon dioxide contents of the MIs are reported (FTIR in Table A.5, SIMS in Table A.6, reproductibility test in Table A.7). Of the 167 samples analyzed by FTIR, 37 were measured by SIMS with no loss or damage during transfer to an indium mount. The difference in water concentration between FTIR and SIMS averages 0.5% and 89 ppm for CO_2 content.

In terms of H_2O and CO_2 concentrations from the central eruptive vent of Villarrica (Table 1, Tables A.5-A.6), the Pucón ignimbrite series records the highest H_2O-CO_2 concentrations (0.1–6.0 wt%; 9–1485 ppm, respectively), followed by the Chaimilla series (0.2–2.4 wt.%; 16–337 ppm; similar to Pioli et al., 2015) and the 2015 eruption (0.1–0.8 wt.%; 160–307 ppm). In the MECs, high values are found for the Los Nevados series (0.1–3.4 wt%; 30–1568 ppm; see also Robidoux et al., 2021), and lower values in the Chaillupén series (0.3–3.6 wt%; 29–329 ppm), and in the Caburgua series (0.6–2.8 wt%; 139–677 ppm).

The S, Cl and F concentrations at the Villarrica center (Pucón ignimbrite, Chaimilla and 2015 eruptions) are highly variable (Appendix I) with the following ranges 103–2055 ppm, 11–1330 ppm and, 81–1556 ppm, respectively. The contents of S, Cl, F from MEC samples have the following ranges: 41–2581 ppm, 13–2356 ppm and 59–2473 ppm, respectively (Table A.8).

4.6 Raman-corrected CO_2 contents

Twenty-five MIs with shrinkage bubble (1.3–10.1 vol.%) were analyzed by Raman micro-spectroscopy in order to calculate their CO_2 bubble contents starting from their CO_2 density (see Methodology). In the studied shrinkage bubbles, the measured density varies between 0.004 and 0.911 g/cm^3 (Table A.9). The calculated (mass / glass density x volume) total CO_2 concentrations (in glass inclusions + bubbles) range between 207–3336 ppm, using the approach described in Robidoux et al. (2018). Since no heating experiment was performed on the naturally quenched MIs of this study, the calculated CO_2 contents are compared with the contents obtained by the experimental and computational model "Mimic" of Rasmussen et al. (2020). For this reason, n = 31 shrinkage bubbles were selected from our MIs measured by EMPA and, according to the model "Mimic", they resulted into correction on the total CO_2 concentrations to 54–3529 ppm. These values exceed the original (uncorrected) shrinkage bubble equivalent glass inclusion CO_2 contents of 24–1413 ppm (Table A.8).

4.7 Noble gas isotopes in fluid inclusions

The analytical results of elemental and isotopic measurements of helium, neon and argon, together with other complementary information, are reported in Appendix K. The ^{4}He and ^{20}Ne concentrations measured in FIs from olivine crystals of scoria and ash samples varied from 2.8 × 10^{-14} to 1.6 × 10^{-13} mol/g (Fig. 3) and from 1.7 × 10^{-15} to 1.7 × 10^{-14} mol/g, respectively. The ^{4}He/^{20}Ne ratio was 3.9–42.9, compared to the atmospheric ^{4}He/^{20}Ne of 0.318 from Porcelli et al. (2002). The concentrations of ^{40}Ar, ^{38}Ar, and ^{36}Ar ranged from 1.5 × 10^{-13} to 1.5 × 10^{-12} mol/g, from 8.9 × 10^{-17} to 8.8 × 10^{-16} mol/g and from 4.9 × 10^{-16} to 5.0 × 10^{-15} mol/g, respectively. The ^{40}Ar/^{36}Ar ratio varied in the range 300–336, whereas the theoretical ratio in the atmospheric is ^{40}Ar/^{36}Ar~296 (Porcelli et al., 2002). Both ^{40}Ar/^{36}Ar and ^{4}He/^{20}Ne indicate that all the gases released by the FIs contain an atmospheric component mixed with the magmatic one. The concentrations of ^{40}Ar* vary from 2.6 × 10^{-15} to 1.1 × 10^{-13} mol/g. The ^{4}He/^{40}Ar* varies from 1.4 to 10.5, with the typical mantle ratio being considered to be in the range of 1–5 (Marty, 2012).

The ^{3}He/^{4}He ratios corrected for atmospheric contamination (expressed as Rc/Ra values) vary between 4.0 and 7.6 Ra (Fig. 3; Table A.10), with a bias with uncorrected ^{3}He/^{4}He ratios generally ≤0.2 Ra, except for the sample HCH-2AS that showed a bias of 0.4 Ra.

5. Discussion

5.1 Mafic magmas degas and transit from deep to shallow volatile saturation levels

At Villarrica, the Pucón ingimbrite is the oldest and best studied postglacial eruption. It is the richest in volatile element contents, but also contains MIs the least affected by post-entrapment crystallization (PEC; Table 3). This section discusses melt inclusion volatile loss between two large sets of pre-eruptive conditions that chronologically describe Villarrica mafic magmas from the Pucón Ignimbrite (~3.7 kyr) to decadal old central crater conditions.

Before extending to discriminate degassing effects and calculating saturation pressures for the different eruptive centers (section 5.2), we first highlight the precision and accuracy of the volatile element contents produced consistent calibration curves using SIMS (Fig. A.1), and the reproducibility of FTIR vs. SIMS gave comparable results (Fig. A.2; Table A.7), although the FTIR technique is limited to larger MIs (>30 µm; Appendix A). The SIMS divergence from 1:1 water line in figure A.2 is mainly due to the precision for smaller MI. The carbon dioxide 1:1 line shifts are greater when MIs contain shrinkage bubbles (Fig. A.2), highlighting the advantages of using smaller beam diameters with the SIMS technique over glass inclusions holding vapor bubble. To estimate minimum saturation pressures, the volatile element contents and major element compositions of the MIs are then integrated into the solubility model from Iacono-Marziano et al. (2012) and Witham et al. (2012) (Figs. 4, 6). Despite H_2O-CO_2 pairs being the focus of this study, the sulfur and halogen (Cl, F) contents remained constant from the start to finish of the Pucón eruption, as well as the subsequent paroxysmal explosions at Villarrica crater (Fig. 4; Appendix A, Table A.8).

Overall integrating observations on MI compositions and olivine hosts, Pucón series contains the most primitive olivine crystals (with Fo content between 76,3 and 88,8 %; Table A.4) and MIs record the highest volatile contents (Fig. 4; Table A.4-A.7). Chaimilla's MI volatile element contents are systematically lower than those of the Pucón ignimbrite MI for similar major element chemistry and cogenetic parental melt differentiation (Figs. 2, 4; Table A.8), while for the 2015 eruption, MI volatile element contents are even lower, representing both strong pre-eruptive degassed melts, and potential post-entrapment effects accentuated by low cooling rates of the transported magmas (Fig. 4). Considering such compositional differences attributed to pre-eruptive conditions, we argue that pre-entrapment degassing is not the only cause of volatile variation in our olivine-hosted MI collection. For example, shallow melt CO_2 saturation may lead to potential gas migration into volatile CO_2-rich transport (Aiuppa et al., 2017), which persists during lava lake bubbling mechanisms (Moussalam et al., 2016). The identified shallow storage conditions may also accentuate lower magma cooling rates and melt differentiation. Such effect is reflected by some lower trapping/ quenching MI temperatures and differentiated MIs series (Chaillupén series; Fig. 2, 5) revealed here with PEC treatment (Appendix A; e.g. Giordano et al., 2008) in MI with low water contents ~<1.5 wt.% (Fig. 5; e.g. Lloyd et al., 2013; Robidoux et al., 2021). Therefore, for some olivine the low MI-trapping temperatures at shallow surface is expected to favor H^+ diffusion because the low quenching rates affect the solidification of MIs and accentuate the water glass/crystal diffusion (Fig. 5; Table 3; e.g. Massare et al., 2002; Gaetani et al., 2012).

Taking into account the temporal variation of volatile contents through mafic magmatic events at Villarrica, we observe a temporal transition in the pre-eruptive minimum saturation pressure conditions at Villarrica during paroxysmal inner crater eruptions (Fig. 5a). As a result, major subdivisions in the Pucón sequence of "Pb" and "P1 to P3" (Silva et al., 2010) represent individually different equilibrium pressure ranges, suggesting a polybaric system that may have transported several masses of ascending magmas. The minimum saturation pressure values were higher during climax of the sub Plinian activity, 4.6±1.6 down to 0.020±0.006 kb while the opening of the eruptive sequence (Pb) represents decompression of volatiles for minimum saturation pressures from 2.15±0.47 to 0.68±0.26 kb (violent strombolian; Table A.8). These pressures are thus traduced in lithostatic depths, resulting among these subsequent batches of Pucón magmas to 2.5–7.9±0.63 km (1SD). When the first magma batch reached the surface as the "Pb" opening sequence, it consisted of hot, volatile-element saturated melts (1070–1140 °C). This phase has been described as evolving from a strombolian to a more explosive sub Plinian eruptive style (Moreno and Clavero, 2006), and our new dataset shows that it was relatively water-rich (<3.6 wt%) and CO_2-rich (1485 ppm corresponding lithostatic depths of 16.6±5.9 km, 1SD) (Figs. 4, 5). This study shows that the last Pucón event (P3) finally recorded ~>1200 ppm CO_2 and a maximum water content of 6.0 wt.%, which is higher than the previous 4.65 wt.% water content estimated with the thermobarometric model by Boschetty et al. (2022) (Figs. 4, 5, 6).

The subsequent explosive events to the present day at Villarrica Central Crater may also represent the potential for magma transport between deeper and shallower parts of the volcano's plumbing system, according to our assessment of pre-eruptive conditions. The Chaimilla fall deposit 3,180±40 yr B.P. (Costantini et al., 2011) is a key explosive eruptive event that occurred when the crater formed after the collapse of the edifice following the eruption of the Pucón ignimbrite (e.g. "C3" in Moreno and Clavero, 2006). On account of the very thin stratigraphic separation between the Pucón and the Chaimilla subsequent deposit (this study; Pioli et al., 2015), our new MI dataset demonstrate that the Chaimilla mafic magma represents a degassed, cooler (<1018–1134 °C) endmember of the Pucón ignimbrite (ibid. for S; Cl, F contents; Table A.8); it records lower pressure ranges (0.4–0.9 kb corresponding to the volatile-rich type 2 magma defined by Pioli et al., (2015) (Fo_{81-85} at 1.2 kb). The subsequent Chaimilla event, although similar in composition, is a shallow (1.7–3.2 km) degassed residual melt, produced in similar conditions to the current feeder system (Fig. 2, 4, 6).

The present-days conditions of mafic magma below Villarrica central crater are still reflecting two ranges of storage depths settings for magma evolutions according to our new MIs dataset. The 2015s low contents of the water-CO_2 pair recorded in this study (0.84 wt.% and 307 ppm, respectively) are consistent with the 2015 volatile contents recorded in the MIs of Cortés et al. (2024) (1.45 wt.% and 468 ppm, respectively), implying that the mafic magmas produced during the last decade at central Villarrica crater are strongly degassed at shallow depths. These volatile element contents are used as starting conditions in our proposed solubility model (Fig. 6) and demonstrate volatile saturation of low-water contents reaches minimum stalling lithostatic depth of 1.7 km. Even our estimated depth results are 3.1 ±0.6 km for CO_2-corrected MIs (±8.3kb) (Fig. 5a), which is still below ≤ 5.3 km crystallization equilibrium during the 2015 Strombolian paroxysm (ca. 1110 °C) (Romero et al., 2022). Given those solubility model results representing magmas that persist below the present-day central crater (Figs. 4, 5, 6), this investigation does not discard that the volatiles reach saturation conditions >14.2–16.6 km, which could then support the existence of a deeper reservoir until present-days (Cortés et al., 2024). The magma still crystallizes olivine at a depth of 19–35 km (Morgado et al., 2015), for this reason, deeper portion of the plumbing systems could persist and launch new magma batches (Edmonds et al., 2022). This range of saturation depths partially matches the ~8–20 km zone of low resistivity detected by magnetotelluric analysis which could be related to a region that favor melt transport below Villarrica (Pavez et al., 2023).

5.2 Deep reservoir inferred from CO_2-rich mafic magmas and volatile saturation at Villarrica and MECs

The eruptions monitored at Villarrica over the last decades still record lower minimum solubility pressures for volatile elements (< 5 km), but these conditions are largely reported for lateral volcanic centers according to the comparative data set of our solubility model. Only post-glacial paroxysms such as Pucón ignimbrite have been able to deliver evidence of a deep zone (> 17 km) for subsequent mafic magma recharges, but such characteristics are even met at lateral MECs.

Systematically, the explosive strombolian to violent strombolian eruptions of Chaimilla and subsequent crater explosions after 1971 (Cortés et al., 2024) did not record the deepest saturation levels despite assuming to represent continuous volatile-rich recharge (>12 km; Edmonds et al., 2022). To support this new observation, we present new MI saturation pressure dataset from all MECs and Villarrica paroxysmal eruptive events are fed by magma coming from similar maximum depth estimates (from volatile saturation; ~17–21 km derived from basaltic andesites with similar pre-eruptive P-T compositional evolution; Figs. 5, 6). Nevertheless, nearby as beyond Villarrica flanks, melt-volatile element chemistry transported as magmatic fluids may reflect a distinct compositional evolution during deep transport beyond the 45 km local cortical thickness (Tassara and Echaurren, 2012,). Therefore, before evaluating such causes of heterogeneities in magmatic fluids (section 5.3-5.4), this section shows that pre-eruptive conditions derived from our MI study support consistent deeper regional starting pressures for volatile saturation since the post-Lican Ignimbrite (13.5 ky) Villarrica volcanic event.

At Villarrica central crater, the entrapment pressure of MIs records the same order of lithostatic depth (≤ 21.3 km), somewhat deeper than the 12.7 km vertical extension of the transcrustal system of Cortés et al. (2024) post-1971 eruptive events. This new depth from MI estimate is now closer to the 22.8–29.2±6.1 km bracket of Morgado et al. (2015) at central Villarrica since the 1971 eruption (Fig. 6). This is consistent even with the case of distant Caburgua (~25 km NE Villarrica), the new MIs here are also below the range of 39.0–41.2 ±6.1 km depths recorded by the same authors for Caburgua (CHSEC). Based on our new CO_2 density-µRaman corrections and derived saturation pressures (3.7–4.8 kb; Fig. 5a), we argue that the regional monogenetic cone of Caburgua has equivalent depth pressure from volatile element saturations down to ~13.5–17.3 km, despite ascending through a lithological basement far from the main stratovolcano.

Under these circumstances, a consistent deep magmatic storage or transport zone exist also at a distance from Villarrica even at several MECs (CO_2-rich MIs and Raman MIs corrected collections). This unique storage level can be identified among the complexity of typical trans-crystalline mush systems (TCMS) but provide even more extended information on lithostatic depths according to our sampling of lateral MECs (e.g., Llaima; DeMaisonneuve et al. 2012; Ruth et al., 2017; Cashman et al., 2017). Within the primary structure of Villarrica Caldera 1, there are also explosive flank volcanic activity, such as the Los Nevados cones (<2600 yr B.P.), which also trapped relatively deep magmatic batches (9.2 km; Robidoux et al., 2021) compared to present-day crater conditions (maximum 5 km at Villarrica; this study and Cortés et al., 2024) (Fig. 6). The new MI-CO_2 content correction at Los Nevados now gives minimum equivalent depth pressure values to saturate volatiles down to 14.2–21.3 km. In comparison, the Chaillupén MEC cones, a few hundred meters south of the central crater of Villarrica, record saturated volatiles below <1.9 kb, (Avg. °T= 1169±8°C)(Fig. 5a), resulting in a lithostatic depth of < 0.3–6.8 km for melts erupting on the southern flanks of Villarrica;

such values may still represent deeper sources if MIs are not affected by shallow olivine-MI diffusive H^+ processes.

5.3 Magmatic fluid evidence for atmospheric and crustal-derived components

The magmatic volatiles transported at Villarrica and MECs in this study reflect a common atmospheric component and probably also other South American volcanoes, according to the magmatic fluid tracer $^3He/^4He$ used in this study. The new dataset here provides evidence that the magmatic fluid isotopic noble gas signature is either recycled into the mantle wedge from the subducting slab and/or acquired during magma ponding within the continental crust. To investigate the role of the subducting slab and continental crust on the composition of the degassed magmatic fluids at Villarica, $^3He/^4He$ measured in Fis from the same MI olivine batches can be used as a useful tracer, coupled with petrological and geodynamic evidence (Fig. 7; Table A.10).

In support of the use of noble gas isotopes as magmatic fluid tracers, Hilton et al. (2002) reported in a global review of arc volcanism that: i) the highest $^3He/^4He$ ratios measured in arc volcanism are in the MORB range (i.e. 8 ± 1Ra; Graham, 2002); ii) in many arc segments (including central and northern Chile, Peru and Ecuador) the highest $^3He/^4He$ ratio is below the MORB range (i.e. below 7 Ra); iii) the mean $^3He/^4He$ ratio of all arc segments is 5.4 ± 1.9 Ra. Volatiles transported as magmatic fluids are thus of great importance since they are cycled between the atmosphere and the Earth's interior at subduction zones (Zellmer et al., 2015). In this geodynamic setting, slab dehydration at depths of several kilometers can differentially influence the composition of magmatic fluids generated in the overlying wedge. Subduction-related fluids are known to contain higher proportions of atmospheric components than intraplate and mid-oceanic ridge environments (Burnard et al., 1997). According to Hilton et al. (2002) and Sano and Fischer (2013), noble gases found in arc magmatic/hydrothermal fluids and trapped as fluid inclusions (FIs) in minerals are important indicators of the relative contributions of the subducted slab, crust and mantle to the fluids emitted by arc volcanoes. A recent compilation of light noble gases in the South American arc revealed that the average $^{40}Ar/^{36}Ar$ signature of all gas-rocks samples is ~339 (Lages et al., 2021b), which is well below that of MORB (~44,000; Moreira et al., 1998) and close to the atmospheric signature (~296; Porcelli et al., 2002). In rocks from Villarica (our samples and ones from Lages et al., 2021b), the observed $^{40}Ar/^{36}Ar$ ratios in FI range from 300 to 336, supporting the low isotopic signature already found along the South American Arc. Similar inferences can be made from the $^4He/^{20}Ne$ range (3.9–50.8), which is not far from the atmospheric ratio (0.318) and well below typical mantle values ($^4He/^{20}Ne$>1,000).

Recent studies in the Central and South American Volcanic Arcs have provided new measurements of helium isotopes in FIs hosted in olivine and pyroxene crystals, clarifying the reasons of $^3He/^4He$ variability in those arc volcanoes (Lages et al., 2021a, 2021b; Rizzo et al., 2022 and references therein). The main findings are that: i) the mantle $^3He/^4He$ signature of the Central and South American Volcanic Arcs is within the MORB range, with the highest values measured in Guatemala (9 Ra, Pacaya volcano) and Colombia (8.8 Ra, Galeras volcano; Fig. 3b); ii) $^3He/^4He$ values below the MORB range are indicative of variable crustal contamination, often with an inverse relationship between Rc/Ra values and crustal thickness (this feature is mainly observed in the South American Volcanic Arc; Lages et al., 2021a, 2021b; Barry et al., 2022); iii) there is a progressive decrease in mantle wedge $^3He/^4He$ values, with $^3He/^4He$ values still within the MORB range, coupled with variations in some key trace element ratios (i.e. Ba/La, Th/La, U/Th), resulting from a higher presence of subducted slab sediment fluids (rich in U and Th, from which radiogenic He is produced). This has been observed particularly in the Central American Volcanic Arc and the SVZ (Lages et al., 2021a, 2021b; Rizzo et al., 2022 and references therein).

5.4 Olivine FIs record primitive magmatic fluid during Villarrica subplinian climax

The present study completes the Villarrica volcanic complex understanding of the magmatic fluid signature by confirming that ^4He contamination is stronger in flank MECs according to systematic variations in FIs $^3He/^4He$. Interestingly, according to MI as bulk rock composition, the systematic FIs ^4He contamination is stronger in differentiated-cortically contaminated MECs as Villarrica typical shallow degassed reservoir but is least contaminated in Pucón paroxysm (Fig. 7b, 8b). As to evaluate variation in magmas that are transporting the volatile phases, the bulk rock sample composition of this study does not indicate yet clear systematic correlation with slab fluid markers within the Caldera 1 complex and beyond its boundary (Figs. 7).

By reviewing closely, the local $^3He/^4He$ variations and bulk rock composition, we present new helium isotopic data in FIs that mostly reflect the measurements presented by Lages et al. (2021b), except for one sample from Pucón that has a value of 7.6 Ra. This value is almost 1 Ra unit higher than the average values for Villarica volcano, suggesting that the continental crust effectively plays a role in lowering the $^3He/^4He$ values of pristine mantle fluids. A helium isotopic signature of 7.6 Ra is still lower than that expected for mantle values. However, in the light of the slab sediment fluid contribution suggested by Plank (2005) for this region of the SVZ and the relation between Rc/Ra and Th/La ratios of Lages et al. (2021b) (Fig. 7ab), we argue that the $^3He/^4He$ signature below Villarica is confirmed to be within the MORB range and that the cortical contamination plays an important role in lowering the original mantle $^3He/^4He$. Close examination of the literature dataset with our bulk rock samples (Fig. 7; Table A.2) shows the regional Th/La trend typical of other volcanic centers in the SVZ (Hickey-Vargas et al., 2016; McGee et al., 2017), but it is difficult to observe coupling with the $^{3}He/^{4}He$ signature at the scale of the Villarrica volcanic complex. It is still not possible to observe this correlation beyond the most distant regional volcanic center, Caburgua, unless larger amounts of FI-hosted olivines are encountered to extend the topic (Appendix A). At a distance from the subducting trench, Caburgua is the only regional MEC that deviates from the slab fluid signature data cluster (Fig. 8; Table A.2), implying that it is significantly modified with respect to asthenospheric slab fluid melting. Chemical tracers of magmatic fluids require systematic studies of regional MECs and stratovolcanoes in the same region (e.g., Quetrupillan and Lanin; Cascades; Mordensky and Wallace, 2018). More work is also required regionally to investigate the variation in radiogenic ^{4}He (bulk mol/g content) in olivine FIs (Lages et al., 2021b and references therein) or fumaroles (Tardani et al., 2017; Barry et al., 2022 and references therein) for the most well-studied polygenetic Villarrica basaltic andesites produced since the postglacial period.

The most interesting observation at the Villarrica polygenetic complex is from the variation of $^{3}He/^{4}He$ between successions of different scales of explosive eruptions between central and peripheral craters. The presence of ^{4}He contamination at most differentiated products and the $^{3}He/^{4}He$ values being the highest in olivine-FIs from the most primitive batch of magma at Pucón Ignimbrite (highest post glacial VEI; Table 1). Regardless of the primitive nature of the olivine (olivine Fo% or MI Mg# show no correlation with our Rc/Ra ratios; Figs. 3, 8), we suggest that the magmatic $^{3}He/^{4}He$ signature decreases with crustal ponding and contamination, when wall rock interaction is more likely to decrease cooling rates of large-scale magma reservoirs. This latter conclusion is already supported petrologically by major element MI trends (Fig. 2), bulk-rock trace element tracers and noble gas isotopes (Figs. 3, 8), but could depend on cooling rates and potential magma chamber timescales (e.g. U-Th-He isotopic systematic; Kuritani et al., 2007; McGee et al., 2017). In addition, figure 8 details peripheral plumbing system contamination effect as a potential source of recycled ^{4}He increase, which also occurs for bulk rock compositions indicating crustal interaction, such as Sr/Y ratios (> 20), and K_2O (wt%) content (Fig. 8cd). This correlation is still not systematic for the Th/La ratio (Fig. 7a), used as an indicator of slab sediment fluid contribution (Plank, 2005). When examining chronological evolution of geochemical markers, this geochemical anomaly is only found for the Pucón recharge event (Th/La >0.2) during the post-glacial period of Villarrica and is absent from the Chaimilla-derived magma and other MEC eruptions (Fig. 8ab; Th/La < 0.2). Thus, ^{4}He contamination is weaker during Plinian events with high VEI explosive paroxysms, and the slab fluid signature is only detected for the parental magma fluids that represent volatile-rich element contents (Pucón). Our olivine FI dataset records the lowest ^{4}He content (g/mol) during the climax eruptive phase (Fig. 8). Taken together, such geochemical parameters (olivine MI as Fis compositional trends) thus indicate that less peripheral contamination is expected in basaltic andesites from the parental magma (Pucón) that feed the main explosive paroxysms of Villarrica.

5. Conclusions

For the first time a joint comparison has been made based on melt volatiles, major and noble gases for a polygenetic volcanic system, that of Villarrica in the southern Andes. This study includes new detailed data on volatile saturation depths, with improved analyses for P-T and compositional pre-eruptive magma conditions based on new geobarometry calculations, and a solubility model that uses novel µRaman dataset to predict the original CO_2 contents in MIs with shrinkage bubbles. The temporal/spatial portrait of pre-eruptive conditions as magmatic fluid compositional variations were explored within this research providing of the following conclusions:

I) **The Villarrica stratovolcano forms a polygenetic system in which the magmatic volatile content decreases from the Pucón event (3.7 ky) to the last decade at central crater:** According to the new rich MI dataset collected during most documented explosive mafic eruptions from Villarrica, significant volatile content decrease is observed. Since the current 2 km-wide caldera formation (post glacial period, see Villarrica Unit 3, <~ 3.7 Kyr AP; Moreno and Clavero, 2006), close evaluation of MI texture characteristics and major oxide composition/volatile contents (SIMS, FTIR), demonstrate clear evidence that parental mafic magma of the Pucón eruption might represents the pre-eruptive conditions of the Chaimilla event (<~ 2.6 Kyr AP (Pioli et al., 2015). The actual central crater setting (post 1970s) may favor shallow depth ~<5km degassing as demonstrated with the lava lake CO_2-rich persistent bubbling (Witter et al., 2004; Moussalam et al., 2016; Aiuppa et al., 2017).

II) **Lateral, regional as Villarrica volcanic vents confirm evidence of both shallow volatile-poor and deep CO_2-rich magma reservoirs:** The presented solubility models in this study confirm lithostatic depth ranges for MI entrapments being within the range of documented crystallized mafic mineral phases from the literature (Morgado et al., 2015; Boschetty et al., 2022; Cortés et al., 2024), but two depth zones are clearly identified at central as peripherical MECs. These key depth zones at Villarrica may represent characteristics like polygenetic volcanic systems in other volcanic arcs (Rasmussen et al., 2022), distinguishing the depth of eruptions controlled by high CO_2 saturation in deep reservoirs from those controlled by water loss in shallow reservoirs. The pre-eruptive conditions evolve similarly at present-days central crater (<1.7–4.4 km), as well as laterally to nearby MECs (Chaillupén, Los Nevados) from post-glacial times.

III) The Pucón ignimbrite during its climax phase represents the post-glacial vestige of parental magmatic fluids at Villarrica and flank MECs: Behind the petrogenetic causes associated to explosive paroxysm with relatively high Rc/Ra in single volcanic complex (Piton de la Fournaise in Boudoire et al., 2020), this study identifies temporal evolution of magmatic differentiation/cortical contamination processes during magma-crustal interactions. The Pucón Ignimbrite holds phases richest in volatile content from MIs and high $CO_2/^3He$ ratio from Fis in olivines for which such petrogenetic effect is much weaker. The $^3He/^4He$ signature attributed by our olivine-hosted Fis collection is lower at the MECs and smaller for VEI eruptions (2015) (<6.7 Ra), while in the high VEI explosive paroxysms of Villarrica (Pucón, Chaimilla) it reaches ~7.6 Ra (closer to a mantle signature of 8–9 Ra expected along the South American arc; Lages et al., 2021). At Villarrica, bulk rock differentiation/contamination is consistent with higher contents of Fis radiogenic ^4He (g/mol), a feature observed consistently in volcanic arcs (Lages et al., 2021a,b).

Acknowledgements

This work is part of ANID, Fondecyt Iniciacion No 11190846 project of Philippe Robidoux (2019–2022). We are grateful to Dra Manuela Nazzari and Dir. Piergiorgio Scarlato for providing access to electron microprobe EMPA at Istituto Nazionale di Geofisica e Vulcanologia Sezione di Roma 1, HP-HT Lab. of Experimental Volcanology and Geophysic. The measurements were also supported by Elisabetta Del Bello and Alessio Pontiselli (INGV-Roma) through participation at the TransNational Access (TNA) in the framework of the EXCITE (Horizon 2020) research infrastructure. Special thanks are for Mariano Tantillo and Mariagrazia Misseri from INGV-Palermo, who helped in mineral preparation and noble gases isotope analysis. Special thanks are also addressed to Dra. We address special acknowledgements for Universidad Mayor, Escuela de Geología Bsc. students Gloria Díaz, Aaron Sancho, Daniela Pasten and Prof. Clavero for active participation in the 2017–2022 field trips. ER-K, YM and PR deeply thank Nordine Bouden and Johan Villeneuve for their flawless support with the SIMS measurements and for the access to the Nancy preparation lab.

CAPTIONS

Table Captions:

Table 1 – Volcanic deposit characteristics. Sieved and non-sieved volcanic deposits are given geographical coordinates for outcrop location and additional material description. The granulometry is in Phi (φ) size. Fragment size and typology distribution (% per 100 randomly selected clasts) are classified strictly on Fisher (1966) classification in addition to the full spectrum of clastic material typology, classified according to White & Houghton (2006).

Table 2 – Volcanic event references for analysis

Table 3 – Parameters of post entrapment crystallization effects

Figure Captions

Figure 1 – Location of study area. a) Map of the subduction zone, including arc segments from the Central Volcanic Zone (CVZ). White lines are inferred tectonic plate boundaries and arrow indicates direction of subduction. Colored dots are sampled spring sites with Rc values marked using quartile color code. All eruptive centers listed in the Smithsonian Global Volcanism Program's Holocene Volcano List (small black triangles). From north to south, oceanic plate segments with fracture zone abbreviations ending in "FZ" are linked to Juan Fernandez Ridge; Mocha FZ, Valdivia FZ, Chiloe FZ, and Chile Rise FZ. b) Stratigraphic extent of Villarrica Pucón ignimbrite for Units P1, P2 and initial Base Surge Deposit "Pb" (Moreno and Clavero, 2006) as delimited by Silva et al. (2010). The Caldera 1,2 and 3 boundaries (Moreno and Clavero, 2006) are marked, as well as extent of for Chaillupén and Los Nevados Groups (modified from same source; Robidoux et al., 2021), with Caburgua MECs restricted to Caburgua cone #1 sector for lava and pyroclastic deposits (modified from Moreno and Clavero, 2006; Morgado et al., 2015). The Chaimilla fallout deposit (Costantini et al., 2011) and Pucón (Silva et al., 2010) are shown with maximum covered areas from isopach ellipsoid.

Figure 2 – Major element compositions. The post entrapment-corrected MIs (colored circles) with their major element contents as a function of SiO_2 wt.% (see corrected dataset in Appendix I). The bulk rock analyses are shown by colored squares for each series. Dashed arrows indicate the approximate trend for groundmass crystallization of plagioclase (Pgl In) ± clinopyroxene (Px In). The trapped melts (MIs) evolve via a parental melt differentiation path (red arrow) or post-entrapment crystallization effects (PEC) (orange arrow). The post-entrapment crystallization effects are interpreted in Table 3. The bulk rock composition of the 1971 Villarrica eruption is represented by grey dots and Caburgua-Huellemolle by a dark grey box (Hickey-Vargas et al., 2002; Morgado et al., 2015).a) K_2O vs SiO_2 classification for the volcanic series, b) CaO wt.%,

c) Al_2O_3 wt.% where plagioclase (Pgl-In) is interpreted as residual melt plagioclase crystallization occurring before/during MI entrapment, d) Na_2O wt.% where the dark arrow represents the general tendency toward cogenetic differentiation in all our MI collection, e) MgO wt.%, f) FeO_T wt.%.

Figure 3 – The FI helium dataset. $^3He/^4He$ (Rc/Ra) ratio vs He concentration (mol/g) collected from analytical data of bulk fluid inclusions (FIs) hosted in olivine (Table A.10). Data from Rizzo et al. (2022) and Lages et al. (2021ab) represent the literature FI data, while our dataset of FIs in olivine crystals is represented by colored symbols (see legend in Figure 2). Samples 2015_B* (Villarrica 2015), HCH2A1* and HCH2A4C* (Chaillupén) are from Lages et al. (2021b) (Appendix K). Data are grouped as combined segments from Central American Volcanic Arc (CAVA; green/black colored symbols) and South American Volcanic Arc (South American VZ; yellow symbols). b) $^3He/^4He$ (R_C/R_A) vs He/Ne data ($^4He/^{20}Ne$) in FIs and free gases. Binary mixing (air-magmatic endmember) curves are from Lages et al. (2020, 2021) and calculated using maximum R_C/R_A values for each segment; grey delimits the MORB range (8±1 R_A). The free gas results are classified according to Lages et al. (2021); Free gases of temperature > 100 °C; Free gases 50–100°C; Free gases < 50 °C.

Figure 4 – Volatile contents from melt inclusions at Villarrica. The solubility model is used for PEC-treated MIs only, applying the Iacono-Marziano et al. (2012) model to calculate isobars and degassing curves. a) CO_2 vs H_2O concentrations in melt inclusions from Villarrica. b) CO_2 vs H_2O concentrations in melt inclusions from MECs, c) Raman-corrected degassing paths (closed system degassing). The µRaman density represents all MIs treated with the method described in Robidoux et al. (2018) (Table A.8-A.9). The Mimic model is applied to all MIs measured by EMPA with vapor bubbles and allows to obtain the CO_2 content as output CO_2vbg (Rasmussen et al., 2020), which is the result of the calculated reconstruction of the total MI volume and CO_2 content using the vapor growth model of the same authors.

Figure 5 – Post entrapment crystallization saturation pressure and temperature conditions: chronological order. a) Saturation pressure (kb) of Villarrica center (red) and MECs (blue) for minimum saturation pressures. The µRaman CO_2-corrected MIs represent pressures with open circle symbols; the vertical black arrow points connect non-corrected to CO_2-corrected contents (Table A.8). b) H_2O wt% content from MIs is represented by vertical bars for Villarrica center (red) and MECs (blue). H^+ diffusion is interpreted for increasing effect (upward arrow) or decreasing effect (downward arrow). c) Inman's (1952) Md grain size parameter indicate increased negative values for larger pyroclast size. Explosive fragmentation is inferred to cause an increased production of large clast sizes at the sampled outcrop (upward arrow), while clast cooling rate decreases (downward arrow) as clast size increases. d) Temperature (°C), of Villarrica center (red) and MECs (blue). The thin vertical bars are minimum to maximum recorded PEC MIs for this study. The colored boxes represent minimum and maximum temperatures (°C) using the Tg output obtained from the Mimic model (Rasmussen et al. 2020), which is the glass transition temperature (Giordano et al., 2008). The "MI quenching rate" variation (interpreted) decreases systematically along the same series

of olivine crystals (downward arrow). The left vertical axis is used for trapping MI temperatures while right vertical axis is used for quenching MI temperatures.

Figure 6 – Villarrica depth cross section for solubility model. West to east Villarrica profile for magma crystallization conditions (lithostatic pressure gradient is 0.27 km/kb). Vertical scale X2 applies to framework below >2.0 km in depth and vertical scale X1 applies to framework between summit (2847 m.) and 2.0 km in depth. Horizontal distances are not to scale. Minimum saturation depths (km) are shown with an abbreviation code for each eruptive event based on the literature (Moreno and Clavero, 2006); same color code as for Figure 2, except for literature Chaimilla black letters abbreviated to "Ch*" are crystallization depths of ascending magmas from Pioli et al. (2015).The boxes with colored borders are minimum and maximum saturation pressures (Bar) recorded by MI solubility models and thin vertical bars are minimum and maximum ranges for µRaman CO_2 corrections applied in the present study. Arrow intervals stand for vertical interval depths in black characters for Magma reservoir* (Lohmar et al. 2012; Delgado et al., 2017), Paroxysm source* (2015) (Romero et al., 2022). Villarrica olivine* (19–35 km) and CHSEC olivine (32–44 km) are from Morgado et al. (2015) and represent assumed olivine crystallization depths calculated using pyroxene-olivine geothermobarometry. Background volcanism is modified from Moreno and Clavero (2006). The Rc/Ra dataset is from this study, except for the Villarrica paroxysm source and the duplicate Chaillupén sample (Lages et al., 2021b).

Figure 7 – $^3He/^4He$ for FIs corrected for atmospheric contamination (Rc/Ra) vs magmatic fluid tracers. a) Mean Th/La in subducting sediment columns (Plank, 2014) and volcanic arc trenches (bulk composition added in this paper for CVZ and Lages et al., 2021b; database filtered for < 58 wt% SiO_2). CAVA bulk composition from Rizzo et al., 2022. The same symbols are used as in previous figures for MIs, with the Pucón ignimbrite series Pb considered as the parental magmatic fluid and/or melt for the rest of the dataset produced in this study. B) The $^3He/^4He$ FIs corrected for atmospheric contamination (Rc/Ra) vs. $CO_2/^3He$ systematics for South American fluids calculated as mol/g from mass spectrometry; the crust-mantle binary mixing line (in blue) assumes an Ra of 7.9 (avg. SVZ taken from Lages et al., 2021b). All lines and “X” symbols are fumarole data taken from Lages et al. (2021ab) and CAVA data from Rizzo et al. (2022).

Figure 8 – The influence of geochemical parameters on trapping conditions of $^3He/^4He$ FIs: chronological order. The bulk rock collection is from the following authors: Hickey-Vargas, 1989; Lohmar et al. 2012; Costantini et al., 2011; Pioli et al., 2015; Morgado et al., 2015; Hickey-Vargas et al., 2016; McGee et al., 2017). a) Th/La slab sediment ratio used to test possible slab control on the $^3He/^4He$ signature of the mantle wedge along the Andes and Villarrica, b) ^4He content (g/mol) from this study, c) Sr/Y to detect peripheral contamination, from our bulk rock collection and the literature d) K_2O wt.% content from PEC melt inclusions, with minimum and maximum interval bars. The median value is arbitrary, representing the range of minimum and maximum K_2O wt.% contents in the dataset by eruptive event. The bulk rock K_2O wt.% contents are from this study and the literature.

Supplementary Material

(File)

Appendix A – Supplementary Material Methodology Review.

(Tables)

Appendix B

Table A.1: Full inclusion reference analysis.

Table A.2: Bulk-rock analysis of Villarrica samples.
Major element analysis based on ICPMS. LOI values were corrected for oxygen uptake in the conversion of FeO to Fe_2O_3T (wt.%) in the furnace. Ratios for each eruptive event were reported as FeO/Fe_2O_3. Trace elements and REE were analyzed by inductively coupled plasma mass spectrometry. Trace element ratios are calculated directly from the values in the table (weight ppm ratio) with no normalization to the standards in the literature.

Table A.3: Olivine populations statistics.
Classification of olivine series described for the presence of the following MI typologies (Robidoux et al., 2018): G1 (no inclusions), G2 glassy inclusions, G3 glassy inclusions+vapor bubble, G4 glassy inclusions+vapor bubble+spinel, G5 crystallized MIs, GR MI associated with boundary (reentrant or hourglass). Inclusion morphologies and dimensions are given in microns.

Table A.4: Electron microprobe analyses of original Villarrica and MEC olivine chemistry.

Table A.5: H_2O-CO_2 contents from FTIR.
a) H_2O (as OH^{-1}) at 3,550 cm^{-1} peak, b) CO_2 content as CO_3^{2-} double peak (1,435-1,515 cm^{-1}).

Table A.6: Volatile contents from SIMS.

Table A.7: FTIR and SIMS reproducibility.
The selected FTIR H_2O - CO_2 contents are compared to H_2O SIMS contents with error bars according to respective error sources. The wt. % error for [H_2O] with FTIR assumes the sum of the following errors: (1) median absorbance (Abs.) graphical error between closest cm^{-1} records on IR spectrum to the left and right of the central peak position 3,550 cm^{-1}, (2) thickness deviation from the wafer (µm), (3) difference between replicate analysis "a" and "b". The STD error on eruption series from the density (g/cm^3) and absorption coefficients (mol^{-1} cm^{-1}) is only considered if EMPA results are not available. The wt. % error for [H_2O] with SIMS uses the %STD error from “^{16}O - ^{1}H“ calibration curves. The wt. % error for [CO_3^{2-}] using FTIR (ppm units) uses the same

parameters as for [H_2O] (in wt.%), but graphical error depends on the double peak 1,435 – 1,515 cm^{-1}. The wt. % error for [CO_2] using SIMS (ppm units) uses the %STD error from "^{12}C" calibration curves.

Table A.8: Major element and volatile chemistry of Villarrica PEC glass inclusions. Olivine compositions are given in Fo%, and geothermobarometer results for solubility models are calculated according to Iacono-Marziano et al. (2012). Conditions for Rasmussen method and Raman corrected volatile contents are given for saturation pressure models.

Table A.9: Raman CO_2 density and spectrum identification in shrinkage bubbles.

Table A.10: Noble gas isotopes.

Supplementary Material (Figures)

Figure A.1: Calibration of SIMS parameters for volatiles species. The set of standards with known volatile contents are given for a) $^{12}C^-$, b) $^{13}C^-$, c) $^{16}OH^-$, d) $^{19}F^-$, e) $^{32}S^-$, f) $^{35}Cl^-$. A Cs^+ primary beam with a current of 1 nA and an electron gun is used to compensate for charge build-up at the sample surface. A 3-minute pre-sputter with a 30 × 30 μm square raster was applied, then analyses were performed on the 15 to 20 μm spot in the centre of the raster-cleaned area by a mechanical aperture placed at the secondary ion image plane. The resolving mass of ≈7000 (with the contrast aperture at 400 μm, the energy aperture at 40 eV, the entrance slit at 52 μm and the exit slit at 173 μm) meant that complete discrimination of mass interferences was achieved ($^{34}S^1H$ from ^{35}Cl, ^{17}O from $^{16}O^1H$, $^{29}Si^1H$ from ^{30}Si and $^{31}P^1H$ from ^{32}S). We collected signals for ^{12}C (8 seconds), ^{17}O (3 seconds), $^{16}O^1H$ (6 seconds), ^{18}O (3 seconds), ^{19}F (4 seconds), ^{27}Al (3 seconds), ^{30}Si (3 seconds), ^{32}S (4 seconds) and ^{35}Cl (6 seconds; counting times in brackets), with 2 seconds waiting time after each switch of the magnet. This cycle was repeated 10 times for each analysis. One measurement lasted 12 min per spot.

Figure A.2: FTIR and SIMS reproductibility. Volatile contents of MIs at Villarrica with H_2O concentrations in MIs from Villarrica. The FTIR H_2O–CO_2 content is compared with the H_2O–CO_2 SIMS content with error bars. The MI samples containing shrinkage bubbles are represented by a circle with a black border. a) Comparison of the H_2O content is shown with error bars from Appendix C. The legend shows the four groups of quartiles used with grey-toned circles and each one represents the following categories in μm^3 unit volume (Vo) Q_1 (3,4E-09 – 8,0E-08); Q_2 (8,0E-08 – 2,5E-07); Q_3 (2,5E-07 – 5,4E-07); Q4 (5,4E-07b – 1,2E-05). b) Comparison of the CO_2 content is shown with error bars. Each eruption is color coded according to the legend.

References

1. Aiuppa, A., Bitetto, M., Francofonte, V., Velasquez, G., Parra, C.B., Giudice, G., Liuzzo, M., Moretti, R., Moussallam, Y., Peters, N. and Tamburello, G., (2017). A CO2-gas precursor to the March 2015 Villarrica volcano eruption. Geochemistry, Geophysics, Geosystems, 18(6), 2120-2132.
2. Barry, P. H., De Moor, J. M., Chiodi, A., Aguilera, F., Hudak, M. R., Bekaert, D. V., ... & Giovannelli, D. (2022). The helium and carbon isotope characteristics of the Andean Convergent Margin. Frontiers in Earth Science, 10, 897267.
3. Battaglia, A., Bitetto, M., Aiuppa, A., Rizzo, A. L., Chigna, G., Watson, I. M., ... & de Moor, M. J. (2018). The Magmatic gas Signature of Pacaya Volcano, with implications for the volcanic CO2 flux from Guatemala. Geochemistry, Geophysics, Geosystems, 19(3), 667-692.
4. Boschetty, F.O., Ferguson, D.J., Cortés, J.A., Morgado, E., Ebmeier, S.K., Morgan, D.J., Romero, J.E. and Silva Parejas, C., (2022). Insights into magma storage beneath a frequently erupting arc volcano (Villarrica, Chile) from unsupervised machine learning analysis of mineral compositions. Geochemistry, Geophysics, Geosystems, 23(4), e2022GC010333.
5. Boudoire, G., Rizzo, A. L., Arienzo, I., & Di Muro, A. (2020). Paroxysmal eruptions tracked by variations of helium isotopes: inferences from Piton de la Fournaise (La Réunion island). Scientific Reports, 10(1), 9809.
6. Brahm, R., Parada, M. A., Morgado, E., Contreras, C., & McGee, L. E. (2018). Origin of Holocene trachyte lavas of the Quetrupillán volcanic complex, Chile: Examples of residual melts in a rejuvenated crystalline mush reservoir. Journal of Volcanology and Geothermal Research, 357, 163-176.
7. Burnard, P., Graham, D., & Turner, G. (1997). Vesicle-specific noble gas analyses of" popping rock": implications for primordial noble gases in Earth. Science, 276(5312), 568-571.
8. Cashman, K. V., Sparks, R. S. J., & Blundy, J. D. (2017). Vertically extensive and unstable magmatic systems: a unified view of igneous processes. Science, 355(6331), eaag3055.
9. Cortés, J. A., Gertisser, R., & Calder, E. S. (2024). Magma recharge in persistently active basaltic–andesite systems and its geohazards implications: the case of Villarrica volcano, Chile. International Journal of Earth Sciences, 1-19.
10. Costantini, L., Pioli, L., Bonadonna, C., Clavero, J., & Longchamp, C. (2011). A late Holocene explosive mafic eruption of Villarrica volcano, Southern Andes: The Chaimilla deposit. Journal of Volcanology and Geothermal Research, 200(3-4), 143-158.
11. Danyushevsky, L. V., & Plechov, P. (2011). Petrolog3: Integrated software for modeling crystallization processes. Geochemistry, Geophysics, Geosystems, 12(7).
12. Delgado, F., Pritchard, M. E., Ebmeier, S., González, P., & Lara, L. (2017). Recent unrest (2002–2015) imaged by space geodesy at the highest risk Chilean volcanoes: Villarrica, Llaima, and Calbuco (Southern Andes). Journal of Volcanology and Geothermal Research, 344, 270-288.
13. De Maisonneuve, C. B., Dungan, M. A., Bachmann, O., & Burgisser, A. (2012). Insights into shallow magma storage and crystallization at Volcán Llaima (Andean

southern volcanic zone, Chile). Journal of Volcanology and Geothermal Research, 211, 76-91.

14. DeMets, C. (2001). A new estimate for present-day Cocos-Caribbean plate motion: Implications for slip along the Central American volcanic arc. Geophysical research letters, 28(21), 4043-4046. https://doi.org/10.1029/2001GL013518
15. Edmonds, M., Liu, E. J., & Cashman, K. V. (2022). Open-vent volcanoes fuelled by depth-integrated magma degassing. Bulletin of Volcanology, 84(3), 28.
16. Esposito, R., Bodnar, R.J., Danyushevsky, L.V., De Vivo, B., Fedele, L., Hunter, J., Lima, A. and Shimizu, N., (2011). Volatile evolution of magma associated with the Solchiaro eruption in the Phlegrean Volcanic District (Italy). Journal of Petrology, 52(12), 2431-2460.
17. Ferrando, S., Petrelli, M., & Frezzotti, M. L. (2019). Gradual and selective trace-element enrichment in slab-released fluids at sub-arc depths. Scientific Reports, 9(1), 16393.
18. Frezzotti, M. L., Tecce, F., & Casagli, A. (2012). Raman spectroscopy for fluid inclusion analysis. Journal of Geochemical Exploration, 112, 1-20.
19. Gaetani, G. A., O'Leary, J. A., Shimizu, N., Bucholz, C. E., & Newville, M. (2012). Rapid reequilibration of H2O and oxygen fugacity in olivine-hosted melt inclusions. Geology, 40(10), 915-918.
20. GiorGiordano, D., Russell, J. K., & Dingwell, D. B. (2008). Viscosity of magmatic liquids: a model. Earth and Planetary Science Letters, 271(1-4), 123-134.
21. Giuliani, L., Iezzi, G., & Mollo, S. (2020). Dynamics of volcanic systems: physical and chemical models applied to equilibrium versus disequilibrium solidification of magmas. Dynamic Magma Evolution, 99-132.
22. Graham, D. W. (2002). Noble gas isotope geochemistry of mid-ocean ridge and ocean island basalts: Characterization of mantle source reservoirs. Reviews in mineralogy and geochemistry, 47(1), 247-317. https://doi.org/10.2138/rmg.2002.47.8
23. Heinrich, M., Cronin, S. J., Torres-Orozco, R., Colombier, M., Scheu, B., & Pardo, N. (2020). Micro-porous pyroclasts reflecting multi-vent basaltic-andesite Plinian eruptions at Mt. Tongariro, New Zealand. Journal of Volcanology and Geothermal Research, 401, 106936.
24. Hickey-Vargas, R., Sun, M., & Holbik, S. (2016). Geochemistry of basalts from small eruptive centers near Villarrica stratovolcano, Chile: evidence for lithospheric mantle components in continental arc magmas. Geochimica et Cosmochimica Acta, 185, 358-382.
25. Hickey-Vargas, R., Roa, H. M., Escobar, L. L., & Frey, F. A. (1989). Geochemical variations in Andean basaltic and silicic lavas from the Villarrica-Lanin volcanic chain (39.5 S): an evaluation of source heterogeneity, fractional crystallization and crustal assimilation. Contributions to Mineralogy and Petrology, 103, 361-386.
26. Hilton, D. R., Fischer, T. P., & Marty, B. (2002). Noble gases and volatile recycling at subduction zones. Reviews in mineralogy and geochemistry, 47(1), 319-370.
27. Iacono-Marziano, G., Morizet, Y., Le Trong, E., & Gaillard, F. (2012). New experimental data and semi-empirical parameterization of H2O–CO2 solubility in mafic melts. Geochimica et Cosmochimica Acta, 97, 1-23.

28. Jarrard, R. D. (1986). Relations among subduction parameters. Reviews of Geophysics, 24(2), 217-284.
29. Kuritani, T., Yokoyama, T., & Nakamura, E. (2007). Rates of thermal and chemical evolution of magmas in a cooling magma chamber: A chronological and theoretical study on basaltic and andesitic lavas from Rishiri Volcano, Japan. Journal of Petrology, 48(7), 1295-1319.
30. Lages, J., Rizzo, A. L., Aiuppa, A., Robidoux, P., Aguilar Contreras, R., Apaza Choquehuayta, F. E., & Masías Alvarez, P. J. (2021a). Crustal controls on light noble gas isotope variability along the Andean Volcanic Arc. uri: issn: 2410339X. https://doi.org/10.1016/j.chemgeo.2020.119966
31. Lages, J., Rizzo, A.L., Aiuppa, A., Samaniego, P., Le Pennec, J.L., Ceballos, J.A., Narvaez, P.A., Moussallam, Y., Bani, P., Schipper, C.I. and Hidalgo, S., (2021b). Noble gas magmatic signature of the Andean Northern Volcanic Zone from fluid inclusions in minerals. Chemical Geology, 559, 119966. https://doi.org/10.1016/j.chemgeo.2020.119966
32. Liu, E.J., Wood, K., Mason, E., Edmonds, M., Aiuppa, A., Giudice, G., Bitetto, M., Francofonte, V., Burrow, S., Richardson, T. and Watson, M., (2019). Dynamics of outgassing and plume transport revealed by proximal unmanned aerial system (UAS) measurements at Volcán Villarrica, Chile. Geochemistry, Geophysics, Geosystems, 20(2), 730-750.
33. Lloyd, A. S., Plank, T., Ruprecht, P., Hauri, E. H., & Rose, W. (2013). Volatile loss from melt inclusions in pyroclasts of differing sizes. Contributions to Mineralogy and Petrology, 165, 129-153.
34. Lohmar, S., Parada, M., Gutiérrez, F., Robin, C., & Gerbe, M. C. (2012). Mineralogical and numerical approaches to establish the pre-eruptive conditions of the mafic Licán Ignimbrite, Villarrica Volcano (Chilean Southern Andes). Journal of Volcanology and Geothermal Research, 235, 55-69.
35. Marty, B. (2012). The origins and concentrations of water, carbon, nitrogen and noble gases on Earth. Earth and Planetary Science Letters, 313, 56-66.
36. Mason, E. M., Edmonds, M., Hammond, S., Ilyinskaya, E., Jenner, F., Kunz, B., ... & Velasquez, G. (2024). Chalcophile element degassing at an active continental arc volcano. Geochimica et Cosmochimica Acta, 367, 72-86.
37. Massare, D., Métrich, N., & Clocchiatti, R. (2002). High-temperature experiments on silicate melt inclusions in olivine at 1 atm: inference on temperatures of homogenization and H2O concentrations. Chemical Geology, 183(1-4), 87-98.
38. McGee, L.E., Brahm, R., Rowe, M.C., Handley, H.K., Morgado, E., Lara, L.E., Turner, M.B., Vinet, N., Parada, M.Á. and Valdivia, P., (2017). A geochemical approach to distinguishing competing tectono-magmatic processes preserved in small eruptive centres. Contributions to Mineralogy and Petrology, 172, 1-26.
39. Moitra, P., Gonnermann, H. M., Houghton, B. F., & Tiwary, C. S. (2018). Fragmentation and Plinian eruption of crystallizing basaltic magma. *Earth and Planetary Science Letters*, *500*, 97-104.
40. Mordensky, S. P., & Wallace, P. J. (2018). Magma storage below Cascades shield volcanoes as inferred from melt inclusion data: A comparison of long-lived and short-lived magma plumbing systems. Journal of Volcanology and Geothermal Research, 368, 1-12.

41. Moreira, M. A., & Kurz, M. D. (2013). Noble gases as tracers of mantle processes and magmatic degassing. The noble gases as geochemical tracers, 371-391.
42. Moreno, H., & Clavero, J. R. (2006). Geología del volcán Villarrica: Regiones de la Araucanía y de Los Lagos. Servicio Nacional de Geología y Minería, Subdirección Nacional de Geología.
43. Morgado, E., Parada, M. A., Contreras, C., Castruccio, A., Gutiérrez, F., & McGee, L. E. (2015). Contrasting records from mantle to surface of Holocene lavas of two nearby arc volcanic complexes: Caburgua-Huelemolle Small Eruptive Centers and Villarrica Volcano, Southern Chile. Journal of Volcanology and Geothermal Research, 306, 1-16.
44. Moussallam, Y., Lee, H.J., Ding, S., DeLessio, M., Everard, J.L., Spittle, E., Lu, G., Baur, J., Glazer, E., Peccia, A. and Zaman, M., (2023). Temperature of the Villarrica lava lake from 1963 to 2015 constrained by phase-equilibrium and a new glass geothermometer for Basaltic Andesites. Journal of Petrology, 64(2), egad003.
45. Moussallam, Y., Bani, P., Curtis, A., Barnie, T., Moussallam, M., Peters, N., Schipper, C.I., Aiuppa, A., Giudice, G., Amigo, Á. and Velasquez, G., (2016). Sustaining persistent lava lakes: Observations from high-resolution gas measurements at Villarrica volcano, Chile. Earth and Planetary Science Letters, 454, 237-247.
46. Moussallam, Y., Towbin, W. H., Plank, T., Bureau, H., Khodja, H., Guan, Y., ... & Rose-Koga, E. F. (2024). ND70 Series Basaltic Glass Reference Materials for Volatile Element (H2O, CO2, S, Cl, F) Measurement and the C Ionisation Efficiency Suppression Effect of Water in Silicate Glasses in SIMS. Geostandards and Geoanalytical Research.
47. Muñoz, F. A., Peña-Cortés, F., Inostroza-Matus, C., & Callejas, R. C. (2024). El riesgo en torno al volcán Villarrica en Chile: Exposición, peligrosidad e instrumentos de gestión del riesgo en Coñaripe, Licán Ray, Pucón y Villarrica. *Revista de Estudios Latinoamericanos sobre Reducción del Riesgo de Desastres REDER*, *8*(1), 115-130.
48. Pavez, M., Brasse, H., Kapinos, G., Díaz, D., Lara, L. E., & Schill, E. (2023). Magma storage and transfer in the Villarrica volcanic chain, South Chile: MT insights into volcano-tectonic interactions. Journal of Volcanology and Geothermal Research, 439, 107832.
49. Plank, T. (2005). Constraints from thorium/lanthanum on sediment recycling at subduction zones and the evolution of the continents. Journal of Petrology, 46(5), 921-944.
50. Plank, T. (2014). The chemical composition of subducting sediments. Elsevier.
51. Pioli, L., Scalisi, L., Costantini, L., Di Muro, A., Bonadonna, C., & Clavero, J. (2015). Explosive style, magma degassing and evolution in the Chaimilla eruption, Villarrica volcano, Southern Andes. Bulletin of Volcanology, 77, 1-14.
52. Porcelli, D., Ballentine, C.J. and Wieler, R. (2002). An introduction to noble gas geochemistry and cosmochemistry. Rev. Min. Geoch. 47: 1-18.
53. Putirka, K. D. (2008). Thermometers and barometers for volcanic systems. Reviews in mineralogy and geochemistry, 69(1), 61-120.
54. Rasmussen, D. J., Plank, T. A., Wallace, P. J., Newcombe, M. E., & Lowenstern,

J. B. (2020). Vapor-bubble growth in olivine-hosted melt inclusions. American Mineralogist, 105(12), 1898-1919.

55. Rasmussen, D. J., Plank, T. A., Roman, D. C., & Zimmer, M. M. (2022). Magmatic water content controls the pre-eruptive depth of arc magmas. Science, 375(6585), 1169-1172.
56. Remigi, S., T. Mancini, S. Ferrando, M.-L. Frezzotti (2021). Interlaboratory Application of Raman CO_2 Densimeter Equations: Experimental Procedure and Statistical Analysis Using Bootstrapped Confidence Intervals. Applied Spectroscopy, 75(7), 867-881.
57. Rizzo, A. L., Robidoux, P., Aiuppa, A., & Di Piazza, A. (2022). 3He/4He Signature of Magmatic Fluids from Telica (Nicaragua) and Baru (Panama) Volcanoes, Central American Volcanic Arc. Applied Sciences, 12(9), 4241.
58. Rizzo, A.L., Pelorosso, B., Coltorti, M., Ntaflos, T., Bonadiman, C., Matusiak-Małek, M., Italiano, F. and Bergonzoni, G., (2018). Geochemistry of noble gases and CO_2 in fluid inclusions from lithospheric mantle beneath Wilcza Góra (Lower Silesia, southwest Poland). Frontiers in Earth Science, 6, 215
59. Robidoux, P., Aiuppa, A., Rotolo, S. G., Rizzo, A. L., Hauri, E. H., & Frezzotti, M. L. (2017). Volatile contents of mafic-to-intermediate magmas at San Cristóbal volcano in Nicaragua. Lithos, 272, 147-163.
60. Robidoux, P., Frezzotti, M. L., Hauri, E. H., & Aiuppa, A. (2018). Shrinkage bubbles: the C–O–H–S magmatic fluid system at San Cristóbal volcano. Journal of Petrology, 59(11), 2093-2122.
61. Robidoux, P., Roberge, J., & Adams, C. (2020). Spatial visualization of geochemical data: application to the Chichinautzin volcanic field, Mexico. In Updates in Volcanology-Transdisciplinary Nature of Volcano Science. IntechOpen.
62. Robidoux, P., Pastén, D., Levresse, G., Diaz, G., & Paredes, D. (2021). Volatile content implications of increasing explosivity of the strombolian eruptive style along the fracture opening on the NE Villarrica Flank: Minor eruptive centers in the Los Nevados Group 2. Geosciences, 11(8), 309.
63. Rose-Koga, E.F., Bouvier, A.S., Gaetani, G.A., Wallace, P.J., Allison, C.M., Andrys, J.A., De La Torre, C.A., Barth, A., Bodnar, R.J., Gartner, A.B. and Butters, D. (2021). Silicate melt inclusions in the new millennium: a review of recommended practices for preparation, analysis, and data presentation. Chemical Geology, 570, 120145.
64. Roedder, E. (1984). Volume 12: fluid inclusions. Reviews in mineralogy, 12, 644.
65. Romero, J.E., Morgado, E., Pisello, A., Boschetty, F., Petrelli, M., Cáceres, F., Alam, M.A., Polacci, M., Palma, J.L., Arzilli, F. and Vera, F. (2022). Pre-eruptive Conditions of the 3 March 2015 Lava Fountain of Villarrica Volcano (Southern Andes). Bulletin of Volcanology, 85(1), 2.
66. Ruth, D. C., Cottrell, E., Cortes, J. A., Kelley, K. A., & Calder, E. S. (2016). From passive degassing to violent Strombolian eruption: the case of the 2008 eruption of Llaima volcano, Chile. Journal of Petrology, 57(9), 1833-1864.
67. Sano, Y., & Fischer, T. P. (2013). The analysis and interpretation of noble gases in modern hydrothermal systems. The noble gases as geochemical tracers, 249-317.
68. Silva Parejas, C., Druitt, T. H., Robin, C., Moreno, H., & Naranjo, J. A. (2010). The

Holocene Pucón eruption of Volcán Villarrica, Chile: deposit architecture and eruption chronology. Bulletin of volcanology, 72, 677-692.

69. Smith, I. E. M., & Németh, K. (2017). Source to surface model of monogenetic volcanism: a critical review. Geological Society, London, Special Publications, 446(1), 1-28.
70. Stern, C. R. (2004). Active Andean volcanism: its geologic and tectonic setting. Revista geológica de Chile, 31(2), 161-206. Revista Geológica de Chile, Vol. 31, No. 2, p http://dx.doi.org/10.4067/S0716-02082004000200001
71. Stimac, J., Goff, F., & Goff, C. J. (2015). Intrusion-related geothermal systems. In The encyclopedia of volcanoes (pp. 799-822). Academic Press.
72. Stix, J. (2007). Stability and instability of quiescently active volcanoes: The case of Masaya, Nicaragua. Geology, 35(6), 535-538.
73. Tardani, D., Reich, M., Roulleau, E., Takahata, N., Sano, Y., Pérez-Flores, P., ... & Arancibia, G. (2016). Exploring the structural controls on helium, nitrogen and carbon isotope signatures in hydrothermal fluids along an intra-arc fault system. Geochimica et Cosmochimica Acta, 184, 193-211.
74. Tassara, A., & Echaurren, A. (2012). Anatomy of the Andean subduction zone: three-dimensional density model upgraded and compared against global-scale models. Geophysical Journal International, 189(1), 161-168.
75. Vetere, F., Iezzi, G., Behrens, H., Holtz, F., Ventura, G., Misiti, V., ... & Dietrich, M. (2015). Glass forming ability and crystallisation behaviour of sub-alkaline silicate melts. Earth-science reviews, 150, 25-44.
76. Wallace, P. J., Plank, T., Bodnar, R. J., Gaetani, G. A., & Shea, T. (2021). Olivine-hosted melt inclusions: a microscopic perspective on a complex magmatic world. Annual Review of Earth and Planetary Sciences, 49, 465-494.
77. Watt, S. F., Pyle, D. M., & Mather, T. A. (2013). The volcanic response to deglaciation: Evidence from glaciated arcs and a reassessment of global eruption records. Earth-Science Reviews, 122, 77-102.
78. Witham, F., Blundy, J., Kohn, S. C., Lesne, P., Dixon, J., Churakov, S. V., & Botcharnikov, R. (2012). SolEx: A model for mixed COHSCl-volatile solubilities and exsolved gas compositions in basalt. Computers & Geosciences, 45, 87-97.
79. Witter, J. B., Kress, V. C., Delmelle, P., & Stix, J. (2004). Volatile degassing, petrology, and magma dynamics of the Villarrica Lava Lake, Southern Chile. Journal of volcanology and geothermal research, 134(4), 303-337.
80. Zellmer, G. F., Edmonds, M., & Straub, S. M. (2015). Volatiles in subduction zone magmatism. Geological Society, London, Special Publications, 410(1), 1-17.

1. Introduction

Composite stratovolcanoes have a central vent that is fed by basaltic magma, and their flanks are dotted with minor eruptive centers (MECs), which give rise to hazards across a broader zone. Villarrica is, located at 39°24'S and 71°55'W (Fig. 1a), is one of the few composite volcanoes worldwide hosting an active lava lake (e.g., Witter et al., 2004; Moussallam et al, 2016, 2023). open ventThe volcano in, one of the most active of the Southern Andes Volcanic Zone (SVZ), which) that formed as a consequence of the subduction of the 12–20 My-old Nazca plate beneath the South American plate (Jarrard, 1986; Stern, 2004). Villarrica), typically produces Strombolian/Hawaiian volcanic activity occurring at its central as well as lateral volcanic vents but has(summit) vent. However, geological evidence also producedexists for more energetic Vulcanian to sub-Plinian eruptions (Silva et al., 2010; Costantini et al., 2011; Lohmar et al., 2012) and for mafic ignimbrite-forming eruptions (Moreno and Clavero, 2006), as observed elsewhere as a consequence of fast ascent, decompressional degassing, and fragmentation of basaltic magma (Moitra et al., 2018; Stix, 2007; Heinrich et al., 2020). mafic ignimbritic eruptions (Moreno and Clavero, 2006). The source and location of these magmatic recharge bodies remains poorly constrained, but the mechanism has been documented in volcanoes with similar mafic magma ascent (Moitra et al., 2018 and references therein). Villarrica volcano, located at 39°24'S and 71°55'W (Fig. 1a), hosts an active Postglacial volcano stratigraphy alsolava lake (e.g., Witter et al., 2004; Moussallam et al, 2016, 2023). The main explosive eruption hazard stems from its central vent (e.g. Santiago pit crater, Masaya, Stix et al., 1998), but could also involve multiple synchronous vents during paroxysmal explosive events (e.g., Mt. Tongariro, New Zealand, Heinrich et al., 2020). The distribution of effusive activity on the flanks of stratovolcanoes is also of concern, as postglacial volcanostratigraphy indicates frequent outbursts of voluminous lava flows accompanied by small explosive eruptions, resulting in the formation of spreading clusters of minor eruptive centers (MECs) (Moreno and Clavero, 2006). In the light of these natural hazards, there are two major petrogenetical problems to be addressed concerning stratovolcano systems dominated by mafic magma replenishment, such as Villarrica:

1. **Temporal depth evolution of magmas and pre-eruptive conditions:** Understanding the evolution and origin of the basaltic andesitic magma identified within the actual morphostructural context of Villarrica volcano (Moreno and Clavero, 2006), which produces Strombolian to subplinian activity requires an examination of pre-eruptive conditions (e.g., Cassidy et al., 2018). On the basis that volatiles are key to interpreting eruptive style and explosivity at volcanic centers (Cashman, 2004), we examine whether evidence from magma and gas compositions can reveal a temporal evolution of magma composition and transport conditions within the plumbing system at Villarrica.

2. **Source and spatial distribution of magmatic fluids and volatiles:** The magma reservoirs feeding the composite Villarrica "polygenetic" system involve a diverse, overlapping system of plumbing levels and magma compositions (Geiger et al, 2018). The formation of mafic flank MECs and/or volcanism may produce a wide range of magma geochemistry resulting from the complex transport history in the Villarrica area (Valentine et al., 2015; Smith and Németh, 2017). Examples of these are the pyroclastic cones and associated lavas ofvolcanic centers

Formatted: Normal, No bullets or numbering

Formatted: Font: 12 pt

are Caburgua-Huelemolle Small Eruptive Centers (CHSEC), located in the southern sector of lake Caburgua, a few kilometers northeast of the Villarrica stratovolcano, ~~with an estimated age of 9,000 yr B.P. (Moreno and Clavero, 2006). Thus, the second challenge at Villarrica is to determine whether degassing processes are driven by the same magmatic fluids, across the post-glacial regional edifices (MECs), and the flank volcanic centers that have formed in the current 2 km-wide caldera (Villarrica Unit 3, <~ 3.7 Kyr AP; Moreno and Clavero, 2006).~~and the small eruptive centers on Villarrica flank itself (McGee et al., 2017). As seen at other mafic volcanoes worldwide (Smith and Németh, 2017; Robidoux et al., 2020), MECs can allow characterizing magma transport from the volcanic edifice towards its peripheries.

Stratigraphic mapping at Villarrica over the last few decades has led to an improved model of the eruptive sequence (Moreno and Clavero 2006~~), while the development of seismic and gas~~) as monitoring ~~techniques has helped understand the present state of volcanic~~ and risk management programs (Muñoz et al., 2024). However, understanding how magma origin, evolve and eruptive properties control the switch between such different activity ~~(Lehr et al., 2022 and references therein). Here, we investigate the~~ styles at Villarrica (Moreno and Clavero, 2006) requires a thorough examination of pre-eruptive magma conditions ~~of the post-glacial magmatic ascent history, using~~since volatiles are especially key factors in controlling eruptive style and explosivity at basaltic volcanoes (Cashman et al. 2017), and the study of melt inclusions (MIs; e.g., Wallace et al., 2021) hosted in mafic phenocrysts from volcanic rocks is especially suitable for investigating pre-eruptive conditions. Hence, our attempt here is to characterize the ~~chemistry of the magmatic fluids associated with eruptive products coming from a deeper source in the volcano~~ magmatic plumbing system~~. Melt~~ that sustains the variety of eruption styles at Villarrica by studying the pre-eruptive volatile contents in the source parental magmas of both central and peripheral volcanic centers. Our aim, in particular, is to determine whether magmas erupted at the post-glacial regional edifices (MECs), and at the flank volcanic centers that formed within the current 2 km-wide caldera (Villarrica Unit 3, <~ 3.7 Kyr AP; Moreno and Clavero, 2006), share the same characteristics (same volatile content) as those erupted at the volcano summit. We complement this analysis of Villarrica pre-eruptive magma conditions (from melt inclusion major volatile contents) with the determination of volatile chemistry and isotope compositions ~~from olivine crystals complement bulk rock analyses to illustrate detailed degassing and differentiation mechanisms occurring at various feeder system locations and intrusive stages from the polygenetic Villarrica volcanic system.~~

~~Villarrica has undergone eruptions of variably degassed magma evolving at shallow crustal depths, sourced from > 45 km depth in the MOHO-lithospheric mantle (Tassara and Echaurren, 2012; Hickey-Vargas et al., 2016). To define the~~ (noble gases) in fluid inclusions (Fis), in the attempt to characterize the magmatic fluid source~~ and spatial distribution of Villarrica's magmatic fluids and volatiles, we combine our MI study with a~~

Formatted: Font: 12 pt

Formatted: English (United States)

Formatted: English (United States)

Formatted: Indent: First line: 0.25"

Formatted: English (United States)

high-resolution isotopic noble gas fluid study on olivine crystals sampled at several regional MECs on the volcano flanks. Previous studies showed that $^3He/^4He$ measurements in olivine-hosted fluid inclusions from the 2015 Villarica eruption have an isotopic signature as high as 6.7 Ra (Lages et al., 2021b). This is still lower than the typical homogeneous Andean signature in the mantle along the South American Arc of 8–9 Ra (Lages et al., 2021a,b). Here, therefore, we investigate the causes of $^3He/^4He$ variations in magma batches generated at different MECs using the chronology of the most highly-studied explosive mafic paroxysms at Villarrica, which all fall within the post-glacial eruptive period.

2. Magmatic context and methodology

2. 2.1 Tectonic context and post glacial magmatic volatile background

Villarrica is part of the oblique Villarrica-Quetrupillán-Lanín chain in front of the Southern Volcanic Zone (SVZ). It is bounded by the Juan Fernandez Ridge at its northern edge (~33°S) and the Chile Rise to the south (~46°S) (Fig. 1 a). Volcanism in the Andes is the result of the subduction of the Nazca (10–60 My old) and Antarctic oceanic plates (45(<12–24 My old) beneath the South American continental plate (Stern, 2004), which is moving obliquely (20–30°) to the NE a rate of 7–9 cm/yr (DeMets et al.,, 2001). The basement beneath the Pleistocene-to-Holocene SVZ stratovolcanoes consists of continental crust which is ~ 35–60 km in thickness, above a shallowly dipping (< 25°) Benioff zone (Tassara and Echaurren, 2012). Where the mantle wedge is less well developed (~ 50 km thick), the overlying crust is much younger, with Paleozoic pre-Andean basement and Mesozoic-Cenozoic igneous rocks (Stern, 2004). Within the tectonic context, Villarrica has undergone eruptions of magma evolving at shallow crustal depths, sourced from > 45 km depth in the MOHO-lithospheric mantle (Tassara and Echaurren, 2012; Hickey-Vargas et al., 2016).

Villarrica volcano is close to densely populated urban and tourist areas, and has persistent degassing (e.g., Moussallam et al., 2016; Liu et al., 2019) and frequent effusive and explosive activity (Costantini et al., 2011). Petrological studies and the interpretation of seismic and geodetic data indicate a wide range of pre-eruptive magma storage conditions, in the range of 1.5–8 km in depth (Lohmar et al. 2012; Delgado et al., 2017; Lehr et al., 2022), while theconsidering volatile saturation conditions farther below ~12 km depth (Cortés et al., 2024). Pressures conditions determined with crystallization ofgeothermobarometric methods delivered 0.9–3.5 kb values using augite-melt pair (Cortés et al., 2024) and may reach > 7 kb with olivine-augite pair models indicating >7 kb pressureto represent post-1971 actual crater conditions (Boschetty et al., 2022)

Formatted: English (United States)

Formatted: Indent: First line: 0", Line spacing: Multiple 1.15 li

Formatted: Font: Bold

Formatted: Font: Bold

Formatted: List Paragraph, Outline numbered + Level: 1 + Numbering Style: 1, 2, 3, … + Start at: 2 + Alignment: Left + Aligned at: 0.25" + Indent at: 0.5"

(8.1±1.7 kb; Morgado et al., 2015). According to mineral-liquid geothermobarometry, the last Strombolian paroxysm, characterized by lava fountaining, may have been sourced from magma stored at a depth of 9.4–16.3 km and a Temperature around 1140 °C (Romero et al., 2022, Moussallam et al., 2023).conditions of 0.2–3.5 kb pressure range and a temperature around ~1140 °C (Romero et al., 2022, Moussallam et al., 2023). Farther beyond Villarrica flank and regional MEC such as CHSEC, between 10.8 and 11.4 1.7 kb were measured in Caburgua according to olivine-augite phenocrysts (Morgado et al., 2015). Since Caburgua have been classified between 8,6 and 6, Kyr AP according to stratigraphic relationship with Villarrica Unit 2 (Moreno and Clavero, 2006), Caburgua cone could exceed the age of Pucón ignimbrite, but younger than Licán Ignimbrite.

Three major evolutionary steps define the construction and collapse of Villarrica stratovolcano, with respect to past deglaciation ages (Moreno and Clavero, 2006; Watt et al., 2013). The occurrence of major VEI events has been identified from volcano stratigraphy and ^{14}C geochronology, from the oldest identified intra-glacial Pyroclastic Deposit of 40–14 ky to several post-glacial to Holocene events (Moreno and Clavero, 2006). The history associated with the development of the stratovolcano is divided into Villarrica units 1, 2, and 3, but the overall volatile data is very scarce, except for the Chaimilla fallout deposit produced from Unit 3 to the present-day (Pioli et al., 2015).. We focus here on Unit 3 of Villarrica because it represents the series of volcanic layers that cover the current structure of Caldera 2 (Fig. 1b; Moreno and Clavero, 2006), which formed after the 14.5–13.5 ky BP (^{14}C date) Licán ignimbrite and reached a minimum depth of 1.5 km (6.8 kb) and marked the end of a major volcanic cycle at Villarrica (Lohmar et al., 2012).

At central crater, so far 5 eruptive events, Pucón Ignimbrite, Chaimilla (Pioli et al., 2015), 1971, 1984 and 2015 have been studied to quantify S and Cl contents in MIs by electron microprobe. These studies report maximum contents of 1230 ppm S and 963 ppm Cl (Pioli et al., 2015; Cortés et al., 2024; Mason et al., 2024). In sequences from Chaimilla fallout, the 1971 to 2000s tephra series, H_2O and CO_2 were determined by Fourier Transform Infrared Microspectrometry (FTIR) technique used and the following maximums values were determined; 2.7 wt.% and 500 ppm, respectively (Pioli et al., 2015; Cortés et al., 2024). Elsewhere on NE Villarrica flanks, in the Los Nevados sector (Gr. 2), the H_2O and CO_2 contents have reached values up to 3.0 wt.% and 1586 ppm, respectively (Robidoux et al., 2021).

2.2 3. Methodology

Formatted: Normal, Indent: Left: 0.49", No bullets or numbering

Formatted: Font: 12 pt, Bold

3.1 Global Strategy

The method proposed here to investigate pre-eruptive conditions is based on the study of MIs hosted in mafic phenocrysts from volcanic rocks. The idea behind this approach is to characterize the chemistry of the magmatic fluids associated with eruptive products coming from a deeper source in the volcano-magmatic plumbing system of the whole Villarrica complex. Specifically, to study the "magmatic volatile" content at saturated conditions, this study relies on the MIs which represent, at a given pressure and temperature, trapped silicate melt, with in some cases, magmatic fluids produced and exsolved during igneous processes. Those fluids are assumed to be the source of volatile elements (H_2O, CO_2, S, Cl, F; e.g. Wallace et al., 2021) and for this reason, the term "magmatic fluids" here refers to the exsolved gases that moves through magmatic conduits to the surface.

It is possible to trace the origin of the magmatic fluids by measuring the specific noble gas isotopic $^3He/^4He$ ratio of fluid inclusions (FIs) in olivine phenocrysts, at the time of eruption (e.g. Hilton et al., 2002). For example, previous authors showed that $^3He/^4He$ measurements in olivine-hosted FIs from the 2015 Villarica eruption have an isotopic signature as high as 6.7 Ra (Lages et al., 2021b). This is still lower than the typical homogeneous Andean signature in the mantle along the South American Arc of 8–9 Ra (Lages et al., 2021a,b).

Even though, uncertainties exist on local cause behind variation on isotopic helium variations at this volcano (Lages et al., 2021a). To explore further on this issue, we investigate $^3He/^4He$ variations in olivine-hosted FIs from magma batches generated within the post-glacial eruptive period at Villarrica. This latter implies sampling additional regional MECs and several pyroclastic deposits pertaining to central crater explosive paroxysm that were supplied by mafic magmas.

3.2 Petrologic Approach

The major eruptive events have been studied through a series of ~~new pyroclastic rocks~~n = 15 volcanic rock units sampled from Villarrica and the MECs (Table 1). The most well-documented explosive mafic eruptions at Villarrica were selected because they were produced chronologically after the Licán ignimbrite, so that we can focus on the syn- to postglacial context of the actual Villarrica edifice. The list of samples and analytical methods is given in Tables 1 and 2, with full details of the methodology given in Appendix A “Supplementary Material Methodology Review~~”.~~” as result tables in Appendix B (Tables A.1 to A.10).

To obtain preserved volcanic rock products, volcanic deposits known from literature were systematically sampled between 2017 and 2022 on Villarrica flanks (Fig.

Formatted: Line spacing: Multiple 1.15 li

Formatted: Font: Not Bold

1), targeting juvenile pyroclasts representing rapid cooling rates to best preserve original fluids and volatile compositions from melt as fluid inclusions (MIs and FIs) (Lloyd et al., 2013; Wallace et al., 2021). Total grain size distributions (TGSDs) of entire fall deposits are examined to confirm the fragmentation processes associated with sampled outcrop pyroclast deposits known from the literature in order for name assignation of pyroclastic flow deposits, surge and fallout deposits (details in Appendix A). Olivine-hosted MIs are carefully exposed by polishing single crystals (see details of analytical methods in Appendix A; e.g. Rose-Koga et al., 2021). Special attention was given to the diversity of naturally quenched and preserved MI textural groups (Roedder, 1984) and textural statistics on MI typologies (Robidoux et al., 2018). Quantitative parameters related to post-entrapment crystallization (PEC) are reported in Table 3 and Appendix B and the PEC correction procedure is detailed in Appendix A.

3.2.1 Bulk rock chemistry of sampled volcanic pyroclasts

Bulk rock chemistry was carried out to compare with literature compositional ranges of magmas. n = 26 bulk rock samples are analysed by inductively coupled (IC) plasma mass spectrometry (PMS) as plasma-optical emission spectroscopy (POES). The methods determine the major, trace and rare earth element compositions of the collected samples (Table 2, A.1, A.2). Powders are prepared at the U. Mayor, Escuela de Geologia using a sample pulveriser and sent to a private laboratory for analysis (ActLabs, Canada). The standards, duplicates and blanks accuracy are detailed in Appendix C for the following analysis: major/trace elements fusion ICPOES/ICPMS, fluorine titration for FeO content and H_2O content by gravimetry.

3.2.2 Electron microprobe analysis (EMPA)

To provide the chemistry of the major elements from pre-eruptive magmatic processes, the selected MIs were measured with n = 163 electron microprobe analysis (EMPA) in mineral samples as for the glass inclusions they host (Table 2, A.1). The surfaces were probed with an electron microprobe analyser (EMPA), model JXA-8200 (JEOL), equipped with five wavelength dispersive X-ray spectrometers and one energy dispersive X-ray spectrometer analyser, at the HPHT (high pressure/high temperature) laboratory of the Istituto Nazionale di Geofisica e Vulcanologia (INGV) in Rome (see technical conditions in Robidoux et al., 2021).

Formatted: English (Canada)

3.2.3 Volatile element contents of glass inclusions

Volatile element contents (H_2O, CO_2, Cl, F, S) in glassy MIs, embayments and matrix glasses were determined using a Cameca IMS 1280 ion microprobe at the CRPG-CNRS-Nancy. The smallest range of MIs sizes (2-100 µm) was selected for SIMS (Table A.3), and a total of n = 57 MIs were measured to allow double calibration of CO_2 and H_2O, on the smallest MIs measured by microFTIR (here using abbreviation FTIR for consistency) (Table 1, Table A.1, A.5-A.7); a total of n = 37 inclusion duplicates were obtained by both SIMS and FTIR to fit for correlation tests (Table A.7), while n = 167 MIs FTIR analyses were performed on the total set of inclusions.

SIMS concentrations were determined using calibration curves (Fig. A.1). Maximum errors, based on reproducibility over 10 cycles of analyses, were less than 15% for CO_2, 3% for Cl, 4% for S, and 5% for H_2O and F. The FTIR technique, in comparison, determines the content of water and carbon species according to the Beer-Lambert law, following the same procedure for data treatment as Robidoux et al. (2021). The parameters of the volatile element content calculations are described in detail in Appendix A.

3.2.4 Correction for CO_2 contents and solubility models

Due to the need to account for the shrinkage bubble for the CO_2 content estimation (e.g. Rasmussen et al., 2020), the Raman microspectrometer was used for the measurement of CO2 in 25 bubbles (diameter 2 to 20 µm) of 25 unexposed MIs. The instrument is the Horiba Jobin Yvon high-resolution HR800 LABRAM of the Interdepartmental Center 'G. Scansetti' (Dipartimento di Scienze della Terra, University of Torino). The excitation source was a 532 nm green laser, with power at the emission source of 100 mW (e.g. Robidoux et al., 2017, 2018). The analyses were performed with a confocal setup, with the resulting spot size, calibration and spectral treatment (e.g. Frezzotti et al., 2012), being the same procedure as in Robidoux et al. (2018). The CO_2 bubble contents have been calculated starting from the Fermi diad split. The CO_2 Raman spectrum is characterized by two intensity peaks at ~1285 and ~1380 cm^{-1}, defined as Fermi diad peaks; in melt and fluid inclusions, the Fermi diad split is proportional to the fluid density inside the bubble (Esposito et al., 2011; Frezzotti et al., 2012; Remigi et al., 2021). 2.2.1 Micro analytical approach for determining P-T-X magma conditions.

To understand magma evolution with depth and pre-eruptive conditions, we measured the major elements using electron microprobe analysis (EMPA) and volatile contents of naturally quenched olivine-hosted MIs with secondary ion microprobe spectrometry (SIMS) (e.g. volatile collection H_2O-CO_2-S-Cl-F) comparing with Fourier

~~Transform Infrared microspectrometry (mFTIR) (e.g. dependent-pressure H_2O-CO_2 volatile pair). Quantitative parameters related to post-entrapment crystallization (PEC) are reported in Table 2 and Appendix B and the PEC correction procedure is detailed in Appendix A. The depth of magma evolution for each Villarrica magma sequence is determined using solubility models, taking into account the CO_2 in the shrinkage bubbles measured by µRaman (e.g. Robidoux et al., 2018) for the bubble-corrected CO_2 estimates. Petrographic characterization is applied to basalt-to basaltic andesite pyroclasts from central Villarrica and to regional MECs (including a potential monogenetic volcanic system, Caburgua cone #1; Caburgua-Huellemole Group). In all cases, the MIs provide a snapshot of the melt compositions during magma crystallization and/or degassing, which depends on transport conditions. The comprehensive dataset of olivine and major element measurements in melt inclusions, including information on volatile contents, is provided in Appendix A. This section encompasses a detailed account of the analytical approach, precision, and reproducibility for each method, along with complete instrument specifications.~~

~~2.2.2 Bulk analysis of whole rock and~~ The chosen densimeter is able to accommodate a large range of Fermi diad space (102,65 – 105,47 cm^{-1}) that fit the polynomial equation from the previous authors and the used instrumental setting (Robidoux et al., 2018). The MIs not corrected for CO_2 content (no shrinkage bubbles) are used in solubility model from Iacono-Marziano et al. (2012) to calculate isobars, degassing curves and calculate saturation depths. The selected MIs corrected for CO_2 contents (µRaman or alternative model Mimic from Rasmussen et al., 2020) are treated with the same criteria. The degassing curve models are proposed as second alternative to minimum saturation pressure conditions.

3.2.5 Bulk analysis of isotopic noble gases

To explore the source and spatial distribution of magmatic fluids and volatiles, eleven isotopic analyses of He-Ne-Ar were carried out in fluid inclusions (FIs) trapped in olivine crystals from the Villarica volcanic system at the laboratory of INGV, Sezione di Palermo (Italy). These measurements were combined with three other samples previously studied by Lages et al. (2021b), which are part of the same suite of samples. Those FIs occur within pyroclasts of mafic composition for each investigated eruptive event, and the whole-rock composition was also analyzed (Table 2, ~~Appendix B~~Table A.2). Approximately 0.1–1.2 g of unaltered crystals were hand-picked for noble gas analysis. After cleaning in an ultrasonic bath under nitric acid, acetone and deionised water, the crystals were loaded into a single-stage crusher and then baked under pumping to achieve ultra-high vacuum conditions. After crushing, the gas mixture released from the opening of the fluid inclusions was purified in a preparation system capable of separating noble gases from the main components, and then further

Formatted: Indent: First line: 0", Line spacing: Multiple 1.15 li

Formatted: English (Canada)

separating helium from neon from argon (see Rizzo et al., 2018, 2022, Lages et al., 2021a, 2021b for further details).

Two distinct split-flight-tube mass spectrometers (Helix SFT-Thermo) were used to measure the isotopes of helium (^{3}He and ^{4}He) and ^{20}Ne, independently. The $^{3}He/^{4}He$ ratios are stated in ~~R~~Rc/Ra units, where Ra represents the $^{3}He/^{4}He$ of atmospheric air, which is 1.39×10^{-6}. The analytical error for the ^{20}Ne (1σ) was <0.8%. The He-isotope ratio measurements had an uncertainty (1σ) of less than 6%. According to Rizzo et al. (2018), the ^{20}Ne has been corrected for isobaric interferences at m/z values of 20 ($^{40}Ar^{2+}$). A multicollector mass spectrometer (GVI Argus) was used to measure the stable argon isotopes (^{36}Ar, ^{38}Ar, and ^{40}Ar) with an analytical uncertainty of $^{40}Ar/^{36}Ar < 0.2\%$. For the elemental and isotopic recalculations of He, Ne, and Ar, a pre-purified air standard separated into tanks was utilized. The standards for ^{4}He, $^{3}He/^{4}He$, ^{20}Ne and ^{40}Ar had analytical reproducibilities of less than 2.4%, 2.6%, 2.5% and 2.4%, respectively, over a period of >1 year for He and Ne and ~ 4 years for Ar. For He, Ne, and Ar, the typical blanks were at least two orders of magnitude lower than samples and standard signals. Additional information regarding sample preparation and analytical techniques can be found in Rizzo et al. (2018, 2022) and Lages et al. (2021a, 2021b).

Helium isotopic ratios are expressed as Rc/Ra, where Rc is the air-corrected $^{3}He/^{4}He$ ratio of the sample, determined using the $^{4}He/^{20}Ne$ ratios. The Rc/Ra value is equal to:

$[(R_m/R_a)(He/Ne)_m – (He/Ne)_{air}]/[(He/Ne)_m – (He/Ne)_{air}]$, where "m" and "air" denote air and measured values, respectively.

Because the argon concentration in the atmosphere is much higher than in magmatic fluid inclusions, it was necessary to make a correction, which assumes that all of the ^{36}Ar in the gas phase is atmospheric in origin. Thus, in the samples with $^{40}Ar/^{36}Ar>300$, the ^{40}Ar concentration can be corrected as follows:

$^{40}Ar^* = {}^{40}Arm-[({}^{40}Ar/{}^{36}Ar)air \times {}^{36}Arm]$, where m is the measured value and $^{40}Ar^*$ is the corrected isotope value.

~~3~~4. Results

~~3~~4.1 Pyroclastic deposit classification and fragment size distribution

Sample collection and preparation for the study of volatiles in glassy inclusions (e.g. Lloyd et al., 2013) and olivine separation for bulk isotopic noble gas analyses (Robidoux et al., 2021) were carried out to select material below lapilli size granulometry. Both the pyroclasts of this size and the olivine mineral inclusions will have cooled rapidly, providing ideal trapping conditions for the inclusion in the host mineral and avoiding significant loss of H_2O due to H+ diffusion (Gaetani et al., 2012). The study covers all the pyroclastic deposits in both the monogenetic center, MECs and the adjacent Villarrica stratovolcano.

At each site, ~5,000 grams of sample were sieved in the laboratory to retrieve the granulometric parameter and ~~compared~~compare it with datasets in the literature from Silva et al. (2010).

~~————~~ The full description of the samples is resumed by 3 undergraduate theses at Universidad Mayor (Santiago, Chile) and summarized in Table 1, where key statistical parameters for the distribution are the median Mdφ (50), then the graphical standard deviation σ (φ). The comparison with datasets from Silva et al. (2010) classification fields confirm volcanostratigraphy assignations (details in Appendix A). To compare the different volcanic deposits, the median weight was calculated for grain size distribution in pyroclastic flow deposits, surge, and fallout deposits (Table 1, and Appendix A). The Pucón ignimbrite data represents the initial fall deposit (TVP10E; Md = -1.547; σ = 1.449) and matches the onset of the "Pb" eruptive phase of the Pucón ignimbrite (Moreno & Clavero, 2006), preceding the ignimbrite pyroclastic flow sequence (P1, P2; Silva, 2010, and references therein). The extreme end member for well-sorted and small fragments is associated with the Chaimilla and Caburgua fallout deposits (TVP06 series; Md = -0.97 to 1.1; σ = -2.1 to -1.41). Los Nevados, Chaillupén and the March 2015 Villarrica volcanic episode all fall below -2 and -6 Mdφ (50), due to the sampling collection of single lapilli- to bomb-sized fragments.

~~3~~4.2 Bulk rock geochemistry

The major element compositions of the bulk rock samples are presented in Table A.2. The rocks are classified within the CA and HK-CA series fields (Fig. ~~Appendix B~~2a), according to Peccerillo and Taylor (1976) diagram classification as for distinguishing sodium from potassium enrichment between bulk rock and MI datasets. The Villarrica samples are heterogeneous at Pucón, ranging from basaltic to andesitic (SiO_2=52.1–61.9 wt.%, K_2O=0.52–1.47 wt.%, MgO=2.52–4.84 wt.%), homogeneous at Chaimilla (SiO_2=~53.1 wt.%, K_2O=0.57–0.61 wt.%, MgO=3.9–4.0 wt.%), and overlapping in SiO_2 concentration with the lava fountain scoria composition from 2015 (SiO_2=~53.1 wt.%, K_2O=0.77–0.86 wt.%, MgO=5.31–5.56 wt.%). The range of bulk rock compositions for MEC is restricted to basaltic andesites at Los Nevados (SiO_2=52.3–55.1 wt.%, K_2O=0.67–1.02 wt.%, MgO=4.10–4.47 wt.%) and Chaillupén (SiO_2=53.5–54.5 wt.%, K_2O=0.77–0.84 wt.%, MgO=4.84–5.07 wt.%), but strictly basaltic at Caburgua (SiO_2=50.8–51.9 wt.%, K_2O=0.67–0.75 wt.%, MgO=6.87–6.97 wt.%).~~ The rocks are classified within the CA and HK-CA series fields (Fig. 2a).~~

The trace element compositions of the Villarrica rocks show a slight enrichment in light rare earth elements (LREEs), compared to the moderate and heavy rare earth elements, typical of MORB (Appendix C; Hickey-Vargas et al., 2016). The rocks are slightly enriched in large-ion lithophile elements (e.g., Cs, Rb, Sr, and Ba) relative to N-MORB, but overlap with E-MORB. Most samples have low contents of the high field strength elements (HFSE) Ta, Nb, Zr, and Hf. A detailed systematic use of slab-fluid ratios is resumed in Table A.2 as calculated geochemical ratios (Robidoux et al., 2020).

~~3~~4.3 Olivine texture, chemistry, and MI description

The ~~group of~~ olivine crystals from each eruptive event ~~was~~were grouped and characterized for its dominant MI textures ~~by grouping all minerals as populations for each volcanic deposit (Appendix D~~(Table A.3). In this study, olivine hosted MI are referred to as "MI populations" when they are derived from the same layer of a volcanic deposit. The percentage variations of the MI typologies (Robidoux et al., 2018) are classified according to the "cooling rate-dependent" textural description of MI typologies of Roedder (1984). Olivine crystals with no MIs are assigned to “G1”, then the MI typologies are coded, e.g. starting with homogeneous glassy MI assigned to "G2", MI with bubbles to “G3”, and MI with bubbles and oxides to “G4”.

The “G2” group is particularly variable in the Pucón products and reaches the highest percentages in the P2 sequence (>35%). The percentage of olivine crystals with preserved “primary MIs” (G2+G3+G4) also follows a certain order in term of the amount of olivine crystals in each volcanic deposit (considering that all the MI typologies are subject to PEC~~; e.g. Rose-Koga et al., 2021~~); from Pucón Ignimbrite, Chaimilla to the March 2015 eruption, the amount of olivine crystals with primary MIs (G2+G3+G4) decreases, ~~and~~so does the percentage of olivine crystals with vapor bubbles (G3+G4~~)~~ ~~also decreases.~~).

Olivine Mg# are listed in ~~Appendix E~~Table A.4. At the central eruptive vent of Villarrica, the Pucón olivine crystals are Mg-rich ($Fo_{76–88}$), and those from the 2015 eruption have the lowest Fo content (Fo_{76}), although fewer samples were analyzed, which could introduce a sampling bias. The Chaimilla olivine crystals are relatively heterogeneous in composition ($Fo_{76–85}$, Fo_{80}±3%). The MECs show slightly less Mg-rich olivine crystals compared to Villarrica ($Fo_{73–86}$). Los Nevados olivine crystals are heterogeneous in composition ($Fo_{75–85}$, Fo_{80}±3%), Chaillupén has olivine crystals with high Mg# ($Fo_{84–86}$, Fo_{84}±1%), and lastly the Caburgua olivine crystals have heterogeneous Mg# ($Fo_{73–84}$, Fo_{80}±4%).

~~3~~4.4 Major element content from glass inclusions

All original The inclusions shown in Figure 2 have been corrected for post-inclusion crystallisation of the corresponding phenocryst-host according to the method of Robidoux et al. (2021), following the method of Danyushevsky and Plechov, using the Petrolog 3 program (Danyushevsky, L. V., & Plechov, 2011). This data treatment considers the diffusive exchange of FeO and MgO along the walls of the inclusion and the olivine host, and then the loss of Fe from the inclusion into the olivine host. Recalculated compositions from MIs in samples are given in Table A.8 for the corresponding olivine host crystals.

The corrected MI compositions were corrected by adjusting the K_D of the olivine-melt and comparing with bulk rock compositions for the FeO_T/MgO ratio (Fig. 2; Appendix A) (required in 94 samples a range of 0.6–43.5 and average 15.7% olivine to be added. The Fe-loss implied adding a range of 0.3–3.4 and average of 2.1 wt% FeOT. The total Wallace et al., 2021). To correct for Fe-loss, we used Petrolog3 software (Danyushevsky LV, Plechov P. 2011), in addition to adjusting the iron content at equilibrium with the bulk rock MgO. We also considered the Fe^{2+}/Fe^{3+} analyses withassumes that Fe2+ = ΣFe, the best-fit FeOT/MgO regression line (see also Robidoux et al., 2021).was used at each group of volcanic centres, ranging with modelled bulk rock iron species ratios with Fe2+/Fe3+ = 1.1–4.1.

Formatted: Indent: First line: 0.49", Space After: 12 pt, Tab stops: Not at 0.64" + 1.27" + 1.91" + 2.54" + 3.18" + 3.82" + 4.45" + 5.09" + 5.73" + 6.36" + 7" + 7.63" + 8.27" + 8.91" + 9.54" + 10.18"

Formatted: Font color: Auto

The MIs from the Pucón ignimbrite were classified as basaltic to basaltic andesites and a few andesites were observed (SiO_2 = 47.3–62.8 wt.% and K_2O=0.19–1.60 wt.%); data plot in the field from calc-alkaline (CA) to high potassium calc-alkaline (HKCA) rocks (Fig. 2). The Chaimilla series is slightly richer in K_2O (0.20–1.67 wt.%), and olivine-hosted MIs were mostly classified as basaltic andesites, whereas MIs from the 2015 eruption were basaltic-andesites, with lower K_2O contents (0.78–0.91 wt.%).

The total MIs reported by Robidoux et al. (2021), regardless of the specific eruptive center (Gr. 1, 2), were more differentiated in the Los Nevados MEC (47.6–58.0 wt.% SiO_2; 0.27–1.21 wt.% K_2O), with Chaillupén ballistics representing the most felsic MIs (57.1–59.0 wt.%; 0.93–1.35 wt.% K_2O). Caburgua represents intermediate differentiated MIs (51.1–59.3 wt.% SiO_2), but the alkaline content is highest in these samples (0.62–1.78 wt.% K_2O).

34.5 MI description and MI volatile concentrations

A description of the MIs is given in Appendix D (following the classification of Robidoux et al., 2018). The water and carbon dioxide contents of the MIs are reported (mFTIRFTIR in Appendix FTable A.5, SIMS in Appendix GTable A.6, reproductibility test in Appendix HTable A.7). Of the 167 samples analyzed by mFTIRFTIR, 37 were measured by SIMS with no loss or damage during transfer to an indium mount~~ (Appendix H).~~. The ~~%~~ difference in water concentration between ~~mFTIR~~FTIR and SIMS averages 0.5% and 89 ppm for CO_2 content.

~~Of all the volatile analyses~~ In terms of H_2O and CO_2 concentrations from the central eruptive vent of Villarrica (Table 1, ~~Appendix F-G~~Tables A.5-A.6), the Pucón ignimbrite series records the highest ~~volatile contents in terms of the respective~~ H_2O-CO_2 ~~pair~~concentrations (0.1–6.0 wt%; 9–1485 ppm, respectively), followed by the Chaimilla series (0.2–2.4 wt.%; 16–337 ppm; similar to Pioli et al., 2015) and the 2015 eruption (0.1–0.8 wt.%; 160–307 ppm). In the MECs,~~ similarly~~ high values are found for the Los Nevados series (0.1–3.4 wt%; 30–1568 ppm; see also Robidoux et al., 2021), ~~but also~~and lower values in the Chaillupén series (0.3–3.6 wt%; 29–329 ppm), and~~ again~~ in the Caburgua series (0.6–2.8 wt%; 139–677 ppm).

The S, Cl and F concentrations at the Villarrica center (Pucón ignimbrite, Chaimilla and 2015 eruptions) are highly variable (Appendix I) with the following ranges 103–2055 ppm, 11–1330 ppm and, 81–1556 ppm, respectively. The contents of S, Cl, F from MEC samples have the following ranges: 41–2581 ppm, 13–2356 ppm and 59–2473 ppm~~ (anomalous spot >4000 ppm F content susceptible to represent mineral inclusion that contain solid fluorine phase), respectively.~~, respectively (Table A.8).

~~3~~4.6 Raman-corrected CO_2 contents

Twenty-five ~~MI~~MIs with shrinkage bubble (1.3–10.1 vol.%) were analyzed by Raman micro-spectroscopy ~~for~~in order to calculate their CO_2 bubble contents ~~to be calculated according to the presence of two intensity peaks at ~1285 and ~1380 cm^{-1} in the Raman spectrum, defined as Fermi diad peaks (Esposito et al.,~~ starting from their CO_2 ~~2011; Frezzotti et al., 2012; Remigi et al., 2021). The Fermi diad spacing is proportional to the fluid~~ density ~~inside the bubble~~ (see ~~Appendix A), with results varying~~Methodology). In the studied shrinkage bubbles, the measured density varies between 0.004 and 0.911 g/cm^3 ~~in n = 25 shrinkage bubbles (Appendix J). The densimeter was chosen to accommodate larger range of Fermi diad space (102,65 – 105,47 cm^{-1}) that fit the polynomial equation from the previous author and accordingly to instrumental setting used in Robidoux et al.~~(Table A.9). The calculated ~~(2018). The derived~~ (mass / glass density x volume) total CO_2 concentrations (in glass inclusions + bubbles) ~~all~~ range between 207–3336 ppm, using the approach described in Robidoux et al. (2018). ~~according to our µRaman density results on the 25 shrinkage bubbles using the technique of Robidoux et al. (2018). In addition~~Since no heating experiment was performed on the naturally quenched MIs of this study, the calculated CO_2 contents are compared with the contents obtained by the experimental and computational model "Mimic" of Rasmussen et al. (2020). For this reason, n = 31 shrinkage bubbles were measured to correctselected from our MIs measured by EMPA and, according to the model “Mimic”, they resulted into correction on the total CO_2 concentrations to 54–3529 ppm according to the model Mimic of Rasmussen et al. (2021) (Appendix I).. These values exceed the original (uncorrected) shrinkage bubble equivalent glass inclusion CO_2 contents of 24–1413 ppm (Appendix ITable A.8).

34.7 Noble gas isotopes in fluid inclusions

The analytical results of elemental and isotopic measurements of helium, neon and argon, together with other complementary information, are reported in Appendix K. The ^{4}He and ^{20}Ne concentrations measured in FIs from olivine crystals of scoria and ash samples varied from 2.8×10^{-14} to 1.6×10^{-13} mol/g (Fig. 3) and from 1.7×10^{-15} to 1.7×10^{-14} mol/g, respectively. The $^{4}He/^{20}Ne$ ratio was 3.9–42.9, compared to the atmospheric $^{4}He/^{20}Ne$ of 0.318 from Porcelli et al. (2002). The concentrations of ^{40}Ar, ^{38}Ar, and ^{36}Ar ranged from 1.5×10^{-13} to 1.5×10^{-12} mol/g, from 8.9×10^{-17} to 8.8×10^{-16} mol/g and from 4.9×10^{-16} to 5.0×10^{-15} mol/g, respectively. The $^{40}Ar/^{36}Ar$ ratio varied in the range 300–336, whereas the theoretical ratio in the atmospheric is $^{40}Ar/^{36}Ar$~296 (Porcelli et al., 2002). Both $^{40}Ar/^{36}Ar$ and $^{4}He/^{20}Ne$ indicate that all the gases released by the FIs contain an atmospheric component mixed with the magmatic one. The concentrations of $^{40}Ar^*$ vary from 2.6×10^{-15} to 1.1×10^{-13} mol/g. The $^{4}He/^{40}Ar^*$ varies from 1.4 to 10.5, with the typical mantle ratio being considered to be in the range of 1–5 (Marty, 2012).

The $^{3}He/^{4}He$ ratios corrected for atmospheric contamination (expressed as Rc/Ra values) vary between 4.0 and 7.6 Ra (Appendix K; Fig. 3; Table A.10), with a bias with uncorrected $^{3}He/^{4}He$ ratios generally ≤0.2 Ra, except for the sample HCH-2AS that showed a bias of 0.4 Ra.

45. Discussion

45.1 The oldest magmatic batch preserves original magmaMafic magmas degas and transit from deep to shallow volatile contentssaturation levels

At Villarrica, the Pucón ingimbrite is the oldest and best studied postglacial eruption, the least degassed endmember. It is the richest in volatile element contents, but also contains MIs the MIs least affected by parameters of post-entrapment crystallization (PEC; Table 3). This section discusses melt inclusion volatile loss between two large sets of pre-eruptive conditions that chronologically describe Villarrica mafic magmas from the Pucón Ignimbrite (~3.7 kyr) to decadal old central crater conditions.

Before extending to discriminate degassing effects (Appendix L). The and calculating saturation pressures for the different eruptive centers (section 5.2), we first highlight the precision and accuracy of the volatile element contents produced consistent calibration curves using SIMS (Appendix MFig. A.1), and the reproducibility of mFTIRFTIR vs. SIMS gave comparable results (Appendix NFig. A.2; Table A.7), although the mFTIRFTIR technique is limited to larger MIs (>30 µm). The Villarrica and MEC samples were therefore selected for inclusion using both techniques.

At Villarrica, the Pucón ingimbrite contain the highest volatile contain in the MI collection. Despite the presence of vapor bubbles (except for two samples of Pucón and Gr. Los Nevados 1: TVPI5AB and HLN1A3D, respectively) and PEC glasses subject to volatile diffusion, the Pucón series contains the most primitive olivine crystals and MIs recording the highest volatile contents (Fig. 4; Appendices E; F-H). Chaimilla's MI volatile contents are systematically lower than those of the Pucón ignimbrite for similar major element chemistry and cogenetic parental melt differentiation (Figs. 2, 4; Appendix I) while MI volatile contentsA). The SIMS divergence from the 2015 eruptions are even lower (increasing degassing effect during MI entrapment; Fig 4).

Degassing is not the only cause for volatile variation in our samples. In order to evaluate why the Pucón ignimbrite magma represents the least degassed mafic explosive event and highest saturation pressures (Fig. 5a), we examined a series of geochemical parameters for the olivine crystals and grain size distributions of the respective volcanic deposits sampled in this study. There are two main points favoring the preservation of pre-eruptive volatile contents in the Pucón MI series; (i) high juvenile clast cooling rates, and (ii) high natural inclusion quenching rates. Firstly, since the smaller clast size favors a high cooling rate (Loyd et al., 2013), we infer that decreasing cooling rates may explain the variation in PEC-related artefacts observed in MI populations from successive Chaimilla and MEC eruptive sequences. Regardless of the eruptive center, the presence of juvenile clasts with a low degree of crystallinity is likely to indicate high magma cooling rates (e.g. Los Nevados, 1:1Robidoux et al., 2021). Previously, the larger clast sizes had been identified as the most crystalline (Robidoux et al., 2021), but their water contents are the lowest in our collection of MIs (Fig. 5c).line in figure A.2 is mainly due to the precision for smaller MI. The inverse correlation of grain size with MI water content in the same batch of olivine crystals (Fig. 5b, d) may be explained by an increase in H^+ diffusion which affects all of the pyroclasts (Fig. 5b-c). Secondly, we infer that low MI-trapping temperatures favor H^+ diffusion because of MIs with low water contents (Fig. 5bcd). This effect is explicitly related to low quenching rates which affect the solidification of MIs and accentuate the water diffusion into the olivine host (Fig. 5; Appendix L) (e.g. carbon dioxide 1:1 line shifts are greater when MIs contain shrinkage bubbles (Fig. A.2), highlighting the advantages of using smaller beam diameters with the SIMS technique overMassare et al., 2002; Gaetani et al., 2012). The estimated silicate glass transition

Formatted: English (Canada)

temperature (inclusions holding vapor bubble. To estimateGiordano et al., 2008), as well as the trapping MI temperatures (Putirka et al., 2008), in our data set correspond to the highest water contents measured in the MIs (Fig. 5d). Consequently, we would expect high MI quenching rates to prevent H^+ diffusion in samples from the Pucón ignimbrite.

4.2 Post-glacial magma degassing and chronological volatile saturation depth below Villarrica

There is a temporal transition in the pre-eruptive minimum saturation pressure conditions of eruptive centres at Villarrica between paroxysmal inner crater eruptions (C3) and clustered flank MECs in the primitive Villarrica caldera (C1-2) (Moreno and Clavero, 2006). We characterize the variation in saturation depth conditions of magmas that erupted at volcanic centers around Villarrica (Appendix A). The volatile pressures, the volatile element contents and major element compositioncompositions of the MIs are then integrated into the solubility model from Iacono—-Marziano et al. (2012) and WhitamWitham et al. (2012) (Figs. 4, 6; Appendix A). Despite H_2O-CO_2 pairs being the focus of this study, the sulfur and halogen (Cl, F) contents remained constant from the start to finish of the Pucón eruption, as well as the subsequent paroxysmal explosions at Villarrica crater (Fig. 4; Appendix A, I).Table A.8).

Overall integrating observations on MI compositions and olivine hosts, Pucón series contains the most primitive olivine crystals (with Fo content between 76,3 and 88,8 %; Table A.4) and MIs record the highest volatile contents (Fig. 4; Table A.4-A.7). Chaimilla's MI volatile element contents are systematically lower than those of the Pucón ignimbrite MI for similar major element chemistry and cogenetic parental melt differentiation (Figs. 2, 4; Table A.8), while for the 2015 eruption, MI volatile element contents are even lower, representing both strong pre-eruptive degassed melts, and potential post-entrapment effects accentuated by low cooling rates of the transported magmas (Fig. 4). Considering such compositional differences attributed to pre-eruptive conditions, we argue that pre-entrapment degassing is not the only cause of volatile variation in our olivine-hosted MI collection. For example, shallow melt CO_2 saturation may lead to potential gas migration into volatile CO_2-rich transport (Aiuppa et al., 2017), which persists during lava lake bubbling mechanisms (Moussalam et al., 2016). The identified shallow storage conditions may also accentuate lower magma cooling rates and melt differentiation. Such effect is reflected by some lower trapping/ quenching MI temperatures and differentiated MIs series (Chaillupén series; Fig. 2, 5) revealed here with PEC treatment (Appendix A; e.g. Giordano et al., 2008) in MI with low water contents ~<1.5 wt.% (Fig. 5; e.g. Lloyd et al., 2013; Robidoux et al., 2021). Therefore, for some olivine the low MI-trapping temperatures at shallow surface is expected to favor H^+

diffusion because the low quenching rates affect the solidification of MIs and accentuate the water glass/crystal diffusion (Fig. 5; Table 3; e.g. Massare et al., 2002; Gaetani et al., 2012). The Pucón ignimbrite 3,510–3,710 yr B.P. (Silva et al., 2010) records the highest volatile content preserved in MI-hosted olivines among the entire studied volcanic deposits. Consequently, the Pucón ignimbrite potentially represent the deepest degassing processes inducing mafic magma ascent from below Villarrica, but also the oldest magma recharge event (<17.0 km; this study). The

Taking into account the temporal variation of volatile contents through mafic magmatic events at Villarrica, we observe a temporal transition in the pre-eruptive minimum saturation pressure conditions at Villarrica during paroxysmal inner crater eruptions (Fig. 5a). As a result, major subdivisions in the Pucón sequence of "Pb" and "P1 to P3" (Silva et al., 2010) represent individually different equilibrium pressure ranges (Appendix A),, suggesting a polybaric system that may have transported several masses of ascending magmas. AmongThe minimum saturation pressure values were higher during climax of the sub Plinian activity, 4.6±1.6 down to 0.020±0.006 kb while the opening of the eruptive sequence (Pb) represents decompression of volatiles for minimum saturation pressures from 2.15±0.47 to 0.68±0.26 kb (violent strombolian; Table A.8). These pressures are thus traduced in lithostatic depths, resulting among these subsequent batches of Pucón magmas, when to 2.5–7.9±0.63 km (1SD). When the first magma batch reached the surface, as the "Pb" opening sequence, it consisted of hot, volatile-element saturated melts (1070–1140 °C) with saturation occurring between 2.5–7.9±0.63 km (1SD).). This phase has been described as evolving from a strombolian to a more explosive sub Plinian eruptive style (Moreno and Clavero, 2006), and our new dataset shows that it was relatively water-rich (<3.6 wt%) and CO_2-rich (1485 ppm) (corresponding lithostatic depths of 16.6±5.9 km, 1SD) (Figs. 4, 5). This study shows that the last Pucón event (P3) finally recorded ~>1200 ppm CO_2 and a maximum water content of 6.0 wt.%, which is higher than the previous 4.65 wt.% water content estimated with the thermobarometric model by Boschetty et al. (20202022) (Figs. 4, 5, 6).

The subsequent explosive events to the present day at Villarrica Central Crater may also represent the potential for magma transport between deeper and shallower parts of the volcano's plumbing system, according to our assessment of pre-eruptive conditions. The Chaimilla fall deposit 3,180±40 yr B.P. (Costantini et al., 2011) is a key explosive eruptive event that occurred when the crater formed after the collapse of the edifice following the eruption of the Pucón ignimbrite (e.g. "C3" in Moreno and Clavero, 2006). On account of the very thin stratigraphic separation between the Pucón and the Chaimilla subsequent deposit (this study; Pioli et al., 2015), our new MI dataset demonstrate that the Chaimilla mafic magma represents a degassed, cooler (<1018–1134 °C) endmember of the Pucón ignimbrite (ibid. for S; Cl, F contents; AppendixTable A.8); it records lower pressure ranges (0.4–0.9 kb corresponding to the volatile-rich type

2 magma defined by Pioli et al., (2015) (Fo_{81-85} at 1.2 kb). This explosive paroxysm was saturated in volatiles for minimum depths of between 3.24 to 1.68±0.6 km. To illustrate the model for present-day conditions of mafic magma below Villarrica central crater, our new MI dataset indicates volatile saturation to at least 1.7 km in depth (Fig. 6), considering lithospheric depths of 3.1 ±0.6 km for CO_2-corrected MIs (±8.3kb). The crystallization equilibrium during the 2015 Strombolian paroxysm was ≤ 5.3 km (ca.The subsequent Chaimilla event, although similar in composition, is a shallow (1.7–3.2 km) degassed residual melt, produced in similar conditions to the current feeder system (Fig. 2, 4, 6). 1110 °C) (Romero et al., 2022).

Given theThe present-days conditions of mafic magma below Villarrica central crater are still reflecting two ranges of storage depths settings for magma evolutions according to our new MIs dataset. The 2015s low contents of the water-CO_2 pair recorded in this study (0.84 wt.% and 307 ppm, respectively) are consistent with the 2015 volatile contents recorded in the MIs of Cortés et al. (2024) (1.45 wt.% and 468 ppm, respectively), implying that the mafic magmas produced during the last decade at central Villarrica crater are strongly degassed at shallow depths. These volatile element contents are used as starting conditions in our proposed solubility model (Fig. 6) and demonstrate volatile saturation of low-water contents reaches minimum stalling lithostatic depth of 1.7 km. Even our estimated depth results are 3.1 ±0.6 km for CO_2-corrected MIs (±8.3kb) (Fig. 5a), which is still below ≤ 5.3 km crystallization equilibrium during the 2015 Strombolian paroxysm (ca. 1110 °C) (Romero et al., 2022).of Given those solubility model results representing magmas that persist below the present-day central crater (Appendix A; Figs. 4, 5, 6), this investigation does not discard that the volatiles reach saturation conditions at >14.2–16.6 km while the magma starts crystallizing, which could then support the existence of a deeper reservoir until present-days (Cortés et al., 2024). The magma still crystallizes olivine at a depth of 19–35 km (Morgado et al., 2015).2015), for this reason, deeper portion of the plumbing systems could persist and launch new magma batches (Edmonds et al., 2022). This saturation depth range depth range of saturation depths partially matches the ~8–20 km zone of low resistivity detected by by magnetotelluric analysis which could be related to a region that favor melt transport below Villarrica (Pavez et al., 2023). Although

5.2 Deep reservoir inferred from CO_2-rich mafic magmas and volatile saturation at Villarrica and MECs

The eruptions monitored at Villarrica over the chronologicallast decades still record lower minimum solubility pressures for volatile elements (< 5 km), but these conditions are largely reported for lateral volcanic centers according to the comparative data set of our solubility model. Only post-glacial paroxysms such as Pucón ignimbrite have been able to deliver evidence of a deep zone (> 17 km) for subsequent mafic magma recharges, but such characteristics are even met at lateral MECs.

Systematically, the explosive strombolian to violent strombolian eruptions of Chaimilla and subsequent crater explosions after 1971 (Cortés et al., 2024) did not record the deepest saturation levels despite assuming to represent continuous volatile-rich recharge (>12 km; Edmonds et al., 2022). To support this new observation, we present new MI saturation pressure dataset from all MECs and Villarrica paroxysmal eruptive events are fed by magma coming from similar maximum depth estimates (from volatile saturation; ~17–21 km derived from basaltic andesites with similar pre-eruptive P-T compositional evolution of magmatism at Villarrica may illustrate a ; Figs. 5, 6). Nevertheless, nearby as beyond Villarrica flanks, melt-volatile element chemistry transported as magmatic fluids may reflect a distinct compositional evolution during deep transport beyond the 45 km local cortical thickness (Tassara and Echaurren, 2012,). Therefore, before evaluating such causes of heterogeneities in magmatic fluids (section 5.3-5.4), this section shows that pre-eruptive conditions derived from our MI study support consistent deeper regional starting pressures for volatile saturation since the post-Lican Ignimbrite (13.5 ky) Villarrica volcanic event.

At Villarrica central crater, the entrapment pressure of MIs records the same order of lithostatic depth (≤ 21.3 km), somewhat deeper than the 12.7 km vertical extension of the transcrustal system of Cortés et al. (2024) post-1971 eruptive events. This new depth from MI estimate is now closer to the 22.8–29.2±6.1 km bracket of Morgado et al. (2015) at central Villarrica since the 1971 eruption (Fig. 6). This is consistent even with the case of distant Caburgua (~25 km NE Villarrica), the new MIs here are also below the range of 39.0–41.2 ±6.1 km depths recorded by the same authors for Caburgua (CHSEC). Based on our new CO_2 density-µRaman corrections and derived saturation pressures (3.7–4.8 kb; Fig. 5a), we argue that the regional monogenetic cone of Caburgua has equivalent depth pressure from volatile element saturations down to ~13.5–17.3 km, despite ascending through a lithological basement far from the main stratovolcano.

Under these circumstances, a consistent deep magmatic storage or transport zone exist also at a distance from Villarrica even at several MECs (CO_2-rich MIs and Raman MIs corrected collections). This unique storage level can be identified among the complexity of typical trans-crystalline mush systems (TCMS model that persists into the present () but provide even more extended information on lithostatic depths according to our sampling of lateral MECs (e.g., Llaima; DeMaisonneuve et al. 2012; Ruth et al., 2017; Cashman et al., 2017; Boschetty et al., 2022). The Pucón ignimbrite provides petrological evidence for an early mantle-rooted magma that may transport derived melt at shallower depths. Although similar in composition (section 4.3), the subsequent Chaimilla event is a shallow (1.7–3.2 km) degassed residual melt, produced in similar conditions to the current feeder system (Fig. 6) (Blundy and Cashman, 2008).

4.3 Villarrica Caldera: volatile saturation depth and magma composition

Based on our new collection of bulk rock compositions and the dataset from the literature, we propose that Villarrica is a polygenetic system which has the potential to link its deeper central magmatic system to similar depth chambers beneath lateral MECs (Smith and Németh, 2017). The volatile content and degassing conditions reviewed in previous sections suggest a common mantle-derived volatile source, but entrapment pressure of MI that record the same order of lithostatic depths (≤ 21.3 km). On the other hand, compositional heterogeneities of the transported magmas are reported from bulk rock as MI chemistry between the center and the outer region of Villarrica (Fig. 5, 6).

Within the primary structure of Villarrica Caldera 1 structure, there are minor lateral eruptive fieldsalso explosive flank volcanic activity, such as the Los Nevados cones (<2,6002600 yr B.P.), which also tappedtrapped relatively deep magmatic batches (9.2 km; Robidoux et al., 2021) (Fig. 6). Our new compared to present-day crater conditions (maximum 5 km at Villarrica; this study and Cortés et al., 2024) (Fig. 6). The new MI-CO_2 content correction at Los Nevados now gives minimum saturation equivalent depth pressure values of upto saturate volatiles down to 14.2–21.3 km. In comparison, the Chaillupén MEC cones have , a few hundred meters south of the central crater of Villarrica, record saturated volatiles below <1.9 kb, (Avg. °T= 1169±8°C), which results)(Fig. 5a), resulting in a lithostatic depth of < 0.3–6.8 km for melts erupting on the flanks of Villarrica. In contrast, the regional Caburgua (CHSEC) eruption has magmas that crystallized at 32–44 km (1163 °C) according to the model of Morgado et al. (2015). Based on our new CO_2 density-µRaman corrections (3.7–4.8 kb), we argue that the regional monogenetic cone of Caburgua could dissolve volatiles down to ~13.5–17.3 km, despite travelling up through a lithological basement far from the main stratovolcano. southern flanks of Villarrica; such values may still represent deeper sources if MIs are not affected by shallow olivine-MI diffusive H^+ processes.

5.3 Magmatic fluid evidence for atmospheric and crustal-derived components

The magmatic volatiles transported at Villarrica and MECs in this study reflect a common atmospheric component and probably also other South American volcanoes, according to the magmatic fluid tracer $^3He/^4He$ used in this study. The new dataset here provides evidence that the magmatic fluid isotopic noble gas signature is either recycled into the mantle wedge from the subducting slab and/or acquired during magma ponding within the continental crust. To investigate the role of the subducting slab and continental crust on the composition of the degassed magmatic fluids at Villarica, $^{3}He/^{4}He$ measured in Fis from the same MI olivine batches can be used as a useful tracer, coupled with petrological and geodynamic evidence (Fig. 7; Table A.10).

In support of the use of noble gas isotopes as magmatic fluid tracers, Hilton et al. (2002) reported in a global review of arc volcanism that: i) the highest $^{3}He/^{4}He$ ratios measured in arc volcanism are in the MORB range (i.e. 8 ± 1Ra; Graham, 2002); ii) in many arc segments (including central and northern Chile, Peru and Ecuador) the highest $^{3}He/^{4}He$ ratio is below the MORB range (i.e. below 7 Ra); iii) the mean $^{3}He/^{4}He$ ratio of all arc segments is 5.4 ± 1.9 Ra. The basement characteristics involve compositional heterogeneities of the transported magmas in the region of Villarrica according to our new bulk rock composition results (Fig. 7). Since the post-Licán Ingimbrite ~13.5 ky volcanic event (formation of Caldera 1 at Villarrica), the MEC and Villarrica datasets from previous authors demonstrate progressive sedimentary slab assimilation and/or crustal contamination/assimilation (Sr/Y, K_2O content), with a particularly strong evolution towards sediment-metasediment chemical end members with a "slab fluid" signature (Th/La, Sr/Nd, La/Sm, Th/Nb ratios; Fig. 7). This signature is present at Villarrica Los Nevados Gr.1 (HLN1), initial Pucón (Pb) and early Chaimilla deposits, but diminishes through space at distant MEC and monogenetic MEC Caburgua (Fig. 7; see spatial "slab fluid" vector graphically connecting our sample series from low to strong "slab fluid" signature). Diagnostic plots of Th/La vs. La/Ta show that the mantle wedge source of the magma was metasomatised by slab-derived 'supercritical' fluids in the water-rock system (Ferrando et al., 2019), which is graphically explained by the parallel axis vector (Fig. 7b). The exception in our sample set is the granitic lithic contaminated scoria, which could alternatively be explained by enrichment by hydrous silicate melts (Fig. 7b) and/or crustal assimilation (Fig. 7a, c-d). The "slab fluid" signature (Fig. 7d) also diminishes through time toward the intermediate to final eruptive phases (Los Nevados Gr.2 HLN2, Pucón P2-3, Chaimilla, Chaillupén) (Fig. 7). Spatial dissipation of the geochemical signature exists in other polygenetic-related MECs worldwide, for example, between the peripheral cone of Cono Navidad and the Lonquimay stratovolcano, Chile (Gilbert et al., 2014): The most striking difference is observed in MECs from the monogenetic Chichinautzin volcanic field and Popocatepetl, Mexico, where the slab signature decreases away from the stratovolcano (Robidoux et al., 2020). Away from the Villarrica C1-C3 caldera boundaries, this study clearly supports the idea that the regional Caburgua (CHSEC) monogenetic system is representative of how different mantle-crustal conditions affect magma transport, but more importantly, that potential mantle composition heterogeneities exist along the volcanic arc segment in the SVZ (Morgado et al., 2015; Hickey-Vargas et al., 2016; McGee et al., 2017).

4.4 Evidence of atmospheric and crustal-derived components in magmatic fluids

VolatilesVolatiles transported as magmatic fluids are thus of great importance since they are cycled between the atmosphere and the Earth's interior at subduction zones (Zellmer et al., 2015). In this geodynamic setting, slab dehydration at depths of several kilometers can differentially influence the composition of magmatic fluids generated in the overlying wedge. Subduction-related fluids are known to contain higher proportions of atmospheric components than intraplate and mid-oceanic ridge environments (Burnard et al., 1997). According to Hilton et al. (2002) and Sano and Fischer (2013), noble gases found in arc magmatic/hydrothermal fluids and trapped as fluid inclusions (FIs) in minerals are important indicators of the relative contributions of the subducted slab, crust and mantle to the fluids emitted by arc volcanoes. A recent compilation of light noble gases in the South American arc revealed that the average $^{40}Ar/^{36}Ar$ signature of all gas-rocks samples is ~339 (Lages et al., 2021b), which is well below that of MORB (~44,000; Moreira et al., 1998) and close to the atmospheric signature (~296; Porcelli et al., 2002). In rocks from Villarica (our samples and ones from Lages et al., 2021b), the observed $^{40}Ar/^{36}Ar$ ratios in FI range from 300 to 336, supporting the low isotopic signature already found along the South American Arc. Similar inferences can be made from the $^{4}He/^{20}Ne$ range (3.9–50.8), which is not far from the atmospheric ratio (0.318) and well below typical mantle values ($^{4}He/^{20}Ne$>1,000).

These atmospheric Ar-Ne isotopic signatures suggest significant contamination by an atmospheric component, consistent with their comparatively high abundances in air (compared to helium) (Hilton et al., 2002). Although contamination of surface rocks on exposure is possible, though difficult to confirm or exclude, recycling of atmospheric Ar into the mantle by dehydration of subducting oceanic crust has been suggested in several contexts (Matsumoto et al., 2001; Hopp and Ionov, 2011; Di Piazza et al., 2015; Rizzo et al., 2016, 2022; Robidoux et al., 2017, 2020; Battaglia et al., 2018; Lages et al., 2021a, 2021b). At Villarica volcano, the intricate plumbing system and the fact that it formed in a continental crust at about 45 km in depth must also be taken into account (Hickey-Vargas et al., 2016). Considering that the presence of an atmospheric component is a common feature of many volcanoes in the South American volcanic arc, and that most of these volcanoes were built above a continental crust several tens of kilometers in thickness, we can conclude that the atmospheric component in magmatic fluids from Villarica, and probably also other South American volcanoes, is either recycled into the mantle wedge from the subducting slab and/or acquired during magma ponding within the continental crust.

To investigate the role of the subducting slab and continental crust on the composition of the degassed magmatic fluids at Villarica, $^{3}He/^{4}He$ can be used as a useful tracer, coupled with petrological and geodynamic evidence (Fig. 8; Appendix K). In a global review of arc volcanism, Hilton et al. (2002) reported that: i) the highest $^{3}He/^{4}He$

Formatted: English (United Kingdom)

ratios are in the MORB range (i.e. 8 ± 1Ra; Graham, 2002); ii) in many arc segments (including central and northern Chile, Peru and Ecuador) the highest ^{3}He/^{4}He ratio is below the MORB range (i.e. below 7 Ra); iii) the mean ^{3}He/^{4}He ratio of all arc segments is 5.4 ± 1.9 Ra. Recent studies in the Central and South American Volcanic Arcs have provided new measurements of helium isotopes in FisFIs hosted in olivine and pyroxene crystals, adding to our knowledgeclarifying the reasons of ^{3}He/^{4}He variability in those arc volcanoes (Lages et al., 2021a, 2021b; Rizzo et al., 2022 and references therein). The main results of this recent workfindings are that: i) the mantle ^{3}He/^{4}He signature of the Central and South American Volcanic Arcs areis within the MORB range, with the highest values measured in Guatemala (9 Ra, Pacaya volcano) and Colombia (8.8 Ra, Galeras volcano; Fig. 3b); ii) ^{3}He/^{4}He values below the MORB range are indicative of variable crustal contamination, often with an inverse relationship between Rc/Ra values and crustal thickness (this feature is mainly observed in the South American Volcanic Arc; Lages et al., 2021a, 2021b; Barry et al., 2022); iii) there is a progressive decrease in mantle wedge ^{3}He/^{4}He values, with ^{3}He/^{4}He values still within the MORB range, coupled with variations in some key trace element ratios (i.e. Ba/La, Th/La, U/Th), resulting from a higher presence of subducted slab sediment fluids (rich in U and Th, from which radiogenic He is produced). This has been observed particularly in the Central American Volcanic Arc and the SVZ. (Lages et al., 2021a, 2021b; Rizzo et al., 2022 and references therein).

At Villarica volcano, Lages et al. (2021b) reported ^{3}He/^{4}He values as high as 6.7 Ra, which were interpreted as resulting from crustal contamination, although Plank (2005) pointed out that significant quantities of sediment-derived fluids are transferred to arc magmas in northern and southern Chile. In this work, we present new data on ^{3}He/^{4}He

5.4 Olivine FIs record primitive magmatic fluid during Villarrica subplinian climax

The present study completes the Villarrica volcanic complex understanding of the magmatic fluid signature by confirming that ^{4}He contamination is stronger in flank MECs according to systematic variations in FIs ^{3}He/^{4}He. Interestingly, according to MI as bulk rock composition, the systematic FIs ^{4}He contamination is stronger in differentiated-cortically contaminated MECs as Villarrica typical shallow degassed reservoir but is least contaminated in Pucón paroxysm (Fig. 7b, 8b). As to evaluate variation in magmas that are transporting the volatile phases, the bulk rock sample composition of this study does not indicate yet clear systematic correlation with slab fluid markers within the Caldera 1 complex and beyond its boundary (Figs. 7).

By reviewing closely, the local ^{3}He/^{4}He variations and bulk rock composition, we present new helium isotopic data in FIs that mostly reflect the measurements presented by Lages et al. (2021b), except for one sample from Pucón that has a value of 7.6 Ra. This value is almost 1 Ra unit higher than the average values for Villarica volcano, suggesting that the continental crust effectively plays a role in lowering the ^{3}He/^{4}He values of pristine mantle fluids., A helium isotopic signature of 7.6 Ra is still lower than that expected for mantle values. However, in the light of the slab sediment fluid contribution suggested by Plank (2005) for this region of the SVZ and the relation between Rc/Ra and Th/La ratios of Lages et al. (2021b) (Fig. ~~9ab~~7ab), we argue that the ^{3}He/^{4}He signature below Villarica is confirmed to be within the MORB range and that the ~~complex plumbing system of the volcano plays an important role in lowering the mantle ^{3}He/^{4}He. More work is required to investigate the variation in radiogenic ^{4}He (bulk mol/g content) in olivine FIs~~cortical contamination plays an important role in lowering the original mantle ^{3}He/^{4}He. Close examination of the literature dataset with our bulk rock samples (Fig. 7; Table A.2) shows the regional Th/La trend typical of other volcanic centers in the SVZ (Hickey-Vargas et al., 2016; McGee et al., 2017), but it is difficult to observe coupling with the ^{3}He/^{4}He signature at the scale of the Villarrica volcanic complex. It is still not possible to observe this correlation beyond the most distant regional volcanic center, Caburgua, unless larger amounts of FI-hosted olivines are encountered to extend the topic (Appendix A). At a distance from the subducting trench, Caburgua is the only regional MEC that deviates from the slab fluid signature data cluster (Fig. 8; Table A.2), implying that it is significantly modified with respect to asthenospheric slab fluid melting. Chemical tracers of magmatic fluids require systematic studies of regional MECs and stratovolcanoes in the same region (e.g., Quetrupillan and Lanin; Cascades; Mordensky and Wallace, 2018). More work is also required regionally to investigate the variation in radiogenic ^{4}He (bulk mol/g content) in olivine FIs (Lages et al., 2021b and references therein) or fumaroles (Tardani et al., 2017; Barry et al., 2022 and references therein) for the most well-studied polygenetic Villarrica basaltic andesites produced since the postglacial period.

The most interesting observation at the Villarrica polygenetic complex is from the variation of ^{3}He/^{4}He between successions of different scales of explosive eruptions between central and peripheral craters. The presence of ^{4}He contamination at most differentiated products and the ^{3}He/^{4}He values being the highest in olivine-FIs from the most primitive batch of magma at Pucón Ignimbrite (highest post glacial VEI; Table 1). Regardless of the primitive nature of the olivine (olivine Fo% or MI Mg# show no correlation with our Rc/Ra ratios; ~~Fig~~Figs. 3, 8), we suggest that the magmatic ^{3}He ~~content decrease~~ /^{4}He signature decreases with crustal ponding and contamination ~~and~~, when wall rock interaction is more likely to ~~slow down~~decrease cooling rates of large-scale magma reservoirs. This latter conclusion is already supported petrologically by major element MI trends (Fig. 2), bulk-rock ~~REE (Figs. 7)~~trace element tracers and noble gas isotopes (Figs. 3, 8), but could depend on cooling rates and potential magma chamber timescales (e.g. U-~~TH~~Th-He isotopic systematic; Kuritani et al., 2007; McGee et al., ~~2018~~2017). In addition, figure ~~9~~8 details peripheral plumbing system contamination effect as a potential source of recycled ^{4}He increase, which also occurs for bulk rock

Formatted: English (United States)

compositions indicating crustal interaction, such as Sr/Y ratios (> 20), and K_2O (wt%) content (Fig. ~~9cd~~8cd). This correlation is still not systematic for the Th/La ratio~~,~~ (Fig. 7a), used as an indicator of slab sediment fluid contribution (~~Fig 7b). This~~Plank, 2005). When examining chronological evolution of geochemical markers, this geochemical anomaly is only found for the Pucón recharge event (Th/La >0.2) during the post-glacial period of Villarrica and is absent from the Chaimilla-derived magma and other MEC eruptions (Fig. ~~9ab~~8ab; Th/La < 0.2). Thus, ^{4}He contamination is weaker during Plinian events with high VEI explosive paroxysms~~ (Pucón, Chaimilla).~~, and the slab fluid signature is only detected for the parental magma fluids that represent volatile-rich element contents (Pucón). Our olivine FI dataset records the lowest ^{4}He content (g/mol) during the climax eruptive phase (Fig. ~~9). Such~~8). Taken together, such geochemical parameters (olivine MI as Fis compositional trends) thus indicate that less peripheral contamination is expected in basaltic andesites from the parental magma (Pucón) that feed the main explosive paroxysms of Villarrica.

5. Conclusions

For the first time a joint comparison has been made based on melt volatiles, major and noble gases for a polygenetic volcanic system, that of Villarrica in the southern Andes. This study includes new detailed data on volatile saturation depths, with improved analyses for P-T~~-fO_2~~ and compositional pre-eruptive magma conditions based on new geobarometry calculations, and a solubility model that uses novel µRaman dataset to predict the original CO_2 contents in MIs with shrinkage bubbles. ~~Two major petrogenetical problems~~The temporal/spatial portrait of pre-eruptive conditions as magmatic fluid compositional variations were explored within this research providing of the following conclusions:

~~Temporally since the current 2 km-wide caldera formation (post glacial period, see Villarrica Unit 3, <~ 3.7 Kyr AP; Moreno and Clavero, 2006), the~~

I) The~~,~~ Villarrica stratovolcano forms a polygenetic system in which the magmatic volatile content decreases from the Pucón event (3.7 ky) to the ~~March 2015 paroxysm. The~~**last decade at central crater:** According to the new rich MI dataset collected during most documented explosive mafic eruptions from Villarrica, significant volatile content decrease is observed. Since the current 2 km-wide caldera formation (post glacial period, see Villarrica Unit 3, <~ 3.7 Kyr AP; Moreno and Clavero, 2006), close evaluation of MI texture characteristics and major oxide composition/volatile contents

Formatted: Font: Bold

(SIMS, FTIR), demonstrate clear evidence that parental mafic magma of the Pucón eruption might represents the pre-eruptive conditions of the Chaimilla event (<~ 2.6 Kyr AP (Pioli et al., 2015). The actual central crater setting (post 1970s) may favor shallow depth ~<5km degassing as demonstrated with the lava lake CO_2-rich persistent bubbling (Witter et al., 2004; Moussalam et al., 2016; Aiuppa et al., 2017).

II) Lateral, regional as Villarrica volcanic vents confirm evidence of both shallow volatile-poor and deep CO_2-rich magma reservoirs: The presented solubility models in this study confirm lithostatic depth ranges for MI entrapments being within the range of documented crystallized mafic mineral phases from the literature (Morgado et al., 2015; Boschetty et al., 2022; Cortés et al., 2024), but subsequent explosivetwo depth zones are clearly identified at central as peripherical MECs. These key depth zones at Villarrica may represent characteristics like polygenetic volcanic systems in other volcanic arcs (Rasmussen et al., 2022), distinguishing the depth of eruptions record increasing degassing conditions below minimumcontrolled by high CO_2 saturation pressure depth equivalent (<~ 17.0 km). Mafic magma continued to in deep reservoirs from those controlled by water loss in shallow reservoirs. The pre-eruptive conditions evolve vertically from shallow storage depths tosimilarly at present conditions days central crater (<1.7–4.4 km), as well as laterally to nearby MECs (Chaillupén, Los Nevados) from post-glacial times. According to the noble gas study, the magmatic fluid signature varies with continental contamination during vertical transport of the mafic magmas; the isotopic noble gas MORB signature is richer in radiogenic ^4He at the MECs and smaller VEI eruptions (2015) (<6.7), while the high VEI explosive paroxysms of Villarrica (Pucón, Chaimilla) peak at Ra~7.6 (closer to the homogeneous mantle signature along the South American arc of 8–9 Ra; Lages et al., 2021).

Spatially the contrasting background geology (Caburgua) and divergent magmatic chemical source at 25 km from Caldera 1 confirm that the plumbing system architecture is complex and distinct between Villarrica itself and the flank MECs. The noble gas studies combined with bulk rock datasets for Villarrica (Pucón ignimbrite, Chaimilla, 2015 eruptive sequence) and flank eruptive centers (Grupo Los Nevados and Chaillupén and the closest regional MECs at Caburga) confirm a unique ascent and degassing behavior for each successive batch of mafic magma, due to different degrees of interaction with the crust for each one. All basaltic andesitic Villarrica magmas could be derived from a similar parental end member rooted in the asthenospheric mantle, but their typical slab fluid signature and crustal contamination effect, as evidenced by bulk rock chemistry, are variable in the central Villarrica vent and lateral MECs (see Morgado et al., McGee et al., 2017). The new noble gas dataset finally completes the scenario of spatial magma heterogeneities, confirming that the crustal effect of radiogenic ^4He lowers the original $^3He/^4He$ ratio as magma batches pond in the different zones below the Villarrica central crater and its flank MECs plumbing system.

III) The Pucón ignimbrite during its climax phase represents the post-glacial

Formatted: List Paragraph, Numbered + Level: 1 + Numbering Style: I, II, III, … + Start at: 1 + Alignment: Left + Aligned at: 0.25" + Indent at: 0.75"

Formatted: Font: Bold

vestige of parental magmatic fluids at Villarrica and flank MECs: Behind the petrogenetic causes associated to explosive paroxysm with relatively high Rc/Ra in single volcanic complex (Piton de la Fournaise in Boudoire et al., 2020), this study identifies temporal evolution of magmatic differentiation/cortical contamination processes during magma-crustal interactions. The Pucón Ignimbrite holds phases richest in volatile content from MIs and high $CO_2/^3He$ ratio from Fis in olivines for which such petrogenetic effect is much weaker. The $^3He/^4He$ signature attributed by our olivine-hosted Fis collection is lower at the MECs and smaller for VEI eruptions (2015) (<6.7 Ra), while in the high VEI explosive paroxysms of Villarrica (Pucón, Chaimilla) it reaches ~7.6 Ra (closer to a mantle signature of 8–9 Ra expected along the South American arc; Lages et al., 2021). At Villarrica, bulk rock differentiation/contamination is consistent with higher contents of Fis radiogenic ^4He (g/mol), a feature observed consistently in volcanic arcs (Lages et al., 2021a,b).

Acknowledgements

This work is part of ANID, Fondecyt Iniciacion No 11190846 project of Philippe Robidoux (2019–2022). We are grateful to Dra Manuela Nazzari and Dir. Piergiorgio Scarlato for providing access to electron microprobe EMPA at Istituto Nazionale di Geofisica e Vulcanologia Sezione di Roma 1, HP-HT Lab. of Experimental Volcanology and Geophysic. The measurements were also supported by Elisabetta Del Bello and Alessio Pontiselli (INGV-Roma) through participation at the TransNational Access (TNA) in the framework of the EXCITE (Horizon 2020) research infrastructure. Special thanks are sent for Dr. Andrea Rizzo and staff from INGV-Palermo for analysis on noble gases;for Mariano Tantillo and Mariagrazia Misseri from INGV-Palermo, who helped in mineral preparation with their assistance during and noble gases isotope analysis. Special thanks are also addressed to Dra. Simona Ferrando from University of Torino for Raman studies. We address special acknowledgements for Universidad Mayor, Escuela de Geología as Universidad de Chile (Depart. Geología) Bsc.Bsc. students Gloria Díaz, Aaron Sancho, Daniela Pasten and Prof. Clavero for active participation in the 2017–2022 field trips. ER-K, YM and PR deeply thank Nordine Bouden and Johan Villeneuve for their flawless support with the SIMS measurements and for the access to the Nancy preparation lab.

Formatted: Font: Bold

Formatted: List Paragraph, Indent: Left: 0.75"

Formatted: Font: Not Bold

Formatted: Justified, Space After: 10 pt, Line spacing: Multiple 1.15 li, Adjust space between Latin and Asian text, Adjust space between Asian text and numbers, Tab stops: 0.64", Left + 1.27", Left + 1.91", Left + 2.54", Left + 3.18", Left + 3.82", Left + 4.45", Left + 5.09", Left + 5.73", Left + 6.36", Left + 7", Left + 7.63", Left + 8.27", Left + 8.91", Left + 9.54", Left + 10.18", Left

CAPTIONS

Table Captions:

Table 1 – Volcanic deposit characteristics. Sieved and non-sieved volcanic deposits are given geographical coordinates for outcrop location and additional material description. The granulometry is in Phi (φ) size. Fragment size and typology distribution (% per 100 randomly selected clasts) are classified strictly on Fisher (1966) classification in addition to the full spectrum of clastic material typology, classified according to White & Houghton (2006).

Table 2 – Volcanic event references for analysis

Table 3 – Parameters of post entrapment crystallization effects

Figure Captions

Figure 1 – Location of study area. a) Map of the subduction zone, including arc segments from the Central Volcanic Zone (CVZ). White lines are inferred tectonic plate boundaries and arrow indicates direction of subduction. Colored dots are sampled spring sites with Rc values marked using quartile color code. All eruptive centers listed in the Smithsonian Global Volcanism Program's Holocene Volcano List (small black triangles). From north to south, oceanic plate segments with fracture zone abbreviations ending in "FZ" are linked to Juan Fernandez Ridge; Mocha FZ, Valdivia FZ, Chiloe FZ, and Chile Rise FZ. b) Stratigraphic extent of Villarrica Pucón ignimbrite for Units P1, P2 and initial Base Surge Deposit "Pb" (Moreno and Clavero, 2006) as delimited by Silva et al. (2010). The Caldera 1,2 and 3 boundaries (Moreno and Clavero, 2006) are marked, as well as extent of for Chaillupén and Los Nevados Groups (modified from same source; Robidoux et al., 2021), with Caburgua MECs restricted to Caburgua cone #1 sector for lava and pyroclastic deposits (modified from Moreno and Clavero, 2006; Morgado et al., 2015). The Chaimilla fallout deposit (Costantini et al., 2011) and Pucón (Silva et al., 2010) are shown with maximum covered areas from isopach ellipsoid.

Figure 2 – Major element compositions. The post entrapment-corrected MIs (colored circles) with their major element contents as a function of SiO_2 wt.% (see corrected dataset in Appendix I). The bulk rock analyses are shown by colored squares for each

series. Dashed arrows indicate the approximate trend for groundmass crystallization of plagioclase (Pgl In) ± clinopyroxene (Px In). The trapped melts (MIs) evolve via a parental melt differentiation path (red arrow) or post-entrapment crystallization effects (PEC) (orange arrow). The post-entrapment crystallization effects are interpreted in ~~Appendix L~~Table 3. The bulk rock composition of the 1971 Villarrica eruption is represented by grey dots and Caburgua-Huellemolle by a dark grey box (Hickey-Vargas et al., 2002; Morgado et al., 2015).a) K_2O vs SiO_2 classification for the volcanic series, b) CaO wt.%, c) Al_2O_3 wt.% where plagioclase (Pgl-In) is interpreted as residual melt plagioclase crystallization occurring before/during MI entrapment, d) Na_2O wt.% where the dark arrow represents the general tendency toward cogenetic differentiation in all our MI collection, e) MgO wt.%, f) FeO_T wt.%.

Formatted: Font: Bold, Font color: Auto

Figure 3 – The FI helium dataset. $^3He/^4He$ (~~R~~Rc/Ra) ratio vs He concentration (mol/g) collected from analytical data of bulk fluid inclusions (FIs) hosted in olivine (~~Appendix K~~Table A.10). Data from Rizzo et al. (2022) and Lages et al. (2021ab) represent the literature FI data, while our dataset of FIs in olivine crystals is represented by colored symbols (see legend in Figure 2). Samples 2015_B* (Villarrica 2015), HCH2A1* and HCH2A4C* (Chaillupén) are from Lages et al. (2021b) (Appendix K). Data are grouped as combined segments from Central American Volcanic Arc (CAVA; green/black colored symbols) and South American Volcanic Arc (South American VZ; yellow symbols). b) $^3He/^4He$ (~~R~~Rc/R_A) vs He/Ne data ($^4He/^{20}Ne$) in FIs and free gases. Binary mixing (air-magmatic endmember) curves are from Lages et al. (2020, 2021) and calculated using maximum R_C/R_A values for each segment; grey delimits the MORB range (8±1 R_A). The free gas results are classified according to Lages et al. (2021); Free gases of temperature > 100 °C; Free gases 50–100°C; Free gases < 50 °C.

Figure 4 – Volatile contents from melt inclusions at Villarrica. The solubility model is used for PEC-treated MIs only, applying the Iacono-Marziano et al. (2012) model to calculate isobars and degassing curves. a) CO_2 vs H_2O concentrations in melt inclusions from Villarrica. b) CO_2 vs H_2O concentrations in melt inclusions from MECs, c) Raman-corrected degassing paths (closed system degassing). The µRaman density represents all MIs treated with the method ~~of~~described in Robidoux et al. (2018) ~~using our CO_2 density dataset measured by µRaman.~~(Table A.8-A.9). The Mimic model is applied to all MIs measured by EMPA with vapor bubbles ~~producing new~~and allows to obtain the CO_2 content as output CO_2vbg (Rasmussen et al., 2020), which is the result of the calculated reconstruction of the total MI volume and CO_2 content ~~reconstruction~~ using the vapor growth model of the same authors.

Figure 5 – Post entrapment crystallization saturation pressure and temperature conditions: chronological order. a) Saturation pressure (kb~~),~~) of Villarrica center (red) and MECs (blue) for minimum saturation pressures. The µRaman CO_2-corrected MIs represent pressures with ~~bubble~~open circle symbols ~~and~~; the vertical black arrow ~~point~~points connect non-corrected to CO_2-corrected contents~~.~~ (Table A.8). b) H_2O wt% content from MIs is represented by vertical bars for Villarrica center (red) and MECs (blue). H^+ diffusion is interpreted for increasing effect (upward arrow) or decreasing

effect (downward arrow). c) Inaman'sInman's (1952) Md grain size parameter indicate increased negative values for larger pyroclast size. Explosive fragmentation is inferred to cause an increased production of large clast sizes at the sampled outcrop (upward arrow), while clast cooling rate decreases (downward arrow) as clast size increases. d) Temperature (°C), of Villarrica center (red) and MECs (blue). The thin vertical bars are minimum to maximum recorded PEC MIs for this study. The grey colored boxes represent minimum and maximum temperatures (°(°C-) using the Tg output obtained usingfrom the Mimic model (Rasmussen et al. 2020), which is the glass transition temperature (Giordano et al., 2008). The "MI quenching rate" variation (interpreted) subjectively decreases systematically along the same series of olivine crystals (downward arrow). The left vertical axis is used for trapping MI temperatures while right vertical axis is used for quenching MI temperatures.

Figure 6 – Villarrica depth cross section for solubility model. West to east Villarrica profile for magma crystallization conditions (lithostatic pressure gradient is 3.7 0.27 km/kb/km). Vertical scale X2 applies to framework below >2.0 km in depth and vertical scale X1 applies to framework between summit (2847 m.) and 2.0 km in depth. Horizontal distances are not to scale. Minimum saturation depths (km) are shown with an abbreviation code for each eruptive event based on the literature (Moreno and Clavero, 2006); same color code as for Figure 2, except for literature Chaimilla black letters abbreviated to "Ch*" are crystallization depths of ascending magmas from Pioli et al. (2015).The boxes with colored borders are minimum and maximum saturation pressures (Bar) recorded by MI solubility models and thin vertical bars are minimum and maximum ranges for µRaman CO_2 corrections applied in the present study. Arrow intervals stand for vertical interval depths in black characters for Magma reservoir* (Lohmar et al. 2008 and 2012; Delgado et al., 2017; Pavez et al., 2023), Paroxysm source* (2015) (Romero et al., 2022) and Low Resistivity Zone* (Pavez et al., 2023) where partial melts develop.). Villarrica olivine* (19–35 km) and CHSEC olivine (32–44 km) are from Morgado et al. (2015) and represent assumed olivine crystallization depths calculated using pyroxene-olivine geothermobarometry. Background volcanism is modified from Moreno and Clavero (2006). The Rc/Ra dataset is from this study, except for the Villarricа paroxysm source and the duplicate Chaillupén sample (Lages et al., 2021b).

Figure 7 – Magma source evolution from bulk rock. Trace element and REE ratio trends from bulk rock analyses are compared with literature data. The volcanic arc bulk rocks are compositions for volcanic arc segments combining Central + South Volcanic Zone C-SVZ and North Volcanic Zone NVZ (database in Lages et al., 2021a, b) and CAVA (database in Rizzo et al., 2022) samples. The sediments sampled in the trench seawards of the Mocha FZ Fernandez Ridge MVFZ are all datasets from Lucassen et al. (2010) used to estimate the potential contribution of slab sediments. Volcanic eruption event abbreviations for bulk rock data in this study use the same names as in Moreno and Clavero (2006). The tendency for spatial enrichment and temporal decrease of slab fluid signature is illustrated in each figure with blue line toward black arrow. The primitive mantle PM is from Mc Donought et al., (1995). Our primitive

Formatted: Font: Bold, Font color: Auto

Formatted: Centered

starting member is represented by the Pb abbreviation for Pucón opening phase. a) Th/La vs. Sm/La, where OIB, MORB (Sun and McDonough, 1989) and sediment end members are data from Plank (2005), modified from McGee et al. (2017), modified Oceanic Crust value AOC from Jacques et al. (2014), b) Modified diagnostic Th/La vs. La/Ta diagram to distinguish the nature of natural as experimental slab-derived fluids for supercritical fluids and hydrous-silicate melts in the rock-fluid system released by different lithologies at high P-T conditions (Ferrando et al., 2019). Our dataset and the literature samples are filtered only for analyses having MgO > 4 wt%, LOI < 4 wt%, and Na_2O/K_2O < 8 to be plotted in order to consider the most primitive rocks.), c) Sr/Nd vs. La/Sm, where approximate tendency for addition of slab melt (sediment + AOC) to a depleted (BAM) mantle end member composition attributed to Villarrica model modified from Wieser et al. (2018). Our model identifies for crustal contamination and sediment addition, d) Sr/Th vs. Th/Ce, where arrows point to fluid and assimilation tendencies modified from McGee et al. (2017)'s modelling of end-member components using granitoid xenoliths, linked to samples from this study (Pucón P3 lithic fragments).

Figure 8Figure 7 – $^3He/^4He$ for FIs corrected for atmospheric contamination (Rc/Ra) vs magmatic fluid tracers. a) Mean Th/La in subducting sediment columns (Plank, 2014) and volcanic arc trenches (bulk composition added in this paper for CVZ and Lages et al., 2021b; database filtered for < 58 wt% SiO_2). CAVA bulk composition from Rizzo et al., 2022. The same symbols are used as in previous figures for MIs, with the Pucón ignimbrite series Pb considered as the parental magmatic fluid and/or melt for the rest of the dataset produced in this study. B) The $^3He/^4He$ FIs corrected for atmospheric contamination (Rc/Ra) vs. $CO_2/^3He$ systematics for South American fluids calculated as mol/g from mass spectrometry; the crust-mantle binary mixing line (in blue) assumes an Ra of 7.9 (avg. SVZ taken from Lages et al., 2021b). All lines and "X" symbols are fumarole data taken from Lages et al. (2021ab) and CAVA data from Rizzo et al. (2022).

Figure 98 – The influence of geochemical parameters on trapping conditions of $^3He/^4He$ FIs: chronological order. The bulk rock collection is from the following authors: Hickey-Vargas, 1989; Lohmar, 2008 et al. 2012; Costantini et al., 2011; Pioli et al., 2015; Morgado et al., 2015; Hickey-Vargas et al., 2016; McGee et al., 2017). a) Th/La slab sediment ratio used to test possible slab control on the $^3He/^4He$ signature of the mantle wedge along the Andes and Villarrica, b) ^4He content (g/mol) from this study, c) Sr/Y to detect peripheral contamination, from our bulk rock collection and the literature d) K_2O wt.% content from PEC melt inclusions, with minimum and maximum interval bars. The median value is arbitrary, representing the range of minimum and maximum K_2O wt.% contents in the dataset by eruptive event. The bulk rock K_2O wt.% contents are from this study and the literature.

Formatted: Font: Not Bold

Supplementary Material

(File)

Appendix A – Supplementary Material Methodology Review.

(Tables)

Appendix B ~~–~~

Table A.1: Full inclusion reference analysis.

~~Appendix C –~~ Table A.2: Bulk-rock analysis of Villarrica samples.
Major element analysis based on ICPMS. LOI values were corrected for oxygen uptake in the conversion of FeO to Fe_2O_3T (wt.%) in the furnace. Ratios for each eruptive event were reported as FeO/Fe_2O_3. Trace elements and REE were analyzed by inductively coupled plasma mass spectrometry. Trace element ratios are calculated directly from the values in the table (weight ppm ratio) with no normalization to the standards in the literature.

~~Appendix D –~~ Table A.3: Olivine populations statistics.
Classification of olivine series described for the presence of the following MI typologies (Robidoux et al., 2018): G1 (no inclusions), G2 glassy inclusions, G3 glassy inclusions+vapor bubble, G4 glassy inclusions+vapor bubble+spinel, G5 crystallized MIs, GR MI associated with boundary (reentrant or hourglass). Inclusion morphologies and dimensions are given in microns.

~~Appendix E –~~ Table A.4: Electron microprobe analyses of original Villarrica and MEC olivine chemistry.

~~Appendix F –~~ Table A.5: H_2O-CO_2 contents from FTIR.
a) H_2O (as OH^{-1}) at 3,550 cm^{-1} peak, b) CO_2 content as CO_3^{2-} double peak (1,435-1,515 cm^{-1}).

~~Appendix G –~~ Table A.6: Volatile contents from SIMS.

~~Appendix H –~~ Table A.7: ~~mFTIR~~FTIR and SIMS reproducibility.
The selected ~~mFTIR~~FTIR H_2O - CO_2 contents are compared to H_2O SIMS contents with error bars according to respective error sources. The wt. % error for [H_2O] with ~~mFTIR~~FTIR assumes the sum of the following errors: (1) median absorbance (Abs.) graphical error between closest cm^{-1} records on IR spectrum to the left and right of the central peak position 3,550 cm^{-1}, (2) thickness deviation from the wafer (µm), (3) difference between replicate analysis "a" and "b". The STD error on eruption series from the density (g/cm^3) and absorption coefficients (mol^{-1} cm^{-1}) is only considered if EMPA results are not available. The wt. % error for [H_2O] with SIMS uses the %STD error from "^{16}O - ^{1}H" calibration curves. The wt. % error for [CO_3^{2-}] using ~~mFTIR~~FTIR (ppm units) uses the same parameters as for [H_2O] (in wt.%), but graphical error depends on the double peak 1,435 – 1,515 cm^{-1}. The wt. % error for [CO_2] using SIMS (ppm units) uses the %STD error from "^{12}C" calibration curves.

~~Appendix I –~~ Table A.8: Major element and volatile chemistry of Villarrica PEC glass inclusions.

Olivine compositions are given in Fo%, and geothermobarometer results for solubility models are calculated according to Iacono-Marziano et al. (2012). Conditions for Rasmussen method and Raman corrected volatile contents are given for saturation pressure models.

~~Appendix J –~~ Table A.9: Raman CO_2 density and spectrum identification in shrinkage bubbles.

~~Appendix K –~~ Table A.10: Noble gas isotopes.

~~**Appendix L – Table A.11: Parameters of post entrapment crystallization effects.**~~

Formatted: Font color: Auto

Supplementary Material (Figures)

~~Appendix M –~~ Figure A.1: Calibration of SIMS parameters for volatiles species.

The set of standards with known volatile contents are given for a) $^{12}C^-$, b) $^{13}C^-$, c) $^{16}OH^-$, d) $^{19}F^-$, e) $^{32}S^-$, f) $^{35}Cl^-$. A Cs^+ primary beam with a current of 1 nA and an electron gun is used to compensate for charge build-up at the sample surface. A 3-minute pre-sputter with a 30 × 30 µm square raster was applied, then analyses were performed on the 15 to 20 µm spot in the centre of the raster-cleaned area by a mechanical aperture placed at the secondary ion image plane. The resolving mass of ≈7000 (with the contrast aperture at 400 µm, the energy aperture at 40 eV, the entrance slit at 52 µm and the exit slit at 173 µm) meant that complete discrimination of mass interferences was achieved ($^{34}S^1H$ from ^{35}Cl, ^{17}O from $^{16}O^1H$, $^{29}Si^1H$ from ^{30}Si and $^{31}P^1H$ from ^{32}S). We collected signals for ^{12}C (8 seconds), ^{17}O (3 seconds), $^{16}O^1H$ (6 seconds), ^{18}O (3 seconds), ^{19}F (4 seconds), ^{27}Al (3 seconds), ^{30}Si (3 seconds), ^{32}S (4 seconds) and ^{35}Cl (6 seconds; counting times in brackets), with 2 seconds waiting time after each switch of the magnet. This cycle was repeated 10 times for each analysis. One measurement lasted 12 min per spot.

~~Appendix N –~~ Figure A.2: ~~mFTIR~~FTIR and SIMS reproductibility.

Volatile contents of MIs at Villarrica with H_2O concentrations in MIs from Villarrica. The ~~mFTIR~~FTIR H_2O–CO_2 content is compared with the H_2O–CO_2 SIMS content with error bars. The MI samples containing shrinkage bubbles are represented by a circle with a black border. a) Comparison of the H_2O content is shown with error bars from Appendix C. The legend shows the four groups of quartiles used with grey-toned circles and each one represents the following categories in µm^3 unit volume (Vo) Q_1 (3,4E-09 – 8,0E-08); Q_2 (8,0E-08 – 2,5E-07); Q_3 (2,5E-07 – 5,4E-07); Q4 (5,4E-07b – 1,2E-05). b)

Comparison of the CO_2 content is shown with error bars. Each eruption is color coded according to the legend.

References

1. Aiuppa, A., Bitetto, M., Francofonte, V., Velasquez, G., Parra, C.B., Giudice, G., Liuzzo, M., Moretti, R., Moussallam, Y., Peters, N. and Tamburello, G., (2017). A CO2-gas precursor to the March 2015 Villarrica volcano eruption. Geochemistry, Geophysics, Geosystems, 18(6), 2120-2132.
2. Barry, P. H., De Moor, J. M., Chiodi, A., Aguilera, F., Hudak, M. R., Bekaert, D. V., ... & Giovannelli, D. (2022). The helium and carbon isotope characteristics of the Andean Convergent Margin. Frontiers in Earth Science, 10, 897267.
~~2.~~3. Battaglia, A., Bitetto, M., Aiuppa, A., Rizzo, A. L., Chigna, G., Watson, I. M., ... & de Moor, M. J. (2018). The Magmatic gas Signature of Pacaya Volcano, with implications for the volcanic CO2 flux from Guatemala. Geochemistry, Geophysics, Geosystems, 19(3), 667-692.
~~3. Blundy, J., & Cashman, K. (2008). Petrologic reconstruction of magmatic system variables and processes. Reviews in Mineralogy and Geochemistry, 69(1), 179-239.~~
4. Boschetty, F.O., Ferguson, D.J., Cortés, J.A., Morgado, E., Ebmeier, S.K., Morgan, D.J., Romero, J.E. and Silva Parejas, C., (2022). Insights into magma storage beneath a frequently erupting arc volcano (Villarrica, Chile) from unsupervised machine learning analysis of mineral compositions. Geochemistry, Geophysics, Geosystems, 23(4), e2022GC010333.
5. Boudoire, G., Rizzo, A. L., Arienzo, I., & Di Muro, A. (2020). Paroxysmal eruptions tracked by variations of helium isotopes: inferences from Piton de la Fournaise (La Réunion island). Scientific Reports, 10(1), 9809.
6. Brahm, R., Parada, M. A., Morgado, E., Contreras, C., & McGee, L. E. (2018). Origin of Holocene trachyte lavas of the Quetrupillán volcanic complex, Chile: Examples of residual melts in a rejuvenated crystalline mush reservoir. Journal of Volcanology and Geothermal Research, 357, 163-176.
7. Burnard, P., Graham, D., & Turner, G. (1997). Vesicle-specific noble gas analyses of" popping rock": implications for primordial noble gases in Earth. Science, 276(5312), 568-571.
~~8.~~ Cashman, K. V~~. (2004). Volatile controls on magma ascent and eruption. Washington DC American Geophysical Union Geophysical Monograph Series, 150, 109-124.~~
~~9.~~8. ~~Cashman, K. V~~., Sparks, R. S. J., & Blundy, J. D. (2017). Vertically extensive and unstable magmatic systems: a unified view of igneous processes. Science, 355(6331), eaag3055.
9. ~~Cassidy,~~Cortés, J. A., Gertisser, R., & Calder, E. S. (2024). Magma recharge in persistently active basaltic–andesite systems and its geohazards implications: the case of Villarrica volcano, Chile. International Journal of Earth Sciences, 1-19.

Formatted: Italian (Italy)

Formatted: English (United Kingdom)

~~10. M., Manga, M., Cashman, K., & Bachmann, O. (2018). Controls on explosive-effusive volcanic eruption styles. Nature communications, 9(1), 2839.~~
~~11.~~10. Costantini, L., Pioli, L., Bonadonna, C., Clavero, J., & Longchamp, C. (2011). A late Holocene explosive mafic eruption of Villarrica volcano, Southern Andes: The Chaimilla deposit. Journal of Volcanology and Geothermal Research, 200(3-4), 143-158.
~~12.~~Danyushevsky, L. V., ~~Leslie, R. A., Crawford, A. J., & Durance, P. (2004). Melt inclusions in primitive olivine phenocrysts: the role of localized reaction processes in the origin of anomalous compositions. Journal of Petrology, 45(12), 2531-2553.~~
~~13.~~11. ~~Danyushevsky, L. V.,~~ & Plechov, P. (2011). Petrolog3: Integrated software for modeling crystallization processes. Geochemistry, Geophysics, Geosystems, 12(7).
~~14.~~12. Delgado, F., Pritchard, M. E., Ebmeier, S., González, P., & Lara, L. (2017). Recent unrest (2002–2015) imaged by space geodesy at the highest risk Chilean volcanoes: Villarrica, Llaima, and Calbuco (Southern Andes). Journal of Volcanology and Geothermal Research, 344, 270-288.
~~15.~~13. De Maisonneuve, C. B., Dungan, M. A., Bachmann, O., & Burgisser, A. (2012). Insights into shallow magma storage and crystallization at Volcán Llaima (Andean southern volcanic zone, Chile). Journal of Volcanology and Geothermal Research, 211, 76-91.
~~16.~~14. DeMets, C. (2001). A new estimate for present-day Cocos-Caribbean plate motion: Implications for slip along the Central American volcanic arc. Geophysical research letters, 28(21), 4043-4046. https://doi.org/10.1029/2001GL013518
~~17. Di Piazza, A., Rizzo, A. L., Barberi, F., Carapezza, M. L., De Astis, G., Romano, C., & Sortino, F. (2015). Geochemistry of the mantle source and magma feeding system beneath Turrialba volcano, Costa Rica. Lithos, 232, 319-335.~~
~~18.~~15. Edmonds, M., Liu, E. J., & Cashman, K. V. (2022). Open-vent volcanoes fuelled by depth-integrated magma degassing. Bulletin of Volcanology, 84(3), 28.
~~19.~~16. Esposito, R., Bodnar, R.J., Danyushevsky, L.V., De Vivo, B., Fedele, L., Hunter, J., Lima, A. and Shimizu, N., (2011). Volatile evolution of magma associated with the Solchiaro eruption in the Phlegrean Volcanic District (Italy). Journal of Petrology, 52(12), 2431-2460.
~~20. Fall, A., Tattitch, B., & Bodnar, R. J. (2011). Combined microthermometric and Raman spectroscopic technique to determine the salinity of H2O–CO2–NaCl fluid inclusions based on clathrate melting. Geochimica et Cosmochimica Acta, 75(4), 951-964.~~
~~21.~~17. Ferrando, S., Petrelli, M., & Frezzotti, M. L. (2019). Gradual and selective trace-element enrichment in slab-released fluids at sub-arc depths. Scientific Reports, 9(1), 16393.
~~22.~~18. Frezzotti, M. L., Tecce, F., & Casagli, A. (2012). Raman spectroscopy for fluid inclusion analysis. Journal of Geochemical Exploration, 112, 1-20.
~~23.~~19. Gaetani, G. A., O'Leary, J. A., Shimizu, N., Bucholz, C. E., & Newville, M. (2012). Rapid reequilibration of H2O and oxygen fugacity in olivine-hosted melt inclusions. Geology, 40(10), 915-918.
~~24. Geiger, H., Troll, V. R., Jolis, E. M., Deegan, F. M., Harris, C., Hilton, D. R., &~~

Formatted: English (United States)

Formatted: Italian (Italy)

~~Freda, C. (2018). Multi-level magma plumbing at Agung and Batur volcanoes increases risk of hazardous eruptions. Scientific Reports, 8(1), 10547.~~

~~25. Gherardi, F., Barsanti, M., Principe, C., & Magro, G. (2022). Helium isotopes in Plinian and inter-Plinian volcanic products of Vesuvius, Italy. Frontiers in Earth Science, 10, 1011203.~~

~~26. Gilbert, D., Freundt, A., Kutterolf, S., & Burkert, C. (2014). Post-glacial time series of explosive eruptions and associated changes in the magma plumbing system of Lonquimay volcano, south central Chile. International Journal of Earth Sciences, 103, 2043-2062.~~

20. GiorGiordano, D., Russell, J. K., & Dingwell, D. B. (2008). Viscosity of magmatic liquids: a model. Earth and Planetary Science Letters, 271(1-4), 123-134.

21. Giuliani, L., Iezzi, G., & Mollo, S. (2020). Dynamics of volcanic systems: physical and chemical models applied to equilibrium versus disequilibrium solidification of magmas. Dynamic Magma Evolution, 99-132.

~~27.~~22. Graham, D. W. (2002). Noble gas isotope geochemistry of mid-ocean ridge and ocean island basalts: Characterization of mantle source reservoirs. Reviews in mineralogy and geochemistry, 47(1), 247-317. https://doi.org/10.2138/rmg.2002.47.8

~~28.~~23. Heinrich, M., Cronin, S. J., Torres-Orozco, R., Colombier, M., Scheu, B., & Pardo, N. (2020). Micro-porous pyroclasts reflecting multi-vent basaltic-andesite Plinian eruptions at Mt. Tongariro, New Zealand. Journal of Volcanology and Geothermal Research, 401, 106936.

~~29. Hermann, J., & Rubatto, D. (2009). Accessory phase control on the trace element signature of sediment melts in subduction zones. Chemical Geology, 265(3-4), 512-526.~~

~~30.~~24. Hickey-Vargas, R., Sun, M., & Holbik, S. (2016). Geochemistry of basalts from small eruptive centers near Villarrica stratovolcano, Chile: evidence for lithospheric mantle components in continental arc magmas. Geochimica et Cosmochimica Acta, 185, 358-382.

~~31.~~25. Hickey-Vargas, R., Roa, H. M., Escobar, L. L., & Frey, F. A. (1989). Geochemical variations in Andean basaltic and silicic lavas from the Villarrica-Lanin volcanic chain (39.5 S): an evaluation of source heterogeneity, fractional crystallization and crustal assimilation. Contributions to Mineralogy and Petrology, 103, 361-386.

~~32.~~26. Hilton, D. R., Fischer, T. P., & Marty, B. (2002). Noble gases and volatile recycling at subduction zones. Reviews in mineralogy and geochemistry, 47(1), 319-370.

~~33. Hopp, J., & Ionov, D. A. (2011). Tracing partial melting and subduction-related metasomatism in the Kamchatkan mantle wedge using noble gas compositions. Earth and Planetary Science Letters, 302(1-2), 121-131.~~

~~34.~~27. Iacono-Marziano, G., Morizet, Y., Le Trong, E., & Gaillard, F. (2012). New experimental data and semi-empirical parameterization of H2O–CO2 solubility in mafic melts. Geochimica et Cosmochimica Acta, 97, 1-23.

~~35. Jacques, G., Hoernle, K., Gill, J., Wehrmann, H., Bindeman, I., & Lara, L. E. (2014). Geochemical variations in the Central Southern Volcanic Zone, Chile (38–43 S): the role of fluids in generating arc magmas. Chemical Geology, 371, 27-45.~~

36.28. Jarrard, R. D. (1986). Relations among subduction parameters. Reviews of Geophysics, 24(2), 217-284.

37. Kessel, R., Schmidt, M. W., Ulmer, P., & Pettke, T. (2005). Trace element signature of subduction-zone fluids, melts and supercritical liquids at 120–180 km depth. Nature, 437(7059), 724-727.

38.29. Kuritani, T., Yokoyama, T., & Nakamura, E. (2007). Rates of thermal and chemical evolution of magmas in a cooling magma chamber: A chronological and theoretical study on basaltic and andesitic lavas from Rishiri Volcano, Japan. Journal of Petrology, 48(7), 1295-1319.

39.1. Lages, J., Rizzo, A.L., Aiuppa, A., Samaniego, P., Le Pennec, J.L., Ceballos, J.A., Narvaez, P.A., Moussallam, Y., Bani, P., Schipper, C.I. and Hidalgo, S., (2021a). Noble gas magmatic signature of the Andean Northern Volcanic Zone from fluid inclusions in minerals. Chemical Geology, 559, 119966. https://doi.org/10.1016/j.chemgeo.2020.119966

40.30. Lages, J., Rizzo, A., L., Aiuppa, A., Robidoux, P., Aguilar Contreras, R., Apaza Choquehuayta, F. E., & Masías Alvarez, P. J. (2021b2021a). Crustal controls on light noble gas isotope variability along the Andean Volcanic Arc. uri: issn: 2410339X. https://doi.org/10.1016/j.chemgeo.2020.119966https://doi.org/10.1016/j.chemgeo.2020.119966

41. Lehr, J., Bredemeyer, S., Rabbel, W., Thorwart, M., & Franco, L. (2022). Comparative interevent time statistics of degassing and seismic activity at Villarrica Volcano (Chile). Authorea. May 07, 2020.

31. Lages, J., Rizzo, A.L., Aiuppa, A., Samaniego, P., Le Pennec, J.L., Ceballos, J.A., Narvaez, P.A., Moussallam, Y., Bani, P., Schipper, C.I. and Hidalgo, S., (2021b). Noble gas magmatic signature of the Andean Northern Volcanic Zone from fluid inclusions in minerals. Chemical Geology, 559, 119966. https://doi.org/10.1016/j.chemgeo.2020.119966

42.32. Liu, E.J., Wood, K., Mason, E., Edmonds, M., Aiuppa, A., Giudice, G., Bitetto, M., Francofonte, V., Burrow, S., Richardson, T. and Watson, M., (2019). Dynamics of outgassing and plume transport revealed by proximal unmanned aerial system (UAS) measurements at Volcán Villarrica, Chile. Geochemistry, Geophysics, Geosystems, 20(2), 730-750.

43.33. Lloyd, A. S., Plank, T., Ruprecht, P., Hauri, E. H., & Rose, W. (2013). Volatile loss from melt inclusions in pyroclasts of differing sizes. Contributions to Mineralogy and Petrology, 165, 129-153.

44.34. Lohmar, S., Parada, M., Gutiérrez, F., Robin, C., & Gerbe, M. C. (2012). Mineralogical and numerical approaches to establish the pre-eruptive conditions of the mafic Licán Ignimbrite, Villarrica Volcano (Chilean Southern Andes). Journal of Volcanology and Geothermal Research, 235, 55-69.

45. Lohmar, S. (2008). Petrologia de las ignimbritas Lican y Pucon (Volcan Villarrica) y Curacautín (Volcan Llaima) en los Andes del sur de Chile.

46. Lucassen, F., Wiedicke, M., & Franz, G. (2010). Complete recycling of a magmatic arc: evidence from chemical and isotopic composition of Quaternary trench sediments in Chile (36–40 S). International Journal of Earth Sciences, 99, 687-701.

Formatted: Spanish (Chile)

Formatted: Spanish (Chile)

Formatted: Spanish (Chile)

47.1. Marsh, B. D. (2015). Magma chambers. In The encyclopedia of volcanoes (pp. 185-201). Academic Press.

48.35. Marty, B. (2012). The origins and concentrations of water, carbon, nitrogen and noble gases on Earth. Earth and Planetary Science Letters, 313, 56-66.

36. Mason, E. M., Edmonds, M., Hammond, S., Ilyinskaya, E., Jenner, F., Kunz, B., ... & Velasquez, G. (2024). Chalcophile element degassing at an active continental arc volcano. Geochimica et Cosmochimica Acta, 367, 72-86.

49.37. Massare, D., Métrich, N., & Clocchiatti, R. (2002). High-temperature experiments on silicate melt inclusions in olivine at 1 atm: inference on temperatures of homogenization and H2O concentrations. Chemical Geology, 183(1-4), 87-98.

50. Matsumoto, T., Chen, Y., & Matsuda, J. I. (2001). Concomitant occurrence of primordial and recycled noble gases in the Earth's mantle. Earth and Planetary Science Letters, 185(1-2), 35-47.

51.38. McGee, L.E., Brahm, R., Rowe, M.C., Handley, H.K., Morgado, E., Lara, L.E., Turner, M.B., Vinet, N., Parada, M.Á. and Valdivia, P., (2017). A geochemical approach to distinguishing competing tectono-magmatic processes preserved in small eruptive centres. Contributions to Mineralogy and Petrology, 172, 1-26.

52. McGee, L., Morgado, E., Brahm, R., Parada, M.Á., Vinet, N., Lara, L.E., Flores, A., Turner, M., Handley, H. and Nowell, G., (2019). Stratigraphically controlled sampling captures the onset of highly fluid-fluxed melting at San Jorge volcano, Southern Volcanic Zone, Chile. Contributions to Mineralogy and Petrology, 174, 1-24.

39. Moitra, P., Gonnermann, H. M., Houghton, B. F., & Tiwary, C. S. (2018). Fragmentation and Plinian eruption of crystallizing basaltic magma. *Earth and Planetary Science Letters*, *500*, 97-104.

53.40. Mordensky, S. P., & Wallace, P. J. (2018). Magma storage below Cascades shield volcanoes as inferred from melt inclusion data: A comparison of long-lived and short-lived magma plumbing systems. Journal of Volcanology and Geothermal Research, 368, 1-12.

54.41. Moreira, M. A., & Kurz, M. D. (2013). Noble gases as tracers of mantle processes and magmatic degassing. The noble gases as geochemical tracers, 371-391.

55.42. Moreno, H., & Clavero, J. R. (2006). Geología del volcán Villarrica: Regiones de la Araucanía y de Los Lagos. Servicio Nacional de Geología y Minería, Subdirección Nacional de Geología.

56.43. Morgado, E., Parada, M. A., Contreras, C., Castruccio, A., Gutiérrez, F., & McGee, L. E. (2015). Contrasting records from mantle to surface of Holocene lavas of two nearby arc volcanic complexes: Caburgua-Huelemolle Small Eruptive Centers and Villarrica Volcano, Southern Chile. Journal of Volcanology and Geothermal Research, 306, 1-16.

57.44. Moussallam, Y., Lee, H.J., Ding, S., DeLessio, M., Everard, J.L., Spittle, E., Lu, G., Baur, J., Glazer, E., Peccia, A. and Zaman, M., (2023). Temperature of the Villarrica lava lake from 1963 to 2015 constrained by phase-equilibrium and a new glass geothermometer for Basaltic Andesites. Journal of Petrology, 64(2),

Formatted: Left, Tab stops: Not at 0.64" + 1.27" + 1.91" + 2.54" + 3.18" + 3.82" + 4.45" + 5.09" + 5.73" + 6.36" + 7" + 7.63" + 8.27" + 8.91" + 9.54" + 10.18"

egad003.

~~58.~~45. Moussallam, Y., Bani, P., Curtis, A., Barnie, T., Moussallam, M., Peters, N., Schipper, C.I., Aiuppa, A., Giudice, G., Amigo, Á. and Velasquez, G., (2016). Sustaining persistent lava lakes: Observations from high-resolution gas measurements at Villarrica volcano, Chile. Earth and Planetary Science Letters, 454, 237-247.

~~59. Nuccio, P. M., Paonita, A., Rizzo, A., & Rosciglione, A. (2008). Elemental and isotope covariation of noble gases in mineral phases from Etnean volcanics erupted during 2001–2005, and genetic relation with peripheral gas discharges. Earth and Planetary Science Letters, 272(3-4), 683-690.~~

46. Moussallam, Y., Towbin, W. H., Plank, T., Bureau, H., Khodja, H., Guan, Y., ... & Rose-Koga, E. F. (2024). ND70 Series Basaltic Glass Reference Materials for Volatile Element (H2O, CO2, S, Cl, F) Measurement and the C Ionisation Efficiency Suppression Effect of Water in Silicate Glasses in SIMS. Geostandards and Geoanalytical Research.

47. Muñoz, F. A., Peña-Cortés, F., Inostroza-Matus, C., & Callejas, R. C. (2024). El riesgo en torno al volcán Villarrica en Chile: Exposición, peligrosidad e instrumentos de gestión del riesgo en Coñaripe, Licán Ray, Pucón y Villarrica. *Revista de Estudios Latinoamericanos sobre Reducción del Riesgo de Desastres REDER*, *8*(1), 115-130.

~~60.~~48. Pavez, M., Brasse, H., Kapinos, G., Díaz, D., Lara, L. E., & Schill, E. (2023). Magma storage and transfer in the Villarrica volcanic chain, South Chile: MT insights into volcano-tectonic interactions. Journal of Volcanology and Geothermal Research, 439, 107832.

~~61.~~ Plank, T~~., & Langmuir, C. H. (1998). The chemical composition of subducting sediment and its consequences for the crust and mantle. Chemical geology, 145(3-4), 325-394.~~

~~62.~~49. ~~Plank, T~~. (2005). Constraints from thorium/lanthanum on sediment recycling at subduction zones and the evolution of the continents. Journal of Petrology, 46(5), 921-944.

50. Plank, T. (2014). The chemical composition of subducting sediments. Elsevier.

~~63.~~51. Pioli, L., Scalisi, L., Costantini, L., Di Muro, A., Bonadonna, C., & Clavero, J. (2015). Explosive style, magma degassing and evolution in the Chaimilla eruption, Villarrica volcano, Southern Andes. Bulletin of Volcanology, 77, 1-14.

~~64.~~52. Porcelli, D., Ballentine, C.J. and Wieler, R. (2002). An introduction to noble gas geochemistry and cosmochemistry. Rev. Min. Geoch. 47: 1-18.

53. Putirka, K. D. (2008). Thermometers and barometers for volcanic systems. Reviews in mineralogy and geochemistry, 69(1), 61-120.

~~65.~~54. Rasmussen, D. J., Plank, T. A., Wallace, P. J., Newcombe, M. E., & Lowenstern, J. B. (2020). Vapor-bubble growth in olivine-hosted melt inclusions. American Mineralogist, 105(12), 1898-1919.

55. Rasmussen, D. J., Plank, T. A., Roman, D. C., & Zimmer, M. M. (2022). Magmatic water content controls the pre-eruptive depth of arc magmas. Science, 375(6585), 1169-1172.

~~66.~~56. Remigi, S., T. Mancini, S. Ferrando, M.-L. Frezzotti (2021).

Formatted: English (United States)

Interlaboratory Application of Raman CO 2 Densimeter Equations: Experimental Procedure and Statistical Analysis Using Bootstrapped Confidence Intervals. Applied Spectroscopy, 75(7), 867-881.

67.57. Rizzo, A. L., Robidoux, P., Aiuppa, A., & Di Piazza, A. (2022). 3He/4He Signature of Magmatic Fluids from Telica (Nicaragua) and Baru (Panama) Volcanoes, Central American Volcanic Arc. Applied Sciences, 12(9), 4241.

68.58. Rizzo, A.L., Pelorosso, B., Coltorti, M., Ntaflos, T., Bonadiman, C., Matusiak-Małek, M., Italiano, F. and Bergonzoni, G., (2018). Geochemistry of noble gases and CO2 in fluid inclusions from lithospheric mantle beneath Wilcza Góra (Lower Silesia, southwest Poland). Frontiers in Earth Science, 6, 215

69.59. Robidoux, P., Aiuppa, A., Rotolo, S. G., Rizzo, A. L., Hauri, E. H., & Frezzotti, M. L. (2017). Volatile contents of mafic-to-intermediate magmas at San Cristóbal volcano in Nicaragua. Lithos, 272, 147-163.

70.60. Robidoux, P., Frezzotti, M. L., Hauri, E. H., & Aiuppa, A. (2018). Shrinkage bubbles: the C–O–H–S magmatic fluid system at San Cristóbal volcano. Journal of Petrology, 59(11), 2093-2122.

71.61. Robidoux, P., Roberge, J., & Adams, C. (2020). Spatial visualization of geochemical data: application to the Chichinautzin volcanic field, Mexico. In Updates in Volcanology-Transdisciplinary Nature of Volcano Science. IntechOpen.

72.62. Robidoux, P., Pastén, D., Levresse, G., Diaz, G., & Paredes, D. (2021). Volatile content implications of increasing explosivity of the strombolian eruptive style along the fracture opening on the NE Villarrica Flank: Minor eruptive centers in the Los Nevados Group 2. Geosciences, 11(8), 309.

73.63. Rose-Koga, E.F., Bouvier, A.S., Gaetani, G.A., Wallace, P.J., Allison, C.M., Andrys, J.A., De La Torre, C.A., Barth, A., Bodnar, R.J., Gartner, A.B. and Butters, D. (2021). Silicate melt inclusions in the new millennium: a review of recommended practices for preparation, analysis, and data presentation. Chemical Geology, 570, 120145.

74.64. Roedder, E. (1984). Volume 12: fluid inclusions. Reviews in mineralogy, 12, 644.

75.65. Romero, J.E., Morgado, E., Pisello, A., Boschetty, F., Petrelli, M., Cáceres, F., Alam, M.A., Polacci, M., Palma, J.L., Arzilli, F. and Vera, F. (2022). Pre-eruptive Conditions of the 3 March 2015 Lava Fountain of Villarrica Volcano (Southern Andes). Bulletin of Volcanology, 85(1), 2.

76. Roulleau, E., Tardani, D., Sano, Y., Takahata, N., Vinet, N., Bravo, F., Muñoz, C. and Sanchez, J., (2016). New insight from noble gas and stable isotopes of geothermal/hydrothermal fluids at Caviahue-Copahue Volcanic Complex: Boiling steam separation and water-rock interaction at shallow depth. Journal of Volcanology and Geothermal Research, 328, 70-83.

77.66. Ruth, D. C., Cottrell, E., Cortes, J. A., Kelley, K. A., & Calder, E. S. (2016). From passive degassing to violent Strombolian eruption: the case of the 2008 eruption of Llaima volcano, Chile. Journal of Petrology, 57(9), 1833-1864.

78. Sano, Y., & Marty, B. (1995). Origin of carbon in fumarolic gas from island arcs. Chemical Geology, 119(1-4), 265-274.

79.67. Sano, Y., & Fischer, T. P. (2013). The analysis and interpretation of noble gases in modern hydrothermal systems. The noble gases as geochemical

Formatted: English (United States)

Formatted: English (United States)

Formatted: English (United States)

Formatted: Italian (Italy)

tracers, 249-317.

~~80.~~68. Silva Parejas, C., Druitt, T. H., Robin, C., Moreno, H., & Naranjo, J. A. (2010). The Holocene Pucón eruption of Volcán Villarrica, Chile: deposit architecture and eruption chronology. Bulletin of volcanology, 72, 677-692.

~~81.~~69. Smith, I. E. M., & Németh, K. (2017). Source to surface model of monogenetic volcanism: a critical review. Geological Society, London, Special Publications, 446(1), 1-28.

~~82.~~70. Stern, C. R. (2004). Active Andean volcanism: its geologic and tectonic setting. Revista geológica de Chile, 31(2), 161-206. Revista Geológica de Chile, Vol. 31, No. 2, p http://dx.doi.org/10.4067/S0716-02082004000200001

71. Stimac, J., Goff, F., & Goff, C. J. (2015). Intrusion-related geothermal systems. In The encyclopedia of volcanoes (pp. 799-822). Academic Press.

~~83.~~72. Stix, J. (2007). Stability and instability of quiescently active volcanoes: The case of Masaya, Nicaragua. Geology, 35(6), 535-538.

73. Tardani, D., Reich, M., Roulleau, E., Takahata, N., Sano, Y., Pérez-Flores, P., ... & Arancibia, G. (2016). Exploring the structural controls on helium, nitrogen and carbon isotope signatures in hydrothermal fluids along an intra-arc fault system. Geochimica et Cosmochimica Acta, 184, 193-211.

~~84.~~74. Tassara, A., & Echaurren, A. (2012). Anatomy of the Andean subduction zone: three-dimensional density model upgraded and compared against global-scale models. Geophysical Journal International, 189(1), 161-168.

75. ~~Valentine, G. A., & Connor, C. B~~Vetere, F., Iezzi, G., Behrens, H., Holtz, F., Ventura, G., Misiti, V., ... & Dietrich, M. (2015). Glass forming ability and crystallisation behaviour of sub-alkaline silicate melts. Earth-science reviews, 150, 25-44.

~~85. . (2015). Basaltic volcanic fields. In The encyclopedia of volcanoes (pp. 423-439). Academic Press.~~

~~86.~~76. Wallace, P. J., Plank, T., Bodnar, R. J., Gaetani, G. A., & Shea, T. (2021). Olivine-hosted melt inclusions: a microscopic perspective on a complex magmatic world. Annual Review of Earth and Planetary Sciences, 49, 465-494.

~~87.~~77. Watt, S. F., Pyle, D. M., & Mather, T. A. (2013). The volcanic response to deglaciation: Evidence from glaciated arcs and a reassessment of global eruption records. Earth-Science Reviews, 122, 77-102.

~~88. Wieser, P. E., Turner, S. J., Mather, T. A., Pyle, D. M., Savov, I. P., & Orozco, G. (2019). New constraints from Central Chile on the origins of enriched continental compositions in thick-crusted arc magmas. Geochimica et Cosmochimica Acta, 267, 51-74.~~

78. Witham, F., Blundy, J., Kohn, S. C., Lesne, P., Dixon, J., Churakov, S. V., & Botcharnikov, R. (2012). SolEx: A model for mixed COHSCl-volatile solubilities and exsolved gas compositions in basalt. Computers & Geosciences, 45, 87-97.

~~89.~~79. Witter, J. B., Kress, V. C., Delmelle, P., & Stix, J. (2004). Volatile degassing, petrology, and magma dynamics of the Villarrica Lava Lake, Southern Chile. Journal of volcanology and geothermal research, 134(4), 303-337.

~~90.~~80. Zellmer, G. F., Edmonds, M., & Straub, S. M. (2015). Volatiles in subduction zone magmatism. Geological Society, London, Special Publications, 410(1), 1-17.

Formatted: Italian (Italy)

Formatted: Left, Tab stops: Not at 0.64" + 1.27" + 1.91" + 2.54" + 3.18" + 3.82" + 4.45" + 5.09" + 5.73" + 6.36" + 7" + 7.63" + 8.27" + 8.91" + 9.54" + 10.18"

Formatted: English (United States)

Formatted: English (United States)

Figure 1

Click here to access/download;Figure;Figure 1.jpg

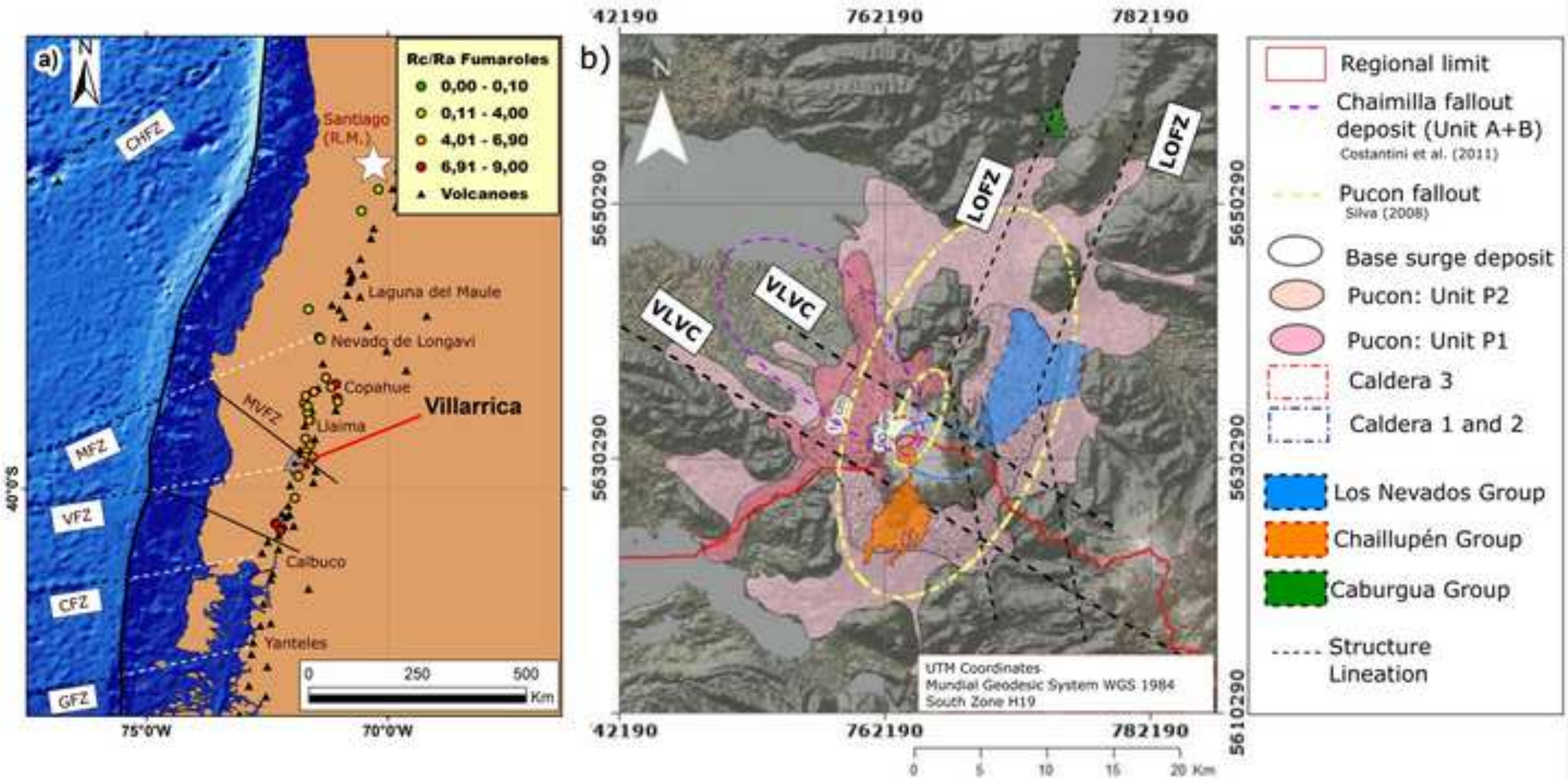

Figure 2

Click here to access/download;Figure;Figure 2.jpg

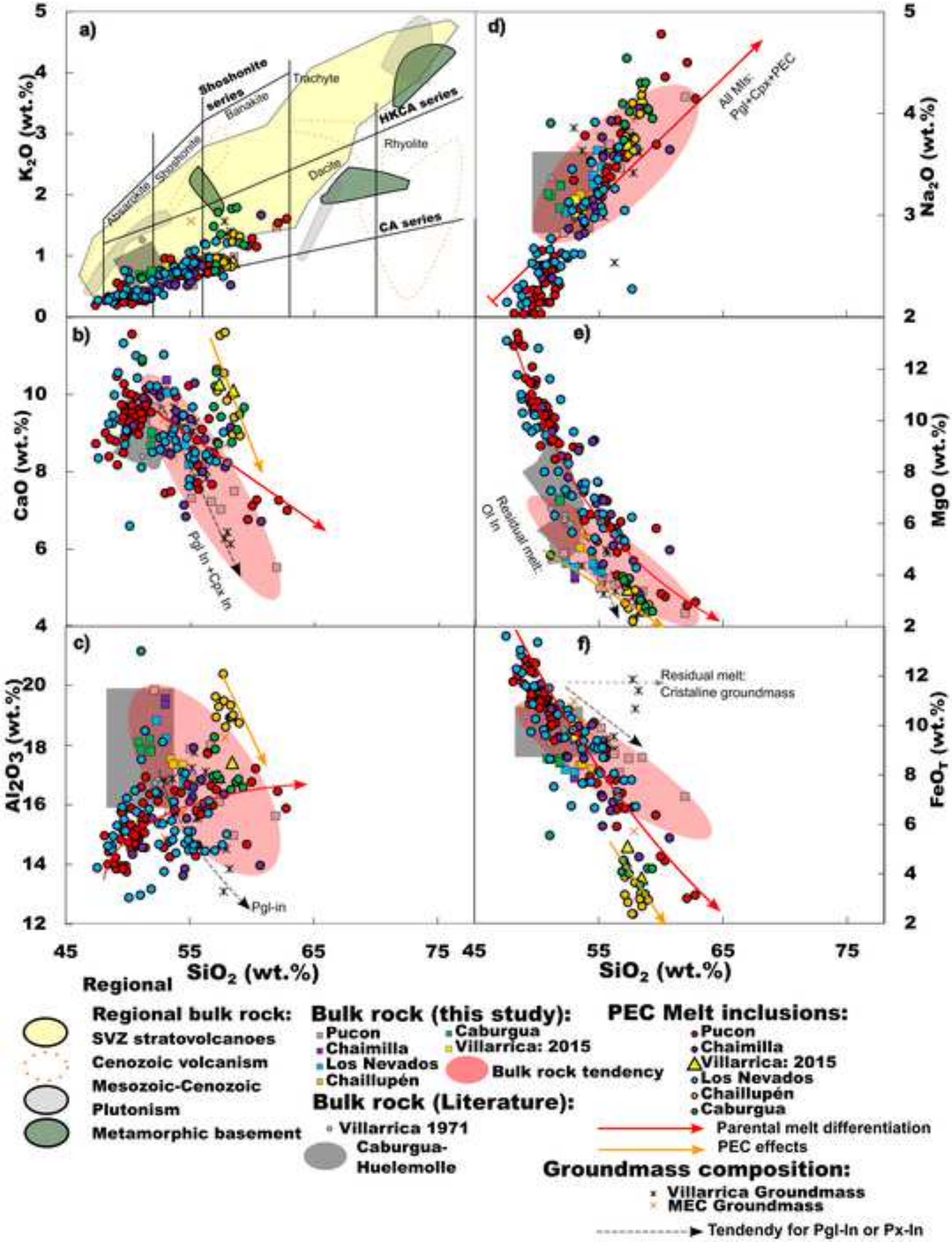

Figure 3

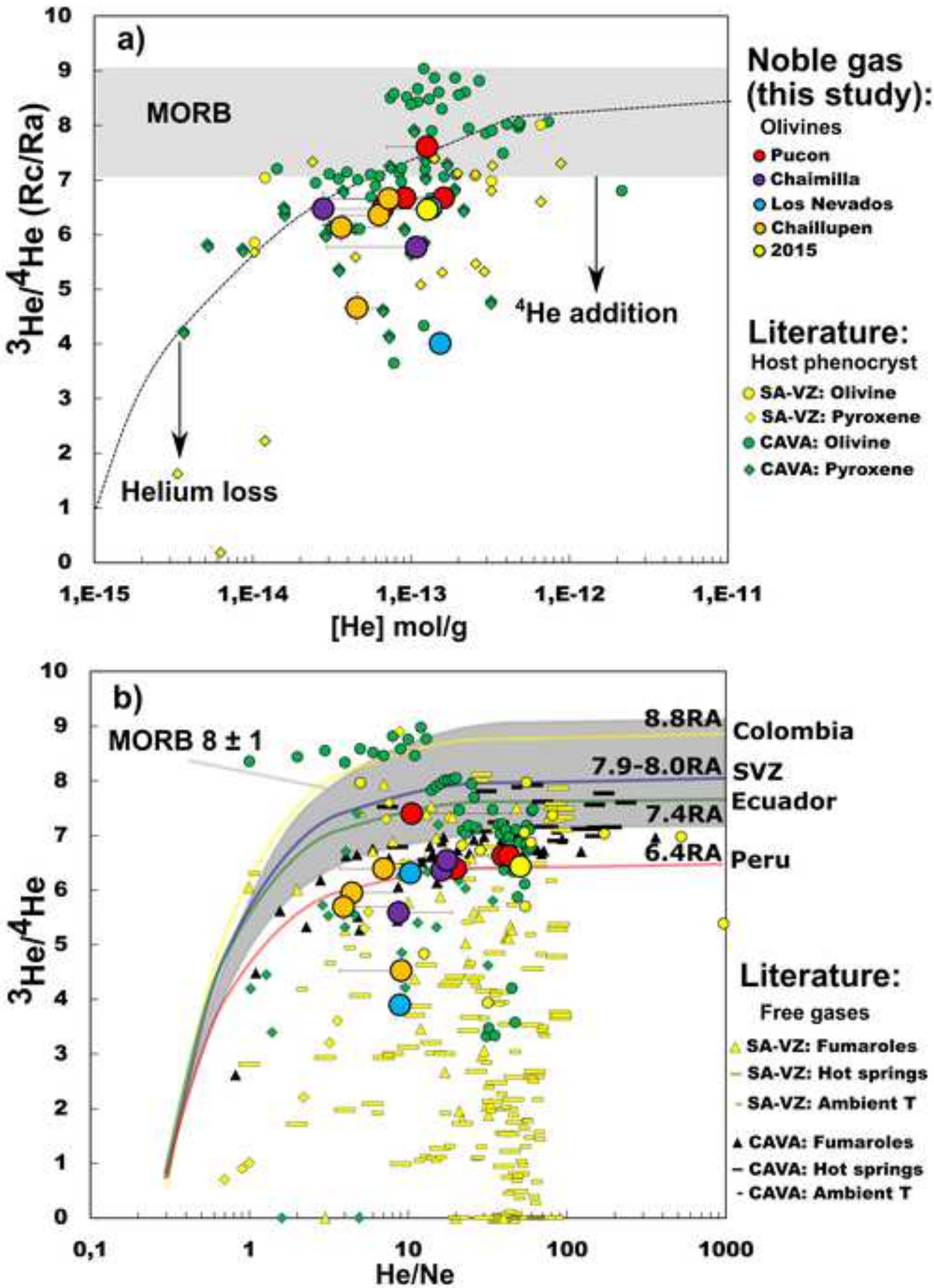

a)
MORB
Noble gas (this study):
Olivines
Pucon
Chaimilla
Los Nevados
Chaillupen
2015
^{4}He addition
Literature:
Host phenocryst
SA-VZ: Olivine
SA-VZ: Pyroxene
CAVA: Olivine
CAVA: Pyroxene
Helium loss
^{3}He/^{4}He (Rc/Ra)
[He] mol/g
1,E-15
1,E-14
1,E-13
1,E-12
1,E-11
b)
MORB 8 ± 1
8.8RA
Colombia
7.9-8.0RA
SVZ
Ecuador
7.4RA
6.4RA
Peru
Literature:
Free gases
SA-VZ: Fumaroles
SA-VZ: Hot springs
SA-VZ: Ambient T
CAVA: Fumaroles
CAVA: Hot springs
CAVA: Ambient T
^{3}He/^{4}He
He/Ne
0,1
1
10
100
1000

Figure 4

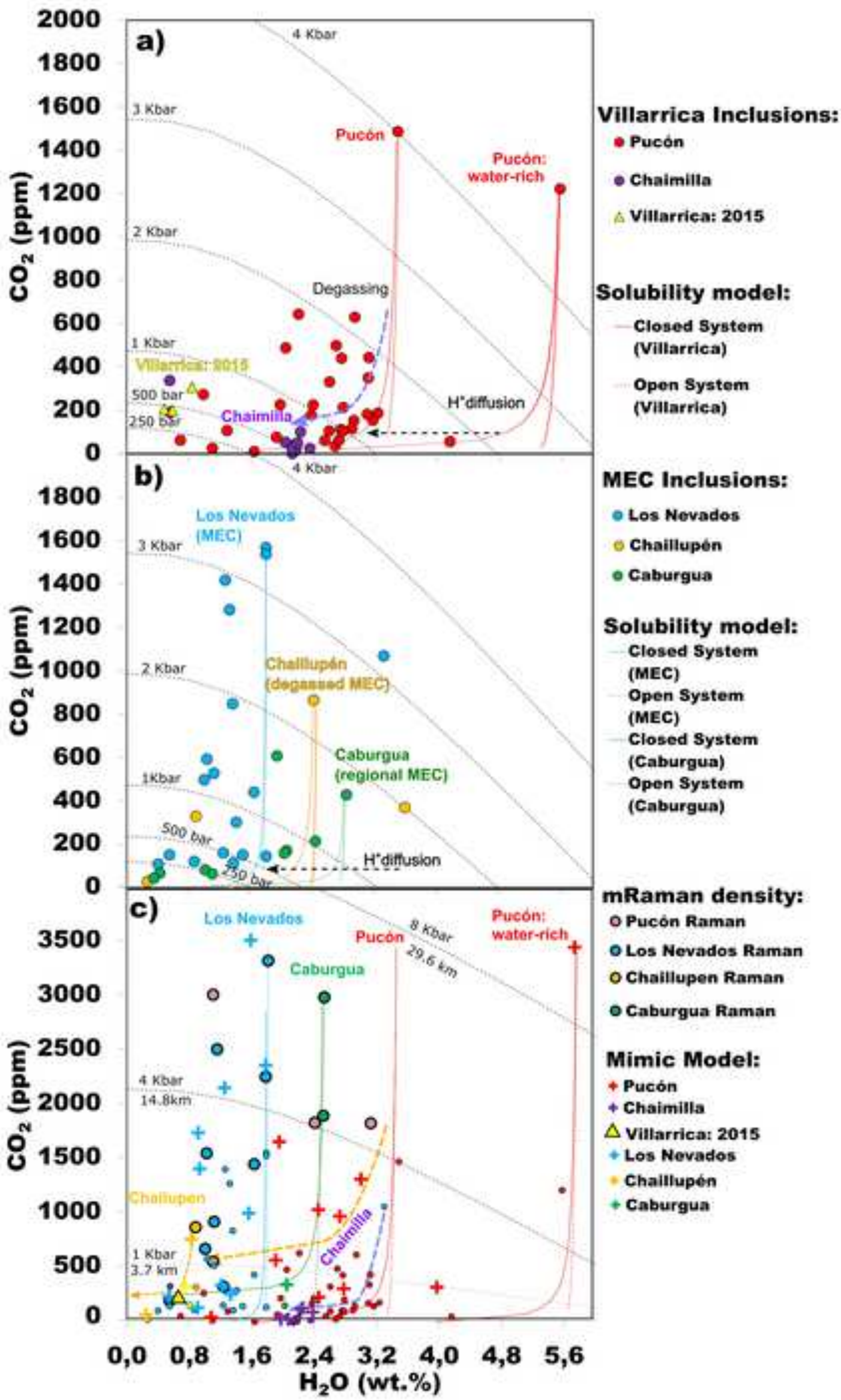

a)
b)
c)
4 Kbar
3 Kbar
2 Kbar
1 Kbar
500 bar
250 bar
Pucón
Pucón: water-rich
Degassing
Villarrica: 2015
Chaimilla
H⁺diffusion
Los Nevados (MEC)
Chaillupén (degassed MEC)
Caburgua (regional MEC)
1Kbar
Los Nevados
Caburgua
Chailupen
8 Kbar
29.6 km
4 Kbar 14.8km
1 Kbar 3.7 km
Chaimilla
CO₂ (ppm)
H₂O (wt.%)
Villarrica Inclusions:
Pucón
Chaimilla
Villarrica: 2015
Solubility model:
Closed System (Villarrica)
Open System (Villarrica)
MEC Inclusions:
Los Nevados
Chaillupén
Caburgua
Solubility model:
Closed System (MEC)
Open System (MEC)
Closed System (Caburgua)
Open System (Caburgua)
mRaman density:
Pucón Raman
Los Nevados Raman
Chaillupen Raman
Caburgua Raman
Mimic Model:
Pucón
Chaimilla
Villarrica: 2015
Los Nevados
Chaillupén
Caburgua

Figure 5

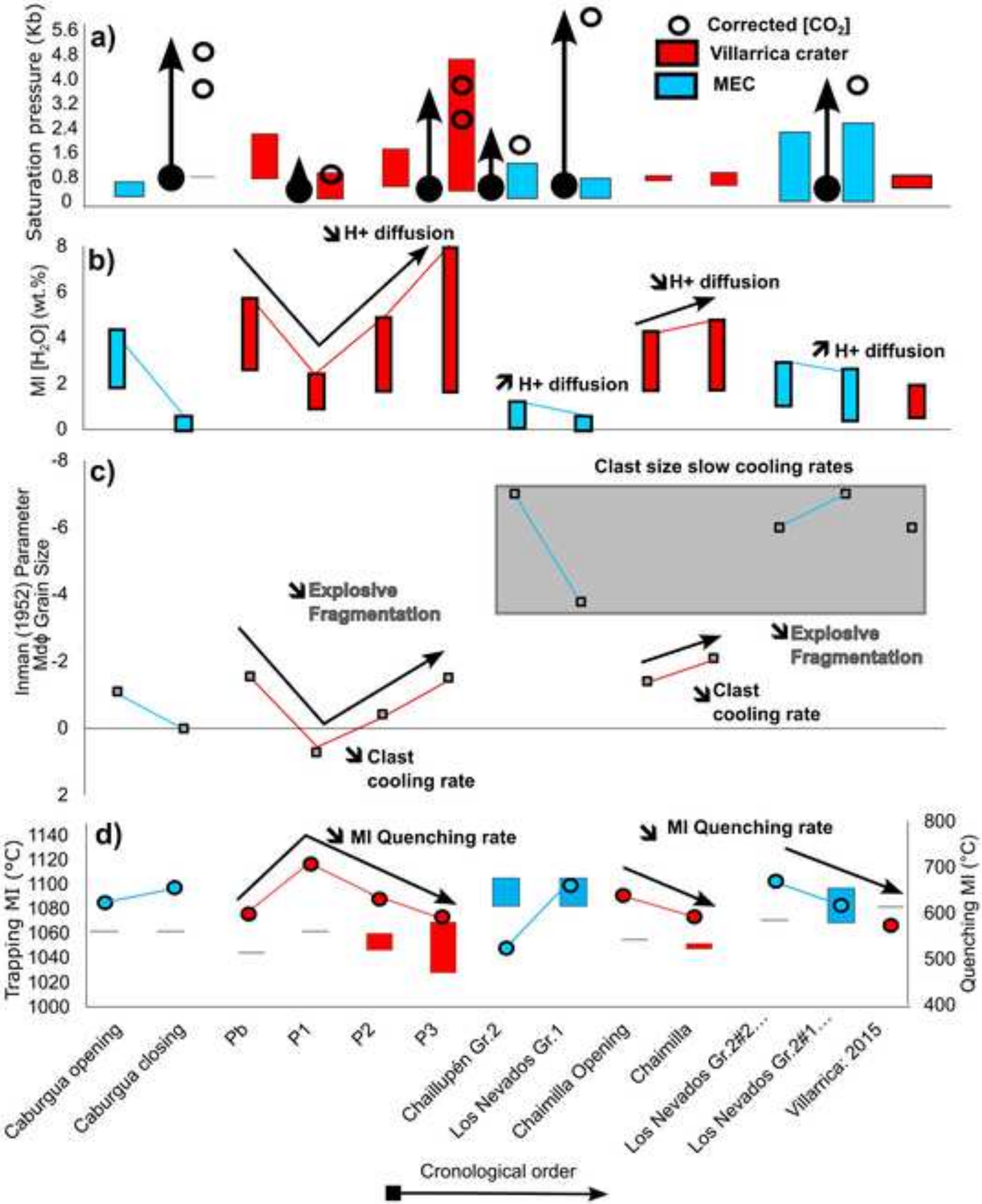

a)
Saturation pressure (Kb)
5.6
4.8
4.0
3.2
2.4
1.6
0.8
0
Corrected [CO2]
Villarrica crater
MEC
b)
MI [H2O] (wt.%)
8
6
4
2
0
H+ diffusion
H+ diffusion
H+ diffusion
H+ diffusion
c)
Inman (1952) Parameter Mdϕ Grain Size
-8
-6
-4
-2
0
2
Clast size slow cooling rates
Explosive Fragmentation
Explosive Fragmentation
Clast cooling rate
Clast cooling rate
d)
Trapping MI (°C)
1140
1120
1100
1080
1060
1040
1020
1000
Quenching MI (°C)
800
700
600
500
400
MI Quenching rate
MI Quenching rate
Caburgua opening
Caburgua closing
Pb
P1
P2
P3
Chaillupén Gr.2
Los Nevados Gr.1
Chaimilla Opening
Chaimilla
Los Nevados Gr.2#2...
Los Nevados Gr.2#1...
Villarrica: 2015
Cronological order

Figure 6

Click here to access/download;Figure;Figure 6.jpg

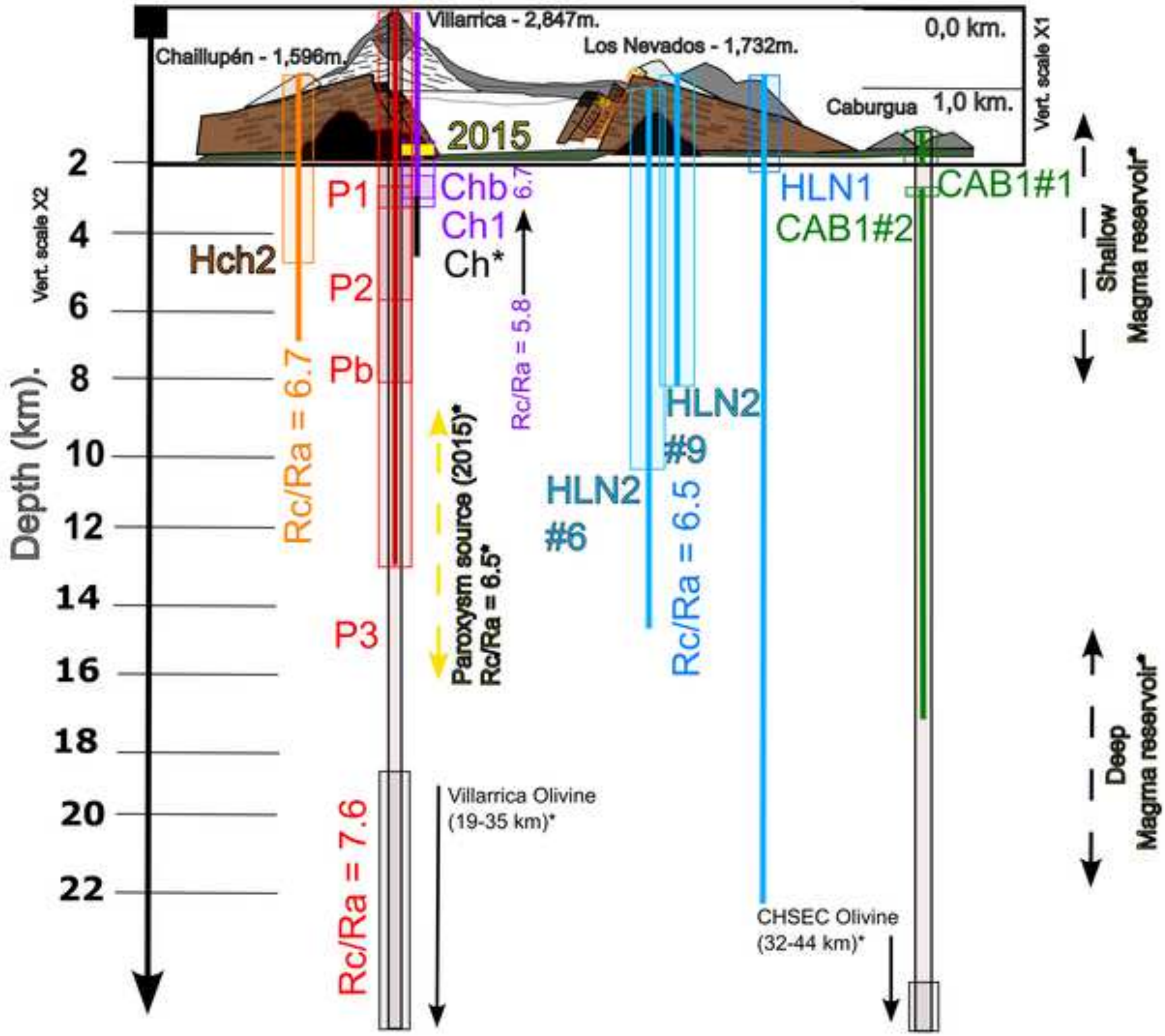

Figure 7

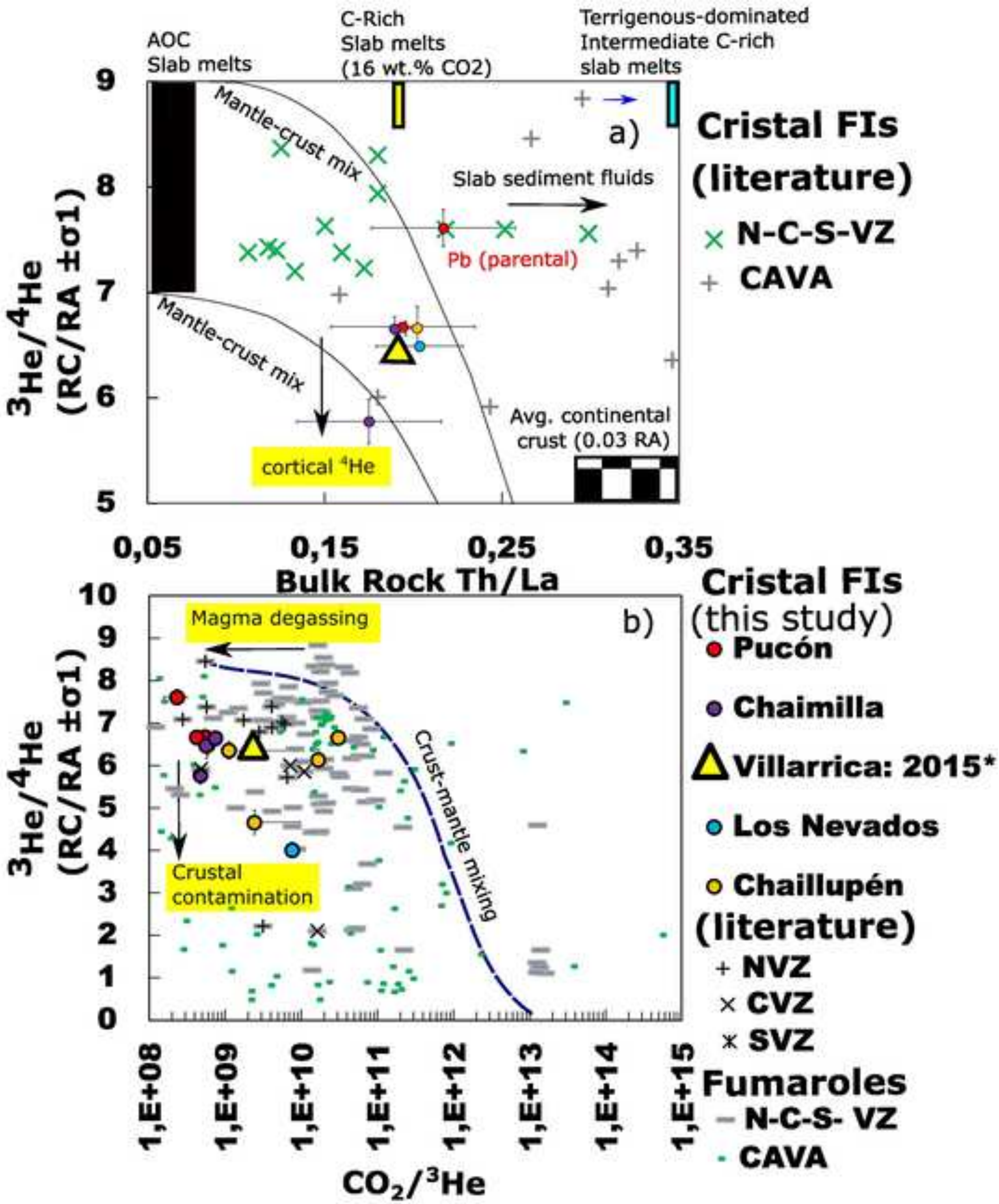
AOC
Slab melts
C-Rich
Slab melts
(16 wt.% CO2)
Terrigenous-dominated
Intermediate C-rich
slab melts
Mantle-crust mix
a)
Slab sediment fluids
Pb (parental)
Mantle-crust mix
Avg. continental
crust (0.03 RA)
cortical ^{4}He
^{3}He/^{4}He (RC/RA ±σ1)
Bulk Rock Th/La
Cristal FIs
(literature)
N-C-S-VZ
CAVA
Magma degassing
b)
Crust-mantle mixing
Crustal
contamination
$CO_2/^3He$
Cristal FIs
(this study)
Pucón
Chaimilla
Villarrica: 2015*
Los Nevados
Chaillupén
(literature)
NVZ
CVZ
SVZ
Fumaroles
N-C-S- VZ
CAVA

Figure 8 Click here to access/download;Figure;Figure 8.jpg

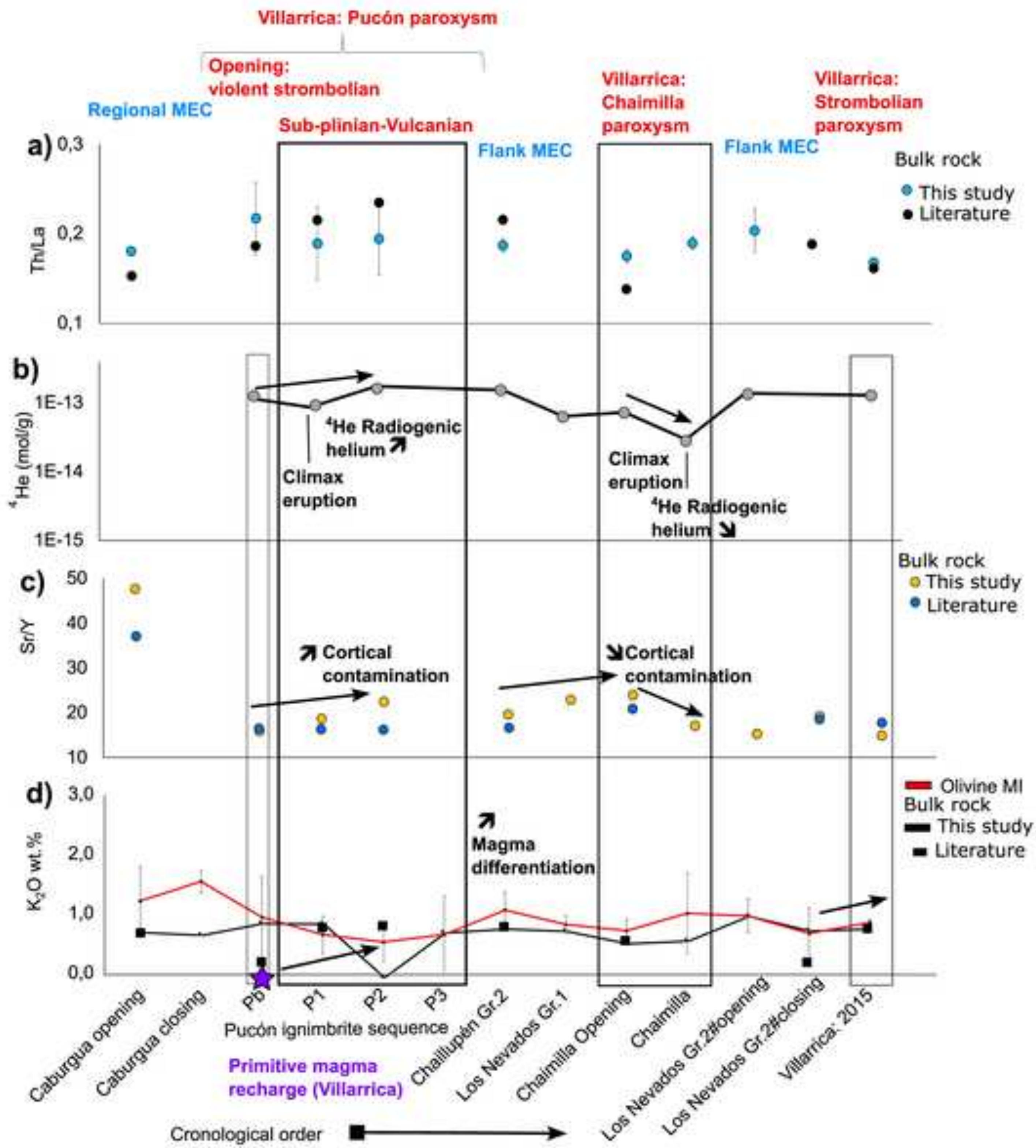

Table 1 Click here to access/download;Table;Table1.xlsx

Eruptive event	VEI	Sample	Deposit
Pucón Ignimbrite[7]	5	TVP10E	Fall deposit
		TVP03[1]	Piroclastic flow deposit rich in juvenile
		TVPI5AB	Piroclastic flow deposit rich in lithic
		TVPI5C	Piroclastic flow deposit rich in lithic
Chaimilla fallout[8]	4	TVP06B	Fallout deposit
		TVP06C	Fallout deposit
		TVP06D	Fallout deposit
March 2015 Paroxysm[9]	2	Villa_p2015+m2015; 2015_B[2]	Piroclast - Scoriaceous bomb
Los Nevados MEC	n.d.	HLN1A3D[3,4]	Piroclast - Scoriaceous bomb
		HLN2A6F[3,4]	Piroclast - Scoriaceous fusiform bomb
		HLN2A9[3,4]	Piroclast - Scoriaceous lapilli-bomb
Chaillués MEC	n.d.	HCH2A5[5]	Piroclast - Scoriaceous fusiform bomb
		HCH2A1[2,5]	Piroclast - Scoriaceous fusiform bomb
		HCH2A4C[2,5]	Lava core
Caburgua MEC	n.d.	CAB1[5]	Fall deposit

Reference list:

1 Gloria Estefanía Díaz Miranda. Universidad Mayor. Memoria de Licenciatura: “Condiciones Pre-Eruptiva

2 Lages, J., Rizzo, A. L., Aiuppa, A., Robidoux, P., Aguilar Contreras, R., Apaza Choquehuayta, F. E., & N

3 Daniela Patricia Pastén Muñoz. Universidad Mayor. Memoria de Licenciatura: “Relación entre Estilos de

4 Robidoux, P., Pastén, D., Levresse, G., Diaz, G., & Paredes, D. (2021). Volatile content implications of

5 Aaron Matías Sancho Escalante. Universidad Mayor. Memoria de Licenciatura: “Rol e implicancias de lo

6 Pioli, L., Scalisi, L., Costantini, L., Di Muro, A., Bonadonna, C., & Clavero, J. (2015). Explosive style, ma

7 Silva Parejas, C., Druitt, T. H., Robin, C., Moreno, H., & Naranjo, J. A. (2010). The Holocene Pucón eru

8 Costantini, L., Pioli, L., Bonadonna, C., Clavero, J., & Longchamp, C. (2011). A late Holocene explosive

9 Romero, J.E., Morgado, E., Pisello, A., Boschetty, F., Petrelli, M., Cáceres, F., Alam, M.A., Polacci, M.,

Unit Asociation	Primary volcanic clast size: Fisher (1966)
Villarrica: Pucon Pb	Toba Lapilli
Villarrica: Pucon P1	Toba Lapilli
Villarrica: Pucon P2-P3	Toba Lapilli
Villarrica: Pucon P2-P3	Toba Lapilli
Villarrica: Chaimilla Lower Sequence (18% lithics= A+B)	Toba Lapilli Breccia
Villarrica: Chaimilla Lower Sequence (18% lithics= A+B)	Toba Lapilli Breccia
Villarrica: Chaimilla Lower Sequence (B-C)[6]	Toba Lapilli Breccia
Villarrica: March, 2015	Breccia lapilli
Los Nevados Gr. 1	Lapilli breccia
Los Nevados Gr. 2	Lapilli breccia
Los Nevados Gr. 2	Lapilli breccia
Chaillupén Gr. 2	-
Chaillupén Gr. 2	-
Chaillupén Gr. 2	-
Caburgua Cone 1	Toba

as De Las Últimas Etapas Del Evento Pucón, Volcán Villarrica (39.5°S); Andes Del Sur". (November 2019). Supervisor: Pro
Masías Alvarez, P. J. (2021). Crustal controls on light noble gas isotope variability along the Andean Volcanic Arc.
e Desgasificación y Eruptivos en los Centros Eruptivos Menores Los Nevados, Andes del Sur". (October 2019). Supervisor:
increasing explosivity of the strombolian eruptive style along the fracture opening on the NE Villarrica Flank: Minor eruptive
os volátiles magmáticos en las condiciones pre-eruptivas de los centros eruptivos menores Caburgua y Chaillupén, Andes
agma degassing and evolution in the Chaimilla eruption, Villarrica volcano, Southern Andes. Bulletin of Volcanology, 77, 1-1
ption of Volcán Villarrica, Chile: deposit architecture and eruption chronology. Bulletin of volcanology, 72, 677-692.
mafic eruption of Villarrica volcano, Southern Andes: The Chaimilla deposit. Journal of Volcanology and Geothermal Rese
Palma, J.L., Arzilli, F. and Vera, F. (2022). Pre-eruptive Conditions of the 3 March 2015 Lava Fountain of Villarrica Volcanc

Volcanic clast components: White y Houghton (2006)	Graphical Std. (σφ) Sorting	Inaman (1952) Parameter (Mdϕ) : Grain Size
Lithic Toba	1.45	-1.55
Vitric Toba	2.68	0.72
Lithic Toba	2.19	-0.43
Lithic Toba	1.35	-1.52
Lithic Toba with 18%lithics	1.1	-1.41
Lithic Toba with 18%lithics	1.1	-1.40
Lithic Toba	0.97	-2.10
Vitric Toba	-	-6.00
Vitric Toba	3.30	-3.78
Vitric Toba	-	-7.00
Vitric Toba	-	-6.00
-	3.50	-7.00
-	3.30	-7.00
-	-	-
Vitric Toba	-0.37	-1.10

f. Philippe Robidoux

Prof. Philippe Robidoux, Review Commission

centers in the Los Nevados Group 2. Geosciences, 11(8), 309.

del Sur". (October 2019). Supervisor: Prof. Philippe Robidoux

14.

arch, 200(3-4), 143-158.

(Southern Andes). Bulletin of Volcanology, 85(1), 2.

Villarrica Eruptive Centre	Granulometry	BR	Olivine Populations
Table(s)	-	Table A.2	Table A.3, A.11
Figure(s)	Fig. SM1	Fig.7,8, A.1, A.7, A.8	
Appendix equivalent	A		
Erupton Series (#analysis)			
Pucón ignimbrite (Pb)	1	3	1
Pucón ignimbrite (P1)	4	1	1
Pucón ignimbrite (P2)	3	2	1
Pucón ignimbrite (P3)	2	3	1
Chaimilla (A+B) Opening	2	1	1
Chaimilla (B+C)	1	1	2
Villarrica: March, 2015	2	2	1
Los Nevados Gr.1	3	3	1
Los Nevados Gr.2	3	3	2
Chaillupén Gr.2	2	3	4
Caburgua	10	5	1

*Lages, J., Rizzo, A. L., Aiuppa, A., Robidoux, P., Aguilar Contreras, R., Apaza Choquehuayta

Noble Gas	Olivine-EMPA	mFTIR	SIMS	MI-EMPA	mRaman	Mimic
Table A.10	Table A.4	Table A.5, A.7	Table A.6, A.7	Table A.8	Table A.9	Table A.8
Fig.3,8, A.7	Fig.A.2	Fig.4, A.4, A.5, A.6	Fig. A.3, A.4, A.5, A.6	Fig.2, Fig. SM2		
				A		
2	37	43	21	34	0	1
1	10	2	2	4	5	1
1	10	22	11	10	0	3
0	24	35	0	19	8	5
1	6	3	5	6	0	1
2	31	10	10	16	0	4
1*	2	7	1	2	0	1
1	6	2	3	6	1	0
1	23	-	6	40	8	10
2+2*	11	12	0	10	1	2
0	13	26	3	13	8	2

a, F. E., & Masías Alvarez, P. J. (2021). Crustal controls on light noble gas isotope variability along th ıe Andean Volcanic Arc. Geochemical Perspectives Letters, uri: issn: 2410339X.

Table 3: Review of melt inclusion compositional dat

A. Chemistry Parameter	A. Changing attribute
KD desviation (avg.)	Increase Mg-Fe diffusion
Los Nevados (0.078)	
Pucon (0.080)	
Chaimilla (0.091)	
Caburgua (0.093)	
2015 (0.141)	
Chaillupén (0.172)	
Water contents (wt.%) (Md)	Increase H^+ diffusion
Pucon Ignimbrite (6.0)	
Caburgua (3.6)	
Los Nevados (3.3)	
Chaillupen (2.8)	
Chaimilla (2.4)	
2015 (0.84)	
The CO_2 content (g/mol)/crystal batch (range)	Decrease mass of CO_2 (bubble+crystal lattices)
Pucón Ignimbrite (3.1–4.6 ·10-10)	
Chaillupén (3.0–7.0 ·10-10)	
Chaimilla (1.8–4.0 ·10-10)	
2015 (? ; Lages et al., 2021)	
Caburgua (n.d.)	
Los Nevados (2.92 ·10-10)	
Maximum CO_2 contents (max. + STD)	Decrease dissolved CO_2
Pucon Ignimbrite (1485 SD 274)	
Chaillupen (863 SD 145)	
Caburgua (607 SD 325)	
Los Nevados (583 SD 176)	
Chaimilla (409 SD 108)	
2015 (307 SD 48)	

aset

B. Complementary observations	B. Changing attribute
(Mdϕ) (Grain Size)	Increase clast size
Chaimilla (-2.1) Caburgua (-1.1) < Pucón Ignimbrite (0.72) Los Nevados (-7.0 to - 3.8) Chaillupén (-7.0) 2015 (-6.0)	
Trapping MI - Glass transition (°C) °T (range+STD)	Decrease cooling °T
Pucón Ignimbrite Te(1135 SD 16) - Tg(580 SD 30) Chaimilla Te(1134 SD 48) - Tg (534 SD 43) Los Nevados Te(1128 SD 19) Tg(653 SD 82) Caburgua Te(1127 SD 14) - Tg(560 SD 140) 2015 Te(1076 SD 10) - Tg (614) Chaillupén Te(1069 SD 8) - Tg (673 SD 43)	
% Total Primary MI + bubble (range)	Decrease amount of vapor bubble
Pucón Ignimbrite (13–81%) Chaillupén (13.8–43.4%) Chaimilla (21.7–24.4%) 2015 (15.5%) Caburgua (14.8%) Los Nevados (11.0–14.0%)	
Maximum %Forsterite contents (max. + STD)	Melt differentiation increase
Pucón Ignimbrite (87 SD 4) Chaillupén (84 SD 0.3) Chaimilla (83 SD 0.4) Los Nevados (82 SD 3.5) Caburgua (80.9 SD 3.4) 2015 (76)	

Click here to access/download
Supplementary material/Appendix (Files for online publication only)
Appendix B.xlsx

Click here to access/download

Supplementary material/Appendix (Files for online publication only)

Appendix C.xlsx

Declaration of interests

☒The authors declare that they have no known competing financial interests or personal relationships that could have appeared to influence the work reported in this paper.

☐The authors declare the following financial interests/personal relationships which may be considered as potential competing interests: